

Inhibition of KRas using Affimers

Ajinkya Rao

Submitted in accordance with requirements for the degree of
Doctor of Philosophy

University of Leeds
Faculty of Biological Sciences
School of Molecular and Cellular Biology

October 2020

The candidate confirms the work submitted is his own, except where work which has formed a part of jointly authored publications has been included. The contributions of candidate and other authors for this work has been explicitly indicated below. The candidate confirms appropriate credit has been given within the thesis where reference has been made to the work of others.

Jointly authored publication:

HAZA, K. Z., MARTIN, H. L., **RAO, A.**, TURNER, A., SAUNDERS, S., PETERSEN, B., TIEDE, C., TIPPING, K., TANG, A. A., AJAYI, M., TAYLOR, T., FISHWICK, K., ADAMS, T. L., GAULE, G. T., TRINH, C. H., JOHNSON, M., BREEZE, A. L., T.A., E., MCPHERSON, M. J. & TOMLINSON, D. C. 2020. RAS-inhibiting biologics identify and probe druggable pockets including an SII- α 3 allosteric site. *BioRxiv*.

The work included from this publication in the thesis; Figure 1b. and 1c and Figure 5, results from which are shown in chapter 3, 4 and 5.

In chapter 3 the screening of KRas-GDP was carried out by Bioscreening technology group. Results are shown in Figure 3.1. SOS^{cat} nucleotide exchange assay was carried out by Dr. Kevin Tipping and is shown in Figure 3.3

In Chapter 4 for X-ray crystallography data collection, processing and refinement analysis was carried out by Dr Chi Trinh.

This copy has been supplied on the understanding that it is copyright material and that no quotation from the thesis may be published without proper acknowledgement.

Acknowledgement

Throughout the writing of this dissertation I have received a great deal of support and assistance. I would first like to offer my thanks to my supervisor Dr Darren Tomlinson for giving me opportunity to do a PhD and for his expertise, guidance and encouragement offered throughout my PhD journey. I would also like to thank my co-supervisor Dr Thomas Edwards for constructive criticism and feedback, your insights and suggestions were very valuable.

Particular thanks to Dr Christian Tiede for all your help and advice, your inputs really helped me understand the research methodology and techniques better. Thanks to all members of Tomlinson and McPherson lab for your advice and encouragement throughout the journey and to make the entire journey enjoyable. The memories of coffee mornings, having a chilled beer after tiring day at Veritas and talking about silly mistakes in the lab would always bring a smile.

My sincere thanks to my friend Dr Amit Kumar for his encouragement and guidance and for critically reading my thesis. I am highly grateful to my friend Dr Bharat Pokharel for his constructive feedback, support and encouragement. Your scientific knowledge is so good, I need to still learn a lot from you!

Finally, I am also highly grateful for my father (Dr Sunil Rao), mother (Anjali Rao) and my brother (Abhinav Rao) for your continuous support throughout my life. You made my dreams to study abroad come true.

Abstract

Ras proteins are small GTP binding and hydrolysing proteins (GTPases) that regulate various signalling pathways responsible for cell proliferation, differentiation, migration and survival. Ras proteins are found to be mutated in 30% of all human cancers. Mutations in Ras or their regulators such as GTPase activating proteins (GAPs) or guanine nucleotide exchange factors (GEFs) render Ras proteins to be in persistently active GTP bound state leading to uncontrolled cell growth and proliferation.

Despite three decades of extensive research, no pharmacological inhibitors of Ras have reached the market. Targeting Ras proteins directly has been challenging process because of lack of deep binding pockets for small molecules to bind to with high affinity and specificity. A novel approach of using non-antibody scaffolds for development of Ras inhibitors has shown great promise. This is being illustrated by recent increase in antibody mimetics targeting Ras such as Intrabodies, Monobodies and DARPins. In this thesis the Affimer, a novel binding protein based on a consensus cystatin scaffold has been used to inhibit KRas, which is most mutated Ras isoform.

The project aims to identify Affimers that are potent inhibitors of KRas function. Three KRas binding Affimers have been identified via phage display that have shown to inhibit KRas activity by inhibiting nucleotide exchange activity. Out of three Affimers, Affimer K3 was identified to exhibit dual mode of inhibition i.e. inhibit nucleotide exchange as well as Ras-Raf interaction. To further understand the binding and inhibition of KRas by K3 Affimer, pulldown assays and nucleotide exchange assays identified that both variable regions of Affimer K3 are important for binding and inhibition of KRas. Furthermore, molecular details of Affimer K3 in complex with KRas revealed a novel Ras conformation with generation of pocket between Switch II and $\alpha 3$ helix. The pocket created by hydrophobic interactions is stabilised by the W44 indole side chain of K3, orienting itself to form hydrogen bonds with H95 present in $\alpha 3$ helix. Mutation of KRas specific residue H95 has shown preferential specificity of Affimer K3 towards KRas, as compared to HRas and NRas. The work presented in this thesis shows Affimer K3 can be used as valuable tool to study KRas function via identification of novel Ras conformer with druggable SII/ $\alpha 3$ pocket.

Table of Contents

Acknowledgement	iii
Abstract	iv
List of Tables	viii
List of figures	ix
List of Abbreviations	xii
Chapter 1	1
Introduction	1
1.1 A brief history, classification and post translational modifications of Ras GTPases	1
1.1.1 The discovery of Ras	1
1.1.2 Ras superfamily of small GTPases	2
1.1.3 Ras synthesis, processing, and maturation	6
2.1 Ras signalling: Mechanism of GTPase activation and regulation	9
2.1.1 Ras regulated signalling pathways	9
2.1.2 Mechanism of Ras GTPase activation	11
2.1.3 Guanine nucleotide exchange factors and GTPase activating proteins	12
2.1.4 Isoform-specific Ras signalling.....	15
3.1 Role of Ras in cancer	16
3.1.1 Incidence and spectrum of Ras mutations in cancer	17
3.1.2 Biochemical and structural properties of Ras mutants	19
4.1 Ras as a therapeutic target	20
4.1.1 Why has Ras been considered 'undruggable'?	20
4.1.2 Early approaches to target Ras.....	21
5.1 Renewed efforts to target Ras directly	24
5.1.1 Inhibition of K-Ras ^{G12C}	24
5.1.2 Pan-Ras inhibitors	26
6.1 Novel approaches to target Ras using non-antibody binding proteins	27
6.1.1 Artificial binding proteins	27
6.1.1.1 Intrabody.....	30
6.1.1.2 Affibody.....	32
6.1.1.3 Monobodies	33
6.1.1.4 DARPins	34
7.1 Affimer Reagents	37
7.1.1 Type I Affimer scaffold.....	37

7.1.2 Type II Affimer.....	38
Objectives	41
Chapter 2	42
Materials and Methods	42
2.1 Materials	42
2.1.1 General reagents.....	42
2.1.2 Bacterial strain genotypes.....	42
2.1.3 Primers used for sub-cloning.....	42
2.1.4 Common buffers and solutions	47
2.1.6 Bacterial cell culture reagents	47
2.1.7 SDS PAGE and western blot reagents	48
2.2 Methods	49
2.2.1 DNA protocols and molecular sub-cloning.....	49
2.2.2 Protein analysis methods	55
2.2.3 Protein production	56
2.2.8 Protein crystallisation.....	62
Chapter 3	68
Biochemical characterisation of Ras specific Affimer	68
3.1 Introduction	68
3.2 Results	75
3.2.1 Affimer K3 inhibits SOS ^{cat} mediated nucleotide exchange	75
3.2.2 Affimer K3 inhibits the interaction of Ras with Ras binding domain of CRaf	78
3.2.3 Both variable regions of Affimer K3 are involved in binding and inhibition of KRas	82
3.2.4 Identification of Affimer K3 residues involved in binding and inhibition of KRas	87
3.3 Discussion	90
Chapter 4	95
Structural characterisation of Affimer-KRas complex	95
4.1 Introduction	95
4.2 Results	97
4.2.1 Generation of Affimer K3-KRas complex.....	97
4.2.2 Crystallisation of Affimer K3-KRas complex.....	99
4.2.3 Optimisation of initial crystal hit from JCSG screen II.....	101
4.2.4 Crystallisation using additional sparse matrix screens.....	101
4.2.5 Binding of Affimer K3 to KRas revealed a druggable SII/ α -3 pocket	102
4.2.6 Crystal structure of Affimer K3 reveals a dynamic VR2 loop.....	106

4.2.7 Crystal structure of Affimer K3	108
4.3 Discussion	110
Chapter 5	115
Understanding Affimer K3 specificity towards KRas	115
5.1 Introduction.....	115
5.2 Results	116
5.2.1 Affimer K3 preferentially binds to KRas isoform.....	116
5.2.2 Structural analysis of Ras-Raf1RBD inhibition via Affimer K3	120
5.3 Discussion.....	124
Chapter 6	126
Discussion and future perspectives	126
6.1 Use of Affimers to inhibit KRas function	128
6.2 Identification of cryptic binding sites in Ras using Affimer K3	129
6.3 Continuation of the project and future applications.....	130
6.3.1 Affimers as therapeutics	132
Conclusions	133
References	134
Appendix A	155
Vector Maps	155
Appendix-B	160
Protein sequences of all proteins used in this thesis	160
Appendix C	161
Additional protein-based inhibitors binding to Ras	161

List of Tables

Table 1.1 Scaffold binding proteins currently approved or in clinical trials.....	35
Table 2.1 Genotypes of bacterial strains used for this project.....	48
Table 2.2 List and sequence of primers used for subcloning.....	49
Table 2.3 List and sequences of alanine mutant primers used for sub-cloning.....	50
Table 2.4 Details of antibody concentration, dilution factor and source.....	52
Table 2.5 Composition of thermal cycling reaction mixture.....	54
Table 2.7- Primers used for DNA sequencing of plasmids.....	55
Table 2.8 Cycling conditions for site directed mutagenesis protocol.....	58
Table 2.9 X-ray crystallographic data collection, processing and refinement statistics for Affimer K3-KRas complex.....	59
Table 3.1 Amino acid sequences of variable regions and the number of appearances of seven unique Affimers against KRas wild type	69
Table 3.2 Calculated IC ₅₀ values of K6 and K37 Affimers for KRas and HRas WT.....	77
Table 3.3 Calculated IC ₅₀ values of K3, K6 and K37 Affimers for oncogenic KRas mutants.....	80

List of figures

Figure 1.1 Ras superfamily of smallGTPases.....	3
Figure 1.2 Schematic representation of functional domains in Ras structure.....	4
Figure 1.3 Ras plasma membrane targeting via post-translational modifications.....	8
Figure 1.4 Ras regulated signaling pathways.....	10
Figure 1.5 Ras GTPase activation.....	12
Figure 1.6 Functional domains and structural analysis of SOS1 and p120GAP.....	14
Figure 1.7 Incidence and spectrum of Ras mutations in cancer.....	18
Figure 1.8 Chemical structure of low affinity inhibitor compound SCH 5429	21
Figure 1.9 Ras/SOS inhibitor DCAI compound.....	22
Figure 1.10 Chemical structures of Ras-Raf interaction	23
Figure 1.11 Pan Ras inhibitor.....	26
Figure 1.12 Co-crystal structure of HRas and intrabody iDab6 binder protein.....	30
Figure 1.13 Co-crystal structure of HRas and monobody binder protein NS1 (PDB: 5E95).....	33
Figure 1.14 Co-crystal structures of Ras and DARPin binder proteins...	35
Figure 1.15 Structure of the Affimer scaffolds.....	39
Figure 3.1 Phage ELISA for 96 Affimer clones isolated against KRas wild type.....	68
Figure 3.2 Diagram of nucleotide exchange assay.....	70
Figure 3.3 KRas binding Affimers inhibited SOS catalysed nucleotide exchange reaction.....	71
Figure 3.4 Production and purification of Ras, Affimer K3 and SOS for nucleotide exchange assay.....	74
Figure 3.5 Affimer K3 inhibits nucleotide exchange on wild type KRas...	75
Figure 3.6 Deconvolution of native mass spectra.....	77
Figure 3.7 Immunoprecipitation of KRas with GST Raf1RBD is inhibited by Ras binding Affimers.....	78

Figure 3.8 Cloning strategy to create mutants with deleted Affimer K3 variable region 1 or 2.	80
Figure 3.9 – Binding studies of Affimer K3, K3 Δ VR1 and K3 Δ VR2 on KRas.....	81
Figure 3.10 Circular dichroism analysis of K3 WT, K3 Δ VR1 and K3 Δ VR2.....	82
Figure 3.11 Nucleotide exchange assay for K3WT, K3 Δ VR1 and K3 Δ VR2	83
Figure 3.12 Expression and purification of K3 alanine mutants.....	85
Figure 3.13 Effect of Affimer K3 variable regions alanine mutants on the ability to bind to KRas.....	86
Figure 3.14 Functional effects of Affimer K3 variable regions alanine mutants on inhibition of nucleotide exchange to active GTP state.....	87
Figure 4.1 Timeline of drug discovery process and steps involved in identification of lead compound.....	93
Figure 4.2 Purification of Affimer K3-KRas complex.....	95
Figure 4.3 Size exclusion chromatography (SEC) of Affimer K3-KRas complex obtained after Ni ²⁺ -NTA chromatography.....	96
Figure 4.4 Summary of initial crystallisation conditions obtained via JSCG screens.....	97
Figure 4.5 Summary of crystallisation conditions for Affimer K3-KRas complex crystals.....	99
Figure 4.6 Co-crystal structure of KRas with Affimer K3.....	100
Figure 4.7 Intermolecular interaction between Affimer K3-KRas	101
Figure 4.8 Conformational shift and hydrogen bonding network facilitated by binding of K3.....	102
Figure 4.9 Elution profile of K3 Affimer.....	104
Figure 4.10 Summary of crystal conditions of Affimer K3 only.....	105
Figure 4.11 Crystal structure of Affimer K3	106
Figure 4.12 Comparison of surface shape and electrostatics of small molecules with K3 Affimer.....	109
Figure 4.13 Intramolecular interactions of Affimer K3.....	111

Figure 5.1 Site directed mutagenesis and sequence of KRas H95Q/L.....	113
Figure 5.2 15% SDS PAGE gel showing protein expression of KRas WT, H95Q, H95L and Affimer K3/Alanine.....	114
Figure 5.3 Immunoprecipitation of K3/K6 with KRas, KRas H95L and KRas H95Q.....	115
Figure 5.4 Structural overlay and comparison between HRas: Raf1RBD and KRas: Affimer K3.....	117
Figure 5.5 SDS PAGE to verify protein expression of KRas WTandGSTRBD.....	118
Figure 5.6 Co-immunoprecipitation assay showing effect of mutation on residues. involved in Ras:Raf inhibition.....	119
Figure 6.1 Comparison of normal, oncogenic Ras signalling and inhibition of oncogenic KRas with help of AffimerK3	122.

List of Abbreviations

ABP	Artificial binding protein
ADAs	Anti-drug antibodies
ANOVA	Analysis of variance
BAP	Biotin acceptor peptide
BCA	Bicinchoninic acid
BCL-6	B cell lymphoma 6
BH3	BCL-2 Homology 3
BRET	Bioluminescent resonance energy transfer
DARPinS	Designed ankyrin repeat proteins
CAAX acid	C=cysteine, A=Aliphatic amino acid, X= terminal amino acid
CDC 25	Cell division cycle 25
CLIA	chemiluminescence assay
COOT	Crystallographic object-oriented tool kit
DCAI	4,6-dichloro-2-methyl-3-aminoethyl-indole
DTT	Dithiothreitol
EGFR	Epidermal growth factor receptor
ER	Endoplasmic reticulum
ERK	Extracellular signal regulated kinase
ESRF	European Synchrotron radiation facility
FDA	Food and Drug Administration
GAP	GTPase activating protein
GEFs	Guanine nucleotide exchange factors
GPCR	G protein coupled receptors
GST	Glutathione-S-transferase
HCC	Heptacellular carcinoma
HRP	Horseradish peroxidase
HVR	Hypervariable regions
IAC	Intracellular antibody capture

IB	Immunoblot
ICMT	Isoprenylcysteine Carboxyl Methyl Transferase
IPA	Isopropyl alcohol
JCSG	Joint Centre for Structural Genomics
KSR	Kinase suppressor of Ras
MANT	2'-or 3'-O- (N-Methylantraniloyl)
MAPK	Mitogen activated protein kinase
MEF	Mouse embryonic fibroblasts
MWCO	Molecular weight cut-off
NCI	National Cancer Institute
NSCLC	Non cell small lung cancer
NTA resin	nitrilotriacetic acid
PB buffer	Binding buffer
PBST	Phosphate buffered saline 1x Tween
PDAC	Pancreatic ductal adenocarcinoma
PDB	Protein data bank
PE Buffer	Wash buffer
POZ	Pox virus and Zinc finger
PPI	Protein-protein interactions
PTM	Post translational modifications
RAL	Ras-related protein
RAP	Rap GTP binding protein
RBD	Ras binding domain
RCE1	Ras converting enzyme
REM	Ras exchange motif
RHEB	Ras homolog enriched in brain
RIT	Ras-like protein in tissues
RMSD	Root mean square deviation
RSK	Ribosomal S6 kinase
SOC	Super optimal broth

SOS	Son of sevenless
SQT	Stefin A Quadropole Mutant –Tracy
SUMO	Small ubiquitin like modifiers
TCEP	Tris(2-carboxyethyl) phosphine

Chapter 1

Introduction

1.1 A brief history, classification and post translational modifications of Ras GTPases

1.1.1 The discovery of Ras

RAS genes were identified from the studies of “tumour-inducing” retroviruses isolated from rats, cats, cows and other animals (Harvey., 1964; Kirsten and Mayer., 1967) (Coffin et al., 1997). Early research dates back to the 1900s when Peyton Rous discovered transmissible leukaemia and solid tumours in chickens (Rous., 1911). In the mid-1960s, Jennifer Harvey and Werner Kirsten isolated two viruses – Harvey murine sarcoma virus and Kirsten murine sarcoma virus that induced tumours in rats (Harvey., 1964; Kirsten and Mayer., 1967). Further studies on these cancer-causing viruses were carried out by Scolnick and colleagues in 1973, which led to the identification of genetic elements responsible for oncogenic transformation. These were then referred to as *SRC* oncogenes (Scolnick et al., 1973). Now these are known as *RAS* oncogenes due to the ability of these retroviruses to cause rat sarcomas (*RAS*), which is an acronym for the current gene name *RAS*. Due to difference in transforming properties of *RAS* retroviruses, discoverers' names were used to distinguish each of them: Harvey (*HRAS*) and Kirsten (*KRAS*) viral *RAS* genes (Malumbres and Barbacid., 2003; Cox and Der., 2010) . In 1981 using the DNA transfection technique established by Weinberg (Krontiris and Cooper, 1981), Krontiris and Cooper isolated DNA from two bladder cancer cell lines and observed transforming activity in NIH 3T3 mouse cell lines (Shih et al., 1979; Der et al., 1982). Following this, three groups in 1982 discovered that transforming genes identified in NIH 3T3 cell lines were similar to Harvey and Kirsten sarcoma viruses. Additionally, they found that the mechanism of Ras oncogene activation was due to single base missense mutation at residue 12 and less frequently at residue 13 and 61 (Reddy et al., 1982; Tabin et al., 1982; Capon et al., 1983) (Mageean., 2014). By 1983, a third transforming human *RAS* gene,

was discovered in neuroblastoma cells and was reported to have weak DNA sequence homology to *HRAS* and *KRAS* and was designated as *NRAS* (Shimizu et al., 1983). It was also found to be structurally related to HRas and KRas. The following section (Section 1) covers Ras superfamily of GTPases, including Ras synthesis, processing, and maturation. Section 2 covers the biochemistry of Ras signalling, including the mechanism of GTPase activation and elaborate on the role of Ras in cancer.

1.1.2 Ras superfamily of small GTPases

More than 150 members of Ras-related small Guanosine Triphosphatases (GTPases) have been identified in the cell so far, which share a conserved protein structure and function. GTPases function as binary molecular switches that get activated by binding to GTP and deactivated by hydrolysis of GTP to GDP (Wennerberg et al., 2005). The Ras superfamily of proteins can be classified into five major subfamilies based on their sequence and functional similarities: Ras, Rho, Rab, Ran, and Arf (Figure 1.1).

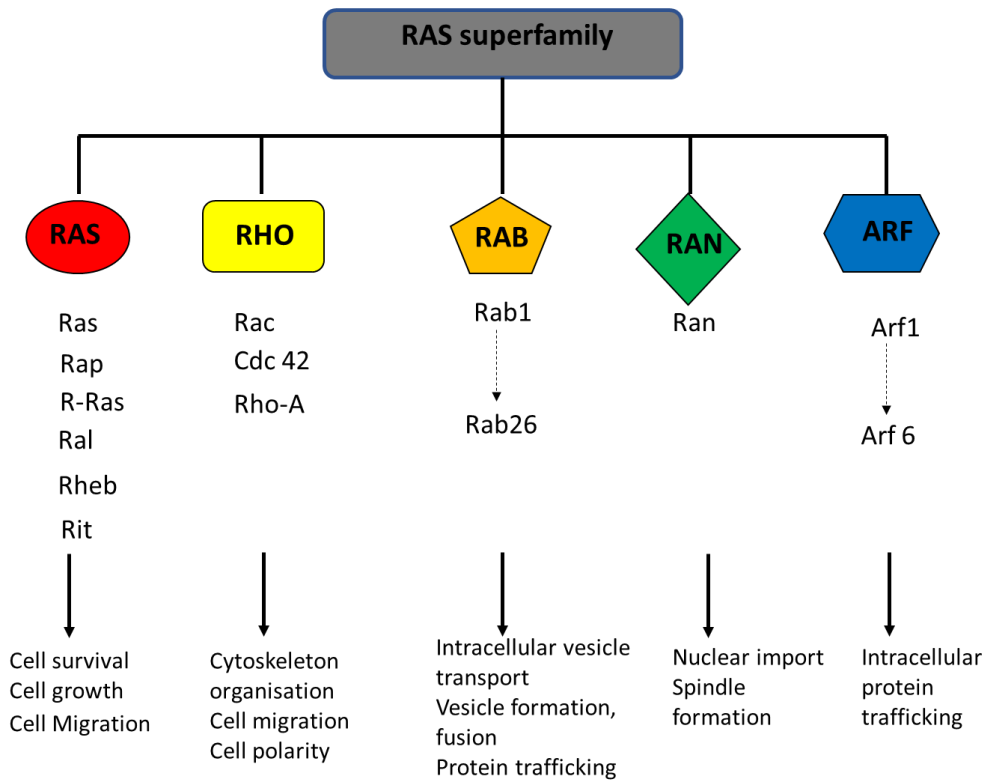


Figure 1.1 Ras superfamily of small GTPases. Ras superfamily consists of five significant subfamilies of GTPases that perform a wide variety of cellular functions. These include Ras, Rho, Rab, Ran, and Arf. Best characterised and studied proteins in each subfamily have been mentioned along with their role in maintaining essential functions in the cell.

All these families have a common core structure, a G domain, which comprises five alpha-helices ($\alpha 1$ - $\alpha 5$) and six beta sheets ($\beta 1$ - $\beta 6$) (Heider et al., 2010). The G domain's basic structure consists of five highly conserved G motifs (G1-G5) (Figure 1.2). The G1 motif (GxxxxGKS/T) encodes the phosphate-binding loop (P-loop). The G2 motif (xTx) contains an invariant threonine residue that mediates hydrogen bonding interactions with the γ phosphate of GTP and coordinates with Mg^{2+} ion in the GTP-bound state. The G3 motif (DxxG) consists of invariant aspartic acid and glycine residues that stabilise Mg^{2+} binding and hydrogen bonding with γ phosphate. Finally, the G4 (N/TKxD) and G5 (xAx) motifs contain residues important for guanine nucleotide-binding specificity (Mishra and Lambright., 2016).

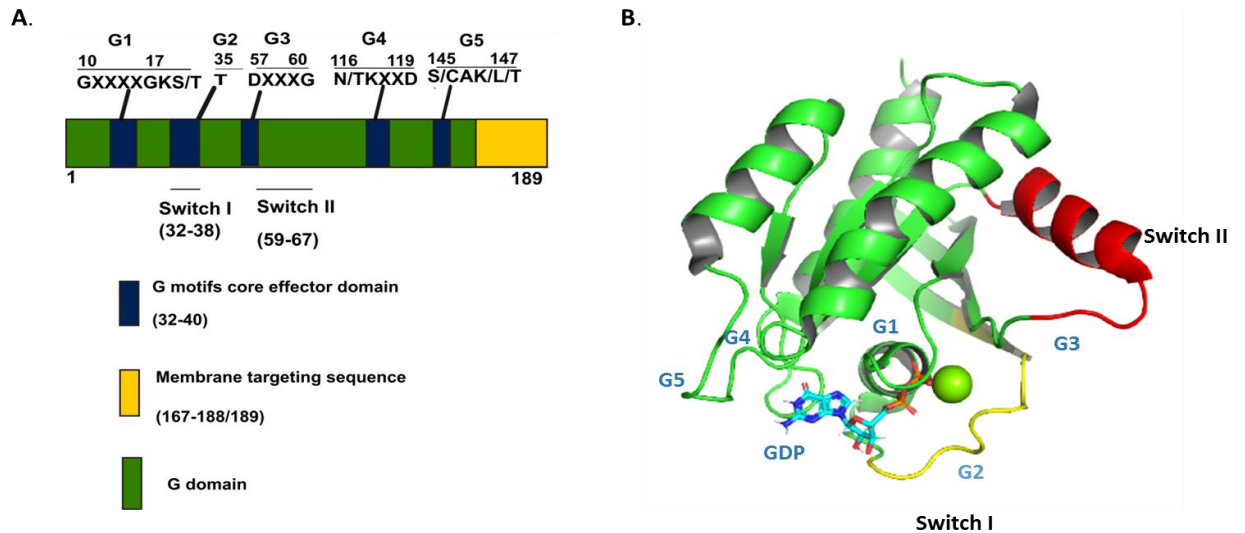


Figure 1.2 Schematic representation of functional domains in Ras structure. **A.** Blue coloured boxes indicate regions participating in GTP and effector binding as represented by G motifs core effector domains. Switch I and switch II regions and membrane targeting CAAX (yellow) motif for post-translational modifications are also shown. **B.** The regions indicated in A are highlighted on KRas structure (PDB: 4OBE). This KRas structure lacks the C terminal CAAX motif. GDP is coloured as per elements present, magnesium in yellow, the switch I and switch II regions are highlighted in yellow and red, respectively. Images were generated in PyMOL.

1.1.2.1 Ras protein subfamily (36 members)

Ras subfamily members show high conservation within G1, G3, G4, and G5 motifs. Ras subfamily contains 36 genes that encode 39 Ras proteins (20-29 kDa) in the human genome (Colicelli., 2004; Karnoub and Weinberg., 2008). The key members of the family include *HRAS*, *KRAS*, *NRAS*, Related Ras viral oncogene homolog (*RRAS*), Rap GTP binding protein (*RAP*), Ras-related protein (*RAL*), Ras homolog enriched in brain (*RHEB*) and Ras-like protein in tissues (*RIT*). The functional differences between these members are mostly quantitative in effector protein engagement and post-translational modifications. Ras proteins (*HRas*, *KRas*, and *NRas*) have been subjected to intense research scrutiny because of their crucial role in human cancers (Wennerberg et al., 2005). Ras proteins are membrane-bound intracellular GTPases activated in response to extracellular ligands that bind to cell surface receptors (Details in section 2.1) (Repasky et al., 2004). The most

characterised cell surface receptors involved in activation of Ras protein are epidermal growth factor receptor (EGFR), and G protein-coupled receptors (GPCR).

1.1.2.2 Rho protein subfamily (23 members)

The Ras homologous (Rho) subfamily of proteins is closely related to the Ras subfamily. The members of this subfamily show vital conservation among their G1-G5 motif. However, most members of this subfamily have insert sequences that are not found in any other Ras superfamily (Colicelli., 2004). Out of 23 members identified Rho A, Ras-related C3 botulinum toxin substrate 1 (Rac1), and cell division control 42 (CDC42) proteins are the most studied. The role of Rho A, Rac1, and Cdc42 in maintaining the assembly of filamentous actins has been verified in animal models such as yeast, flies, and worms. Rho GTPases, besides playing a crucial role in the actin cytoskeleton, are involved in the regulation of cell polarity, vesicular transport, cell cycle progression, microtubule dynamics, and membrane transport pathways (Etienne-Manneville and Hall., 2002).

1.1.2.3 Rab and Ran protein subfamily (71 members)

Ras-like proteins in the brain (Rab) subfamily comprises of the largest branch of the Ras superfamily with 61 members. The majority of Rab GTPases are products of gene duplications since many Rab GTPases have 75-95% sequence similarity with overlapping functions with variation in the carboxy-terminal end, which plays a vital role in subcellular targeting (Stenmark and Olkkonen., 2001). Rab GTPases are involved in the controlling all aspects of intracellular vesicular transport and trafficking of proteins between different organelles using endocytic and secretory pathways. They also facilitate vesicle formation, movement, and fusion. For example, Rab1 is located in the membrane compartment of the endoplasmic reticulum (ER) and Golgi apparatus. It is involved in biosynthesis/transport of proteins and lipids between ER and Golgi apparatus (Zerial and McBride., 2001).

Ras-like nuclear protein (Ran) is the most abundant small GTPase in the cell. Like other GTPases, which act as molecular switch activated Ran GTP is

present in high concentration in the nucleus due to the concentration gradient created due to specific location of Ran regulators within the cell. This concentration gradient created by Ran GTPases helps regulate the nuclear import and export of RNA and proteins. Besides regulating nucleocytoplasmic transport, Ran GTPases are also involved in the formation of nuclear envelope around chromatin after mitosis is finished (Quimby and Dasso., 2003).

1.1.2.4 Arf protein subfamily (30 members)

Similar in function to Rab proteins, the ADP ribosylation factor (Arf) subfamily of proteins is regulators of the trafficking of intracellular proteins. For example, Arf1 regulates the assembly of vesicle coat proteins like coat protein complex I (COP1) and clathrin-coated vesicles. These coat proteins help in the precise sorting of lipids and proteins between cisternae of the Golgi apparatus and the recruitment of proteins to membranes (Memon., 2004).

1.1.3 Ras synthesis, processing, and maturation

Ras proteins are synthesised in the cytosol by polysomes as globular hydrophilic proteins. Ras proteins are subjected to series of post-translational modifications (PTM) to enable them to associate with cell membranes, a key feature required for their biological activity (Willumsen et al., 1984; Ahearn, I. et al., 2018). This PTM takes place at the C terminal region of Ras and ends with a CAAX sequence where C is cysteine, and A is usually aliphatic, and X is any amino acid (Figure 1.3). The CAAX motif undergoes sequential modification by three enzymes. The unmodified CAAX motif serves as a substrate for prenylation by one of the two cytosolic prenyltransferases, farnesyltransferase (FTase) or geranylgeranyltransferase I (GGTase) (Ahearn, I.M. et al., 2011). These enzymes add a 15 or 20 carbon polyisoprene lipid to the sulfhydryl group of the cysteine. If the amino acid in the X position of CAAX sequence is a serine or methionine as in the case of all Ras proteins, then the protein is the primary substrate for FTase. If the X position is replaced by L, then they are modified by GGTase (Ahearn, I. et al., 2018). After farnesylation modified Ras proteins, accumulate on the cytoplasmic face of the endoplasmic reticulum. The modified

Ras proteins are then processed by an enzyme called Ras converting enzyme

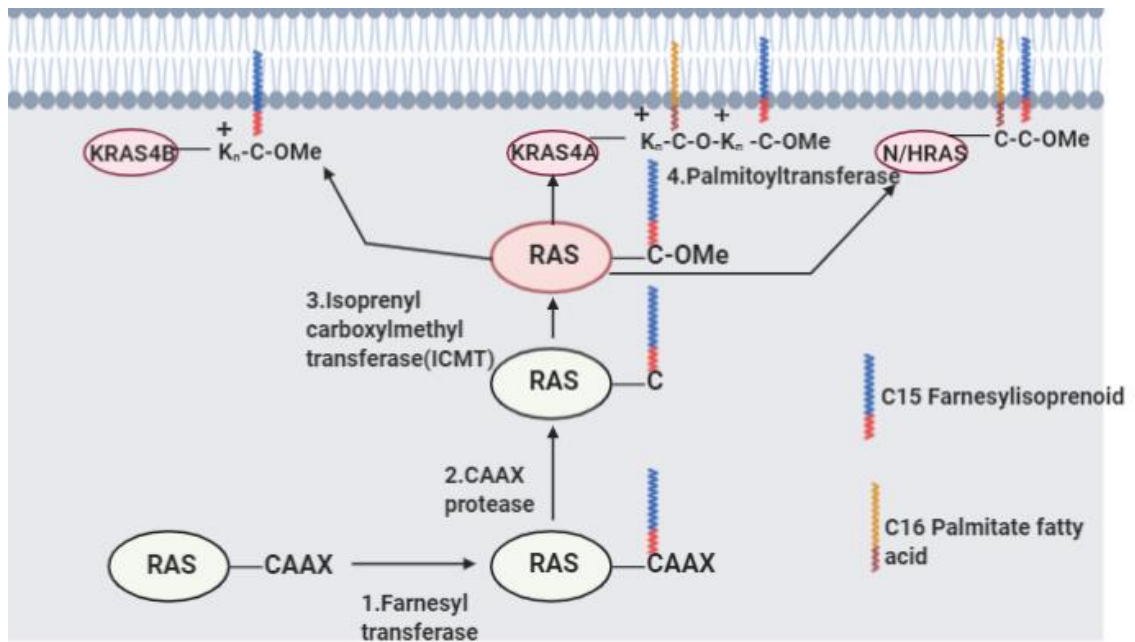


Figure 1.3 Ras plasma membrane targeting via post-translational modifications. Firstly, all Ras isoforms are farnesylated at cysteine residue of the CAAX motif with the help of farnesyl transferase, following which CAAX protease cleaves the terminal AAX peptide. The final step is the CAAX processing involves enzyme ICMT which methyl esterifies α carboxyl group (Dharmaiah et al., 2016). Finally, all Ras isoforms except KRas4B are palmitoylated at cysteine residue close to the carboxyl-terminal end. KRas4B isoform associates itself with the plasma membrane via electrostatic interactions due to a cluster of positively charged lysine residues (Hancock et al., 1990; Haza., 2019). Image was generated in Biorender.com.

(RCE-I), an endopeptidase that removes AAX amino acids converting prenylcysteine into new C terminus (Figure 1.3) (Ahearn, et al., 2011). C terminal prenylcysteines then become substrates for final CAAX processing enzyme isoprenyl cysteine methyltransferase (ICMT). It methyl esterifies the α carboxyl group, thereby neutralising the negative charge at C terminus. The end result of CAAX processing is to remodel the hydrophilic C terminus and render it into hydrophobic one so that it has an affinity for membranes (Ahearn, et al., 2011).

While these CAAX modifications are necessary to render a hydrophobic C terminal end, they would not lead to the stable binding of Ras to the plasma membrane since they require a membrane-targeting signal adjacent to the

CAAX motif (Bar-Sagi., 2001). In HRas, NRas, and KRas4A, the signals involve palmitoylation, once or twice, at cysteine residues upstream of the CAAX motif by Ras palmitoyltransferase. However, in the case of KRas4B, the polybasic lysine domain enables it to interact with anionic phospholipids to support membrane association electrostatically. This property allows KRas4B to forgo palmitoylation and bypass the Golgi to reach the plasma membrane (Mageean., 2014; Silvius et al., 2006). The prenyl binding protein phosphodiesterase- δ (PDE δ) has shown to be specific to KRas4B isoform and binds to prenylated hyper variable region, thereby preventing the binding to endomembranes, which in turn enhances the distribution throughout the cell membranes (Dharmaiah et al., 2016).

2.1 Ras signalling: Mechanism of GTPase activation and regulation

2.1.1 Ras regulated signalling pathways

Once Ras stably associates to the plasma membrane, it can activate more than 20 signalling pathways (Chavan et al., 2015). Mitogen-activated protein kinase/extracellular signal-regulated kinase (MAPK/ERK) pathway is one of the major signalling pathways that play a central role in cell proliferation, cell differentiation, and apoptosis (Figure 1.4). It is activated by growth factors, hormones, and cytokines binding to cell surface receptors, resulting in auto-phosphorylation of receptor tyrosine kinases (RTKs) (Schulze et al., 2005). Phosphorylated tyrosine kinases provide a platform for the recruitment of adaptor proteins such as growth factor receptor binding 2 (GRB2), which is best known to link EGFR tyrosine kinases to activation of Ras and downstream targets. GRB2 consists of Src-homology 2 (SH2) domains flanked by two Src homology 3 (SH3) domains (Zarich et al., 2006). The SH2 domain interacts with phosphotyrosine containing motifs on the receptors, and the SH3 domains interact with proline-rich regions of the guanine nucleotide exchange factor (GEF) son of sevenless (SOS). GEFs catalyse the release of GDP and GTP-loading, which is the rate-limiting step in Ras activation. GTP-bound Ras recruits Raf to the plasma membrane and enables it to phosphorylate its substrates Mek1 and Mek2 (Kern et al., 2011). These dual-specificity kinases subsequently activate extracellular signal-regulated kinases (ERK-1/2), enabling them to phosphorylate a wide variety of substrates that execute processes related to cell cycle progression, differentiation, protein translation and apoptosis (Cseh et al., 2014).

Ras also displays a high affinity with a wide range of effectors, which are involved in regulating a variety of cellular processes (Figure 1.4) (Ponting and Benjamin., 1996). Ras proteins primarily bind to effectors via residues 32-41, which are present in the switch I region. Ras effector proteins are characterised by the putative Ras binding domain (RBD) (Rajalingam et al., 2007). Ras interacts with RBD and forms Ras-RBD complexes through complementary charge interactions. Currently, there are more than ten different Ras effectors

(Rajalingam et al., 2007). Apart from Raf, PI3K, RalGDS, and p120GAP, the growing family of Ras effector proteins includes Rin1, Team, Af6, Nore1, PLC ϵ , and PKC ζ .

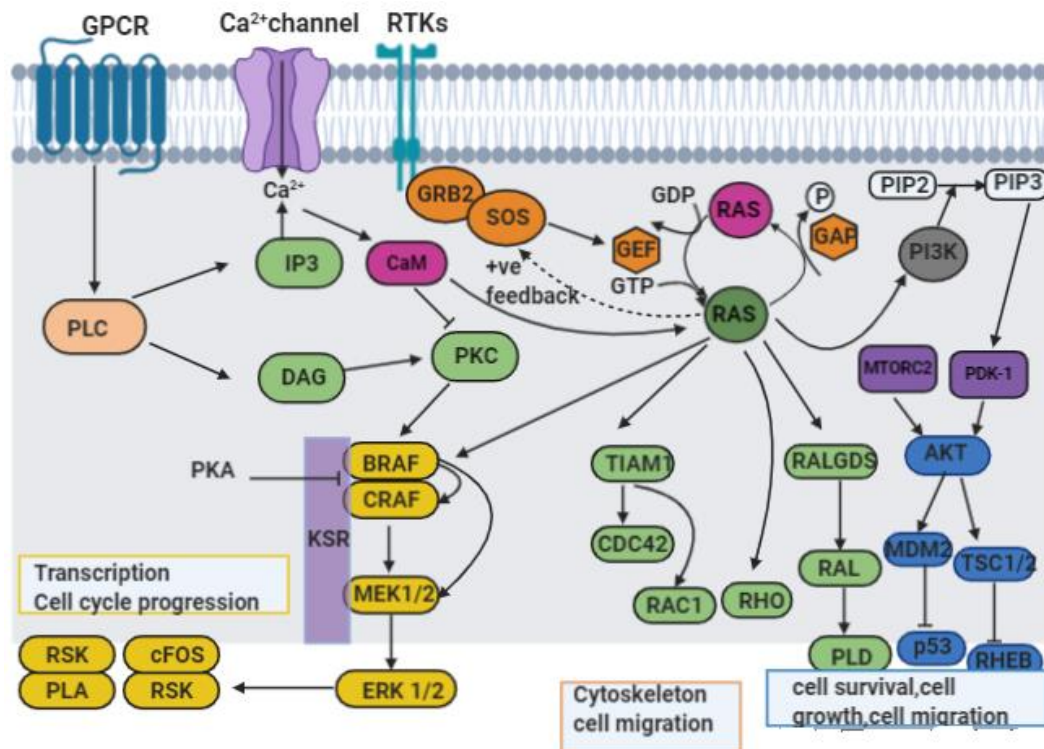


Figure 1.4 Ras regulated signaling pathways. Cartoon depicting an overview of significant Ras regulated signalling pathways. Active Ras (membrane and GTP bound) stimulates a network of downstream signalling pathways with MAPK and PI3K signalling pathways being the two best-characterised pathways. The first Ras effector pathway to be characterized is the Ras-Raf-MAPK pathway (green). Ras becomes activated when ligands (growth factors, hormones, etc.) bind to RTKs with the help of adaptor proteins (GRB2) and GEFs (SOS1) (Dhillon et al., 2007). Activated Ras binds to the Raf family of serine/threonine kinases (ARaf, BRaf, CRaf), by recruiting to the plasma membrane. Active Raf then phosphorylates MEK1/2, which in turn, activates ERK1/2 (Roberts and Der, 2007; Wortzel and Seger, 2011). Activated ERK phosphorylates several cytoplasmic (RSK) and nuclear (Fos, Jun) substrates including regulatory and transcription factors (ELK1) which in turn activate a variety of cellular processes such as cell growth, differentiation and apoptosis (Wortzel and Seger, 2011). Scaffold proteins such as kinase suppressor of Ras (KSR) play an essential role in the spatiotemporal regulation of the MAPK pathway by recruiting the kinases MEK and ERK to Raf (Nguyen et al., 2002). Ras effector family is PI3K signalling pathway (blue), which have essential cellular functions such as cell survival, cell growth and migration. Active PI3K catalyze the conversion of phosphatidylinositol 4.5 bisphosphate (PIP2) into phosphatidylinositol 3,4.5 trisphosphate (PIP3). PIP3 binds to Akt protein

(Figure 1.4 legend continued) stimulating its kinase activity, resulting in phosphorylation of proteins involved in cell cycle entry and cell survival (Hemmings and Restuccia., 2012). Other Ras effector pathways include RalGDS, Rho and TIAM1 play an essential role in cytoskeleton reorganisation and cell migration. Image was generated in Biorender.com.

2.1.2 Mechanism of Ras GTPase activation

Ras becomes activated when GDP-GTP exchange occurs, causing a conformational change in Ras that is critical to its function as a molecular switch in signalling pathways (Milburn et al., 1990). The comparison of the GDP- and GTP-bound structures of Ras has identified two nucleotide sensitive regions referred to Ras switch I (residues 30-40) and switch II (residues 60-76) regions (Figure 1.5). In case of GTP bound Ras, the active site Mg^{2+} coordinates with β and γ phosphates of GTP and side chains of switch I residues T35 and S17 (Hall et al., 2002). The residues in the switch I particularly T35 and G60 in switch II are involved in stabilization of Mg^{2+} bound GTP and form hydrogen bonds with γ phosphate in the active state (Figure 1.5) (Rudack et al., 2012b). Upon GTP hydrolysis, γ phosphate is released and the residues within switch I and switch II return to their flexible conformation in GDP-bound state.

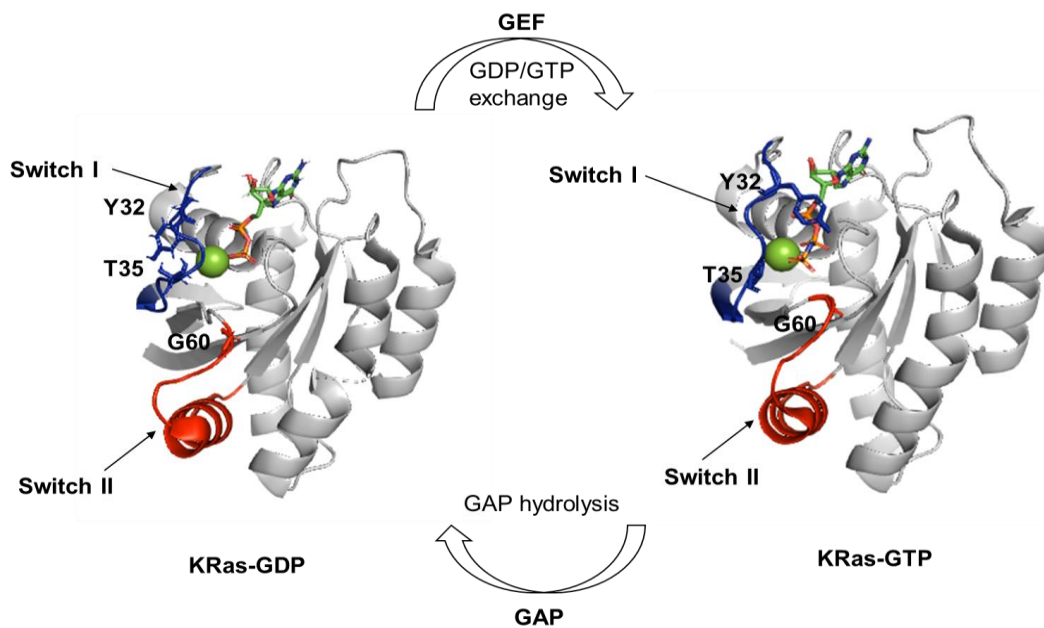


Figure 1.5 Ras GTPase activation. Switch I and switch II regions are coloured red and blue respectively, the side chain residues that undergo large conformational changes as shown in stick representation. Ras GDP (PDB: 4OBE) is activated when GEFs like SOS1, Ras GRP is involved in GDP release. When GTP binds to Ras (PDB: 6GOD), residues Y32, T35 of switch I (blue) forms hydrogen bonds with γ phosphate of GTP and G60 of switch II (red) resulting in activation of a molecular switch. Ras-GTP is inactivated by GTP hydrolysis stimulated by GAP proteins (NF1, p120GAP) and return into an inactive state as represented by open conformation of KRas-GDP. Images were generated via PyMOL.

2.1.3 Guanine nucleotide exchange factors and GTPase activating proteins

Even though Ras proteins possess intrinsic GTPase activity, the function of Ras to act as a molecular switch is highly regulated by the coordinated action of GEFs and GAPs (Rajalingam et al., 2007). Due to tenfold higher cellular concentration of GTP over GDP, GEFs promote the formation of GTP-Ras complex (Hall et al., 2002). Ras GEFs like SOS1 and 2 have a CDC25 homology domain which is specific to Ras followed by Ras exchange motif (REM). They are flanked at N terminal with histone binding domain and DH-PH motif at C terminal with a proline-rich region (Figure 1.6 A) (Boriack-Sjodin et

al., 1998) (Bos et al., 2007). These flanking domains are involved in the activation of GEF by upstream signals. The catalytic domains of GEFs are structurally unrelated, yet they all utilise similar principle to modify the nucleotide-binding pocket, to facilitate the release of GDP. For example, CDC25 domain of SOS covers a large area in the switch II region of Ras. It uses α helical hairpin to perturb the interactions between the phosphate groups of the nucleotide and the magnesium ion in the nucleotide-binding pocket, this allows the GDP to be released and GTP to bind to the pocket (Figure 1.6 B) (Boriack-Sjodin et al., 1998).

Since the intrinsic GTP hydrolysis reaction of Ras is prolonged, Ras GAPs can accelerate the intrinsic GTPase activity of Ras by several orders of magnitude. For example, p120GAP inserts a catalytic arginine residue (called the arginine finger) into Ras nucleotide-binding pocket. It alters the position of Q61, thereby stabilising its position and neutralising negative charge at γ phosphate (Figure 1.6 C). Following which Q61 positions the water molecule for a nucleophilic attack where GTP is cleaved into GDP and Pi. This mechanism of catalysis of GAP induced GTP hydrolysis is being supported by biophysical studies (Bos et al., 2007; Resat et al., 2001; Maertens and Cichowski, 2014; Rudack et al., 2012a). Due to low intrinsic guanine nucleotide exchange and GTP hydrolysis activities, Ras signalling is ordinarily transient. Therefore prolonged Ras signalling due to Ras mutations, inactivation of GAPs or aberrant GEF regulation is the reason for Ras-induced cancers (Vigil et al., 2010).

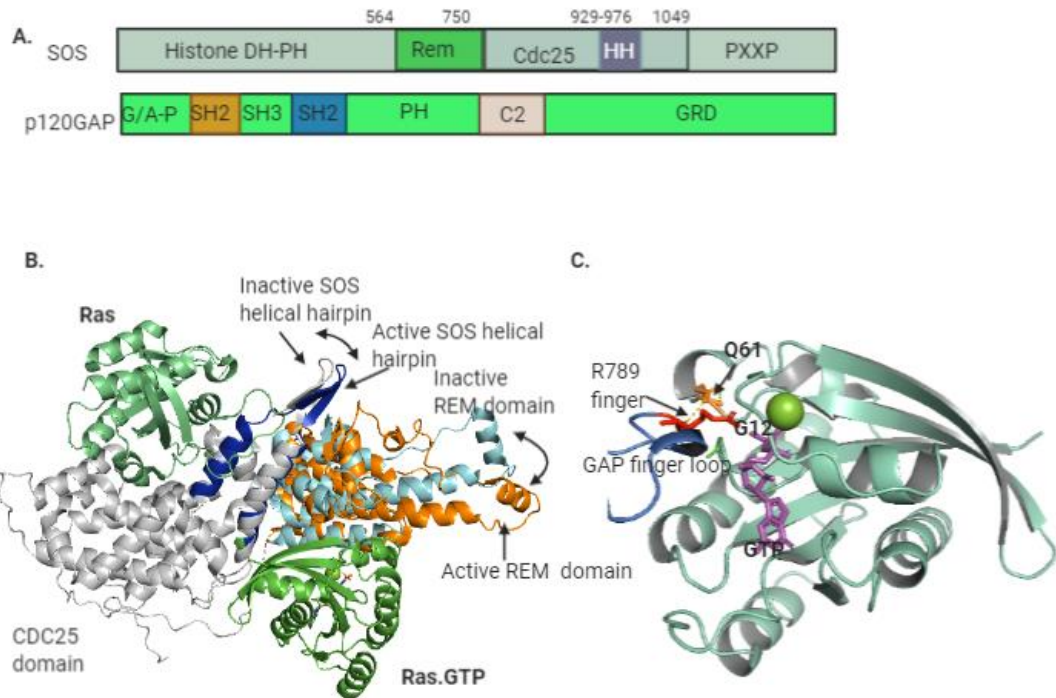


Figure 1.6 Functional domains and structural analysis of SOS1 and p120GAP. **A.** Domain structures of SOS1 and p120GAP. SOS1 contains Rem domain (green) and Cdc25 homolog domains (grey) that includes helical hairpin motif (HH; blue). Created with Biorender.com **B.** Binding of Ras (green) to the allosteric site of SOS results in the activation of SOS through the coordinated rotation of the helical hairpin (blue) and the Rem domain (cyan). The figure shows the structures of uncomplexed SOS (PDB: 2IIO) and Ras-bound SOS (PDB: 2IJE) - adapted from Kuriyan et al., 2006. **C.** This figure illustrates native Ras (cyan) in complex with GAP poised for catalytic reaction (PDB: 1WQ1). The arginine finger (R789) is highlighted in red. Q61 (green) of Ras forms a hydrogen bond to R789. G12 residue located just below the arginine finger, when it becomes mutated, it prevents hydrolysis through a steric clash mechanism. The image was generated in PyMOL and Biorender.com.

2.1.4 Isoform-specific Ras signalling

The four Ras isoforms have a high degree of sequence homology in the G domain (~80%), with most of the variation being observed in hypervariable regions in C terminal end. Despite having a usual cohort of regulators and effectors, Ras isoforms have different mutation frequencies and display a bias towards certain cancers. This suggests isoform-specific function (Hood et al., 2019). One of the primary reasons for the isoform-specific function is thought to lie in different trafficking and subcellular localisation of Ras isoforms. The hypervariable regions in Ras are post-translationally modified to facilitate membrane binding and correct trafficking (Aran and Prior., 2013). Each isoform has a distinct set of modifications and targeting motifs that result in overlapping but distinctive localisations (Aran and Prior., 2013). Another reason for isoform-specific signalling is due to the specific orientation of G domain (residues 1-166) of Ras upon binding to GTP with respect to membranes (Newlaczyk et al., 2014). The differences in presentation of effector binding region due to this reorientation vary between different isoforms, and Ras effectors such as Raf and PI3K are sensitive to this change. Raf binding is favoured by conformation adopted by KRas, while PI3K favours the conformation adopted by HRas (Newlaczyk et al., 2014). Additional factors such as relative expression differences of the different Ras isoforms will influence competition for effector and regulator binding, which will result in variations in signalling responses (Johnson et al., 2017). For example, the *KRAS* gene is poorly expressed as compared to *HRAS* due to a higher presence of rare codons. Rare codons can stall protein translation and conversion of rare codons to common codons can result in increased KRas expression. But since high Ras expression can lead to cellular senescence, it was proposed that rare codons in KRas due to codon bias limit the expression of KRas to a range sufficient to initiate tumorigenesis (Mo et al., 2018; Lampson et al., 2013)

3.1 Role of Ras in cancer

Cancer is characterised by the uncontrolled division of abnormal cells due to loss of cellular regulation in the body. In most cases, cancers arise due to genetic damage caused by exposure to carcinogens such as tobacco smoke, UV radiation and certain chemicals (Carney., 1990; Chia et al., 1991). Mutations in two broad segments of genes: proto-oncogenes and tumour suppressor genes have been implicated in the early onset of cancer. Proto-oncogenes are normal genes involved in cell replication, growth and survival, which when altered due to mutations become oncogenes and resulting in hyperactive proteins involved in growth promotion. (Hanahan and Weinberg., 2000; Hanahan and Weinberg., 2011). Tumour suppressor genes monitor DNA damage and help in repairing damage to DNA before the cell divides. They prevent the expression of genes required for progression to S phase of the cell cycle. Mutations in these genes can result in uncontrolled cell growth.

Ras proteins are encoded by proto-oncogenes that are frequently mutated in human cancers, with an average mutation incidence of 25% in all human cancers (Hobbs et al., 2016; Hobbs and Der., 2019). Mutant Ras proteins promote growth factor independent cell cycle entry. Ras proteins are involved in the regulation of various phases in the cell cycle, especially the G1 phase. Cyclin D1, cyclin-dependent kinase 4 (CDK4), p16 and tumour suppressor Rb are G1 phase regulatory proteins that have shown high expression due to HRas mutation. Cells harbouring oncogenic Ras and Rb can proliferate in the absence of mitogen and loss of cyclin-dependent kinase inhibitors like p16 and p21 makes them anchorage-independent and avoid contact inhibition creating a favourable environment for Ras-mediated tumorigenesis (Sathyan et al., 2007; Macaluso et al., 2002).

3.1.1 Incidence and spectrum of Ras mutations in cancer

Mutational damage in tumour cells results in aberrant Ras signalling. The most obvious of these are activating point mutations in Ras, GAP deletion, growth factor receptor activation and mutation and amplification of Ras effectors (Hobbs et al., 2016). The highest incidence of aberrant Ras signalling is due to single base missense mutations mostly occurring at codon 12, 13 and 61 (Figure 1.7 A). These mutations all impair GAP-induced GTP hydrolysis activity of Ras and therefore causing Ras to be in a permanent active GTP bound state (Prior et al., 2012).

Out of 3 Ras proto-oncogenes, the KRas isoform is most mutated in human cancers. As per Catalog of Somatic Mutations in Cancer analysed, KRas is mutated in 75% of all human tumours analysed compared to 17% with NRas mutations and 7% with HRas (Prior et al., 2020). Mutations in KRas are found in 90% of pancreas, 35% of lung and 45% of colorectal cancers. But in the case of skin cancer NRas is mutated in 18% of all tumours analysed compared to 6% with HRas and 3% with KRas (Tate et al., 2019). These patterns suggest that certain Ras mutations are more prevalent in particular cancer types. In support of this concept, experiments using genetically engineered mice showed that oncogenic KRas^{G12D} promoted stem cell expansion and helped initiate tumours in the colon, but NRas^{G12D} did not promote proliferation and confer resistance to apoptosis. This indicates phenotypic differences between Ras isoform mutants (Haigis et al., 2008). Similar to the isoform bias observed in certain specific cancers, there is a preference of each isoform for certain codon mutations. For example, 80% of KRas mutations occur at codon 12, and 60% of NRas mutations occur at codon 61. HRas mutations are split between 50% and 40% for codon 12 and 61, respectively (Figure 1.7 B) (Prior et al., 2012). In addition to isoform and codon specificity, Ras mutations have shown tissue-specific preferences. For example, in pancreatic ductal adenocarcinoma (PDAC) and colorectal carcinomas KRas^{G12D} (51%) is the dominant mutation. Conversely, KRas^{G12C} is the most common mutation in non-small cell lung cancer (NSCLC) (44%) (Figure 1.7 C) (Serebriiskii et al., 2019). Collectively,

these studies suggest that there is a correlation between Ras isoform mutants with specific cancer types.

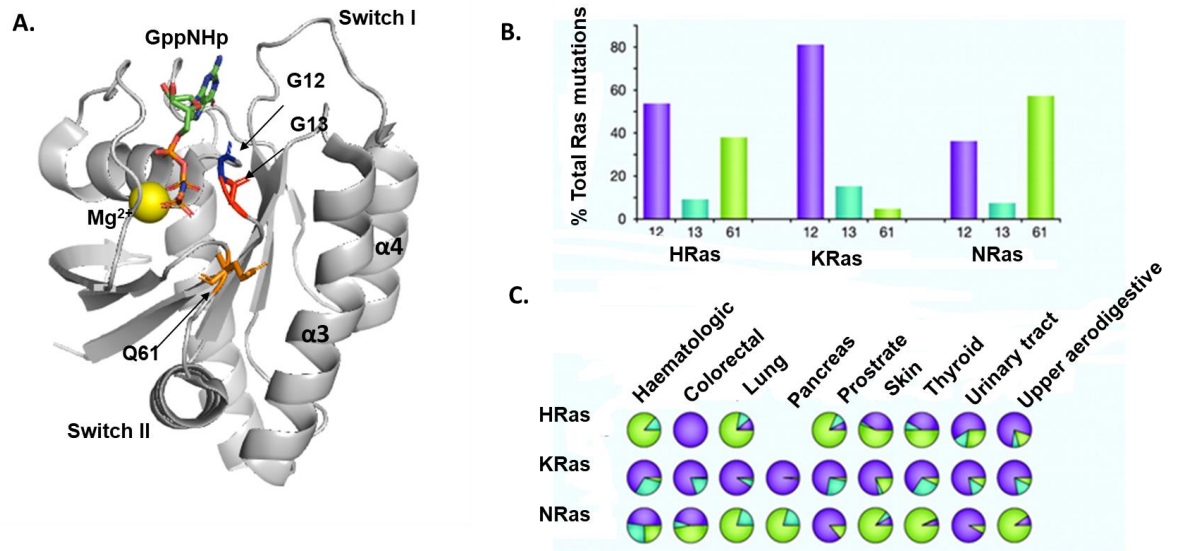


Figure 1.7 Incidence and spectrum of Ras mutations in cancer **A.** Positions of oncogenic mutations at G12, G13 and Q61 on Ras-GTP (PDB: 6GOD). Residue G12 (red), G13 (blue) and Q61 (orange) are drawn explicitly with residues labels in boldface type. Ras-GTP Structure generated in PyMOL. **B.** Ras isoform-specific codon mutation bias showing KRas is typically mutated at codon 12, whereas NRas favours codon 61 and HRas displays intermediate behaviour. **C.** Analysis of individual cancer types reveals isoform-specific patterns of codon mutations even within the same tissue. Pie chart colours: blue, Codon 12; cyan, codon 13 and green, codon 61. Adapted from (Prior et al., 2012).

3.1.2 Biochemical and structural properties of Ras mutants.

The above examples have established the fact that Ras biology is far more complicated and context dependent on type of isoform, codon mutations and protein expression. KRas mutations are more prevalent in particular cancer types, most likely due to a combination of factors ranging from protein expression levels, genetic topology and cellular context. Additionally, based on varied responses of patients with specific KRas mutations, it has been found that different KRas mutations have unique biochemical behaviours based on biochemical and structural data (Hunter et al., 2015).

3.1.2.1 Biochemical analysis of Ras mutants

In terms of biochemical analysis of KRas mutants, it has been found that the nucleotide exchange rates between KRas mutants and wild type have largely been identical. However, in the case of G13D mutant, it was observed that the GTP exchange rate was nine times faster than WT (0.018/s vs 0.002/s) and GDP exchange rate fourteen times faster than wild type (WT) (0.027/s vs 0.002/s), insinuating that the G13D mutant may be able auto-activate more frequently by spontaneously exchanging GDP for GTP (Hunter et al., 2015). This fast exchange kinetics observed for the G13D mutant could explain the more aggressive biology of G13D-associated tumours seen in some studies (Hunter et al., 2015).

3.1.2.2 Structural insights into Ras mutants

Crystal structures of four KRas mutants which include G12V, G12R, G13D, and Q61L have been solved to understand the effect of common KRas mutations on the protein structure (Hunter et al., 2015). Mutations have been found to have a minimal effect on the overall structure of the protein with global Root Mean Square Deviation (RMSD) of 0.115, 0.351, 0.146, and 0.677 Å for G12V, G12R, G13D, and Q61L, respectively when compared with the WT KRas (Hunter et al., 2015).

When Ras is bound to GTP, it exists in two different conformational states (state 1 and state 2) in solution interconverting on a millisecond time scale. These conformational states have been verified using NMR spectroscopy. State 1 has a low affinity towards effectors and more towards GEF whereas state 2 closely resembles conformation when bound to effector binding domain of Ras effectors and has higher GTPase activity (Shima et al., 2010). In case of wild type HRas bound to non-hydrolysable GTP (GppNHp), state 1 exists in $36\pm 2\%$ of the population. However, when mutated to HRasG12V-GppNHp and HRasQ61L-GppNHp, there is a shift in equilibrium between the two states, as state 1 occupies 53% and 58% of the population respectively (Mageean., 2014; Spoerner et al., 2001). Additionally, mutation of residue 12 or 13 to valine or aspartic acid results in displacement of catalytic water molecule, leading to GAP insensitivity (Hobbs et al., 2016). Thus, the above-mentioned structural differences may account for biochemical differences between mutant Ras proteins.

4.1 Ras as a therapeutic target

4.1.1 Why has Ras been considered 'undruggable'?

In the past decade, significant advances have been made in sequencing many cancer driver genes. Large scale genomic sequencing and development of databases such as Cancer Genome Atlas, has helped in understanding the molecular basis of cancer (Dang et al., 2017). Many kinases that drive tumour growth and development have largely been 'druggable' and have yielded significant clinical benefits. However, many known oncogenes such as Ras, Myc, p53 and phosphatases PP2A have been termed as 'undruggable' due to lack of deep binding pockets for small molecules to bind with high affinity and specificity. Due to structural and functional challenges in targeting these 'undruggable' oncoproteins development of new drug discovery technologies have now become one of the critical challenges in cancer research (Stephen et al., 2014; Dang et al., 2017).

Ras has become one of the intensively studied oncogenic targets in drug discovery (Hunter et al., 2015; Ostrem and Shokat., 2016; Haza., 2019). Direct targeting of mutant Ras has been challenging due to various reasons which include a lack of deep hydrophobic pockets to which small molecule can bind to, high intracellular concentration and picomolar affinity of GTP towards the nucleotide-binding pocket, and toxicity related issues arising due to possible inhibition of the wild-type Ras (Ostrem and Shokat., 2016). Despite intensive efforts by researchers to develop effective pharmacological inhibitors of the Ras oncoproteins, no inhibitors of Ras have reached the market, prompting the previously held perception that Ras proteins are “undruggable” (Cox et al., 2014). A resurgence of interest in the targeting of Ras emerged from the National Cancer Institute (NCI) USA, leading to Ras initiative led by Frank McCormick in 2013. Its main mission is to fill critical knowledge gaps essential to target Ras cancer effectively and to and provide as a central resource for data on Ras biology, reagents and therapeutics (Cox et al., 2014).

4.1.2 Early approaches to target Ras

4.1.2.1 GDP-GTP exchange inhibitors

One of the first compounds reported SCH 54292 ($IC_{50}=0.7 \mu M$) was found by NMR spectroscopy and molecular modelling, to bind to a hydrophobic pocket near the critical switch II region of the Ras protein without displacing GDP (Peri et al., 2005). New compounds were optimised in which the sugar of SCH-54292 (Figure 1.8) was replaced with a bicyclic moiety based on molecular modelling. Two of these compounds (SCH 53239 and SCH 53870) have been shown to inhibit Ras-dependent cell growth (Taveras et al., 1997). However, all compounds from this series contain hydroxylamine which is critical for their activity but not an ideal functional group in drug molecule due to toxicity, poor metabolic stability and lack of potency (Taveras et al., 1997).

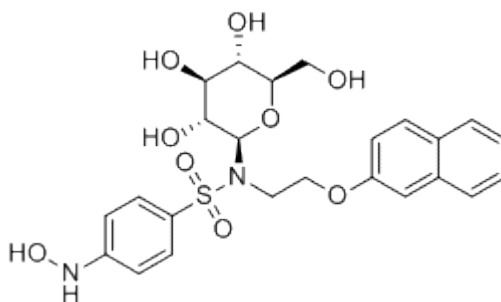


Figure 1.8 Chemical structure of low affinity inhibitor compound SCH 54292. (Ref - SCH 54292 |CAS:188480-51-5 Probechem Biochemicals, 2020).

4.1.2.2 Peptide-based Ras/SOS and Ras/Raf inhibitors

Ras GTP/GDP cycle is regulated by both GAPs and GEFs that facilitate dissociation of GDP and binding of the more abundant GTP (Shima et al., 2010). The most prominent RasGEF is SOS1, which has multiple binding sites for Ras (Winter et al., 2015). A new peptide was designed based on α H helix of SOS (HBS3 peptide), a region that forms contact with Ras in a cleft near switch I and switch II regions (Patgiri et al., 2011). This peptide binds to Ras with a K_d of 158 μ M, and inhibits Ras activation, by interfering in Ras/SOS interaction and significantly reduces EGF induced ERK activation *in vivo*. Although the peptide was not very potent, further optimization of the helical peptide could lead to drug-like molecules (Patgiri et al., 2011).

In 2012, a group from Genentech[®] identified a compound called DCAI (Figure 1.9) via fragment-based screening on KRas4B which binds to the pocket between α 2 helix and core β sheet (β 1- β 3) of KRas (Maurer et al., 2012). SOS mediated nucleotide exchange and release was inhibited by DCAI with an IC_{50} = 340 μ M and 155 μ M respectively. DCAI also has been found to attenuate the EGF stimulated activation of Ras in HEK293 cell lines. In addition to the weak binding (1.1 \pm 0.5 mM), development of small molecule analogues of DCAI with considerable improvements in affinity has been a challenging task (Maurer et al., 2012).

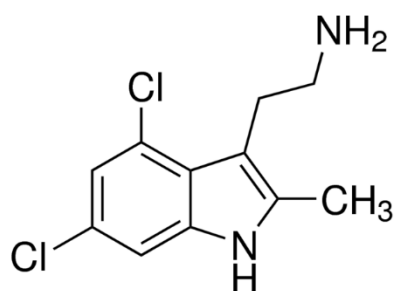


Figure 1.9 Ras/SOS inhibitor DCAI compound (Chemical name 2-(4,6-Dichloro-2-methyl-1H—indol-3-yl) ethanamine. [Ref- (Maurer et al., 2012)].

In another study, using computer docking, several small molecules were selected from a virtual library of compounds for their ability to inhibit Ras-GTP binding to Ras binding domain (RBD) of CRaf (Shima et al., 2013). Two compounds namely compound Kobe0065 and Kobe2602 (Figure 1.10), were identified that inhibited Ras/Raf1 interaction with an inhibitory constant (K_i) of 46 μM and 149 μM (Shima et al., 2013). These compounds reduced the amount of Raf1 binding to mutant HRas^{G12V}, effectively indicating a reduction of cellular activity by Ras (Cox et al., 2014). Using NMR spectroscopy, these compounds were found to bind on the side of the $\alpha 2$ helix of Ras (Switch II region) at a similar but not identical pocket as the Genentech[®] compound- DCAI (Cox et al., 2014). Although the compounds are not very potent, they can serve as a starting point for lead optimisation. However, suitable replacement of toxic semicarbazide ($\text{H}_2\text{NNHC(=O)NH}_2$) is yet to be found (Shima et al., 2013).

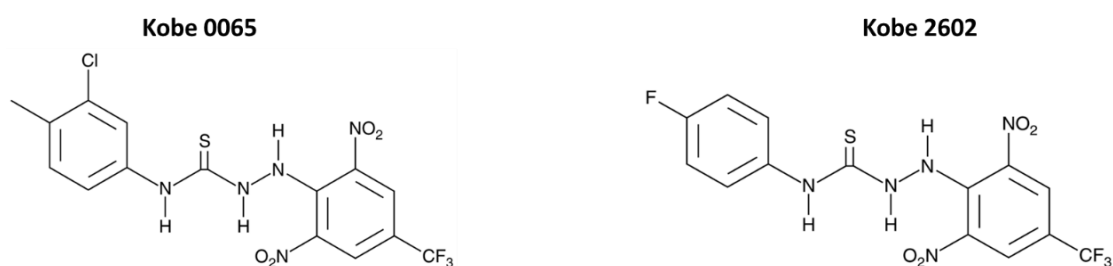


Figure 1.10 Chemical structures of Ras-Raf interaction inhibitors. Kobe 0065 and Kobe 2602. Adapted from Shima et al., 2013.

4.1.2.3 FTase inhibitors

Given the necessity of Ras association with plasma membrane for its oncogenic activity, initial attempts were carried out to develop pharmacological inhibitors of Ras by focussing on inhibiting the enzyme farnesyltransferase (FTase) (details of PTMs of Ras CAAX motif explained in section 1.3). Initial preclinical studies with FTase inhibitors (FTIs) demonstrated blocking tumour growth both *in vitro* and *in vivo* (End et al., 2001). Nevertheless, clinical trials failed owing to lack of efficacy of FTIs due to surprising biochemistry underlying the PTM of the CAAX motif. Since HRas is dependent on COOH terminal lipidation mediated by FTase, FTI treatment of KRas or NRas resulted in alternative lipidation of these proteins by geranylgeranyltransferases (GGTases) (O'Bryan., 2019). As a result, FTIs have proven ineffective in solid tumours, which predominantly harbour KRas mutations. Although FTIs have been combined with GGTase inhibitors, this approach suffers from dose-limiting toxicities that are likely due to over 100 proteins serving as targets for prenylation by these enzymes (O'Bryan., 2019).

5.1 Renewed efforts to target Ras directly

5.1.1 Inhibition of K-Ras^{G12C}

Approaches to develop inhibitors targeting Ras effector binding regions and membrane localization partly failed due to lack of understanding of the complex nature of Ras biochemistry and signalling (Figure 1.9). Therefore targeting specific mutations of Ras could provide an approach in inhibiting oncogenic Ras function and prevent binding to the wild-type protein (Ryan and Corcoran., 2018). While KRas mutations are present in up to 25% of cancers, the oncogenic variants of KRas have different prevalence rates in different cancers. One single type of KRas mutation called KRas^{G12C} account for 44% of all KRas mutations (Ryan and Corcoran., 2018). KRas^{G12C} is particularly prevalent in NSCLC, which makes up to 14% of lung cancer patients in the U.S (Mullard., 2019).

Ostrem, Shokat, and colleagues described a unique approach in targeting oncogenic mutant KRas^{G12C} specifically, without having any effect on wild type KRas (Ostrem et al., 2013). Using a strategy adopted by Earlanon (Earlanon and Hansen., 2004) to identify small molecule drug fragments via reversible site-directed ligand discovery (referred to as “tethering”), small molecules specific to mutant KRas^{G12C} have been identified. The initial screen was carried out using a library of disulphide containing small molecules that react with a native cysteine residue (KRas^{G12C} in this case) under reducing conditions (McCormick., 2019). Those fragments which weakly bind to KRas^{G12C} and have disulphide bond intact during native MS are identified. These fragments were further analysed via X-ray crystallography and optimised to develop lead compounds. (McCormick., 2019). KRas^{G12C} compound 6 identified a druggable pocket between central β sheet, α -2 and α -3 helix of KRas, referred to as SII-P.

Compounds binding to this new allosteric SII-P inhibit Ras activation by binding to the GDP-bound form (inactive) of KRas and not the GTP (active) bound state. Since the intrinsic nucleotide exchange rate of KRas^{G12C} is quite high (the half-life is 30 min) KRas^{G12C} mutant cycles more frequently between GDP- and GTP-bound states which allow the compounds to irreversibly bind to the GDP-bound form and trap KRas^{G12C} in an inactive conformation (Patricelli et al., 2016). Further attempts to identify potent inhibitors of KRas^{G12C} led to the development of ARS 853 and ARS 1620, which potently inhibits G12C in its GDP-bound form and inhibits the growth of NSCLC tumour models (Janes et al., 2018). ARS 1620 has shown mutation-specific selectivity and activity by inhibiting the growth of patient-derived mouse xenografts harbouring the KRas^{G12C} mutation and is also a useful pharmacological tool to understand KRas biology *in-vivo* (Janes et al., 2018).

5.1.2 Pan-Ras inhibitors

While KRas^{G12C} inhibitors have shown promise in preclinical and early-stage clinical trials, these agents would be effective in small populations of patients with specific KRas mutations. Direct targeting of Ras with pan-Ras inhibitors would enable targeting of Ras with multiple mutations. Using fragment-based drug discovery to design compounds that can bind to switch regions of KRas^{G12D}, pan-Ras inhibitor compound 3144 (Figure 1.11) was synthesised (Welsch et al., 2017). Compound 3144 was tested on KRas^{G12D} using biophysical assays such as microscale thermophoresis and protein NMR spectroscopy and binds to KRas^{G12D} with micromolar affinity. Additionally, compound 3144 was found to be cytostatic at some concentrations in MEF containing KRas (IC₅₀= 3.8 µM). Furthermore, it displayed similar levels of lethality in a panel of 11 cancer cell lines with different Ras mutations. However, low efficacy was observed in mutant Ras tumour cell lines with concurrent downstream Raf and PI3K mutations (Welsch et al., 2017). Despite promising results of the Ras inhibitors discussed in sections 4 and 5, none of them has been approved as anticancer therapeutics.

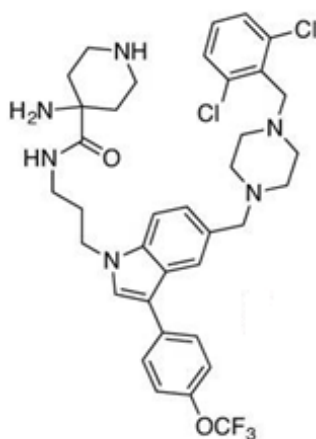


Figure 1.11 Pan Ras inhibitor. Compound 3144. Chemical Formula C₃₆H₄₁Cl₂F₃N₆O₂. Adapted from (Welsch et al., 2017).

6.1 Novel approaches to target Ras using non-antibody binding proteins

6.1.1 Artificial binding proteins

Considering the high incidence and poor prognosis of Ras driven cancers, novel approaches for successful Ras inhibitors were required. Researchers started exploring the possibility of using anti-Ras antibodies as potential cancer therapeutics. Clark and colleagues reported that antibodies that recognize mutant forms of Ras usually at codon 12 or less frequently at codon 61 directly reverse transformed the cancer cells driven by cognate mutant Ras proteins (Clark et al., 1985). However, the antibodies raised against peptide sequences corresponding to codon 12 substitutions were unable to bind since the P loop containing codon 12 is not present on the surface of native nucleotide bound form of Ras protein (Clark et al., 1985). Nevertheless, this early study showed the validity of using anti-Ras antibodies for the treatment of Ras-driven cancers, but their clinical application was hindered due to technical challenges. These include how to deliver the antibodies into cancer cells effectively, and how to maintain the structural integrity of antibodies whose multiple disulphide bonds would be cleaved in the reducing environment of cytosol (Dimitrov., 2012).

To overcome the limitation of antibodies as mentioned above, engineered protein scaffolds were developed which combine the universal antigen recognition function of an antibody with a compact and structurally rigid protein core termed as 'scaffold' (Yu et al., 2017). Candidates for suitable protein scaffolds besides having a compact and structurally rigid core should be able to present surface loops of varying sequence and length. They should also have the ability to tolerate side chain replacement in the contiguous surface region, without significant change in folding properties (Simeon and Chen., 2018). By designing a random library with mutagenesis focused at the loop region or permissible surface area, variants of the engineered scaffold proteins can be selected against a given target by phage display technology (Simeon and Chen., 2018). These antibody alternatives have practical benefits such as robustness, small size and ease of protein expression and can serve as reliable alternatives to conventional antibodies. Such engineered proteins are becoming increasingly prevalent in biotechnology and biomedical applications

(Simeon and Chen., 2018). Over 50 different engineered proteins have been developed in the last two decades, with some reaching clinical trials and a few approved by FDA for clinical use (Table 1.1) (Vazquez-Lombardi et al., 2015).

Table 1.1 Scaffold binding proteins currently approved or in clinical trials. Adapted from (Vazquez-Lombardi et al., 2015).

Scaffold	Name	Affinity	Molecular target	Disease targeted	Company	Clinical trials
Kunitz domain	DX-88 (Ecallantide)	44 pmol/L	Plasma Kallikrein	Hereditary angioedema	Dyax	FDA approval in 2012
	DX 890 (Depelstat)	1 pmol/L	Neutrophil elastase	Pulmonary fibrosis	Dyax	Phase II (NCT00455767)
Knottin	Ziconitide (Prialt)	1 pmol/L	N-type calcium channels	Neuropathic pain	Jazz pharmaceuticals	FDA approved in 2004
	Linaclotide (Linzex)	1nmol/L	Guanylate cyclase-C receptor	Irritable bowel disease	Ironwood pharmaceuticals	FDA approved in 2012
Fynomer	COVA322	0.9 pmol/L	Chymase	Plaque psoriasis	Covagen	Phase I/II (NCT02243787)
DARPin	MP0112	2pmol/L	VEGF-A	AMD,DME	Molecular partners,Allergen	Phase I/II (Campochiaro et.al 2013)
	Abicipar	2pmol/L	VEGF-A	AMD	Molecular partners,Allergen	Phase III (NCT02462486)
	MP0250	<1nmol/L	VEGF,HGF	Tumour suppressor	Molecular partners, Allergen	Phase I (Rodon et.a l 2015)
	MP0274		HER2	Tumour suppressor	Molecular partners, Allergen	Phase I (Reichert et al. 2014)
Adnectin	CT 322	0.06 nmol/L	VEGF receptor	Pancreatic cancer	Bristol Meyers Squib	Phase I, Phase II
	BMS 962476	0.85 nmol/L	PCSK9	Hypercholesterolemia	Bristol Meyers Squib	Phase I
	BMS -986089	0.17 nmol/L	Myostatin	Duchenne Muscular dystrophy	Bristol Meyers Squib	Phase I (NCT02145234 Phase II
Affibody	ABY 025	76 pmol/L	HER 2	Tumour imaging	Affibody	Phase I Phase II (NCT01858116, NCT01216033)

6.1.1.1 Intrabody

Intrabodies are typically single variable fragments (scFv) consisting of heavy (V_H) and light chain (V_L) variable domains linked via a flexible peptide linker (Figure 1.12) (Lobato and Rabbitts., 2004). There are, however few scFv that can work efficiently as intrabodies since scFv cannot form disulphide bonds, which are critical in the folding of almost all antibodies and thus often exhibit insolubility and instability. To overcome this limitation imposed by the cellular environment, intracellular antibody capture (IAC) technology was used (Tanaka and Rabbitts., 2003). It involves selecting intrabodies from diverse phage libraries expressing scFv, which are initially screened with antigen *in vitro* and then subsequently screened using *in vivo* antibody-antigen interaction assay in yeast cells (Tanaka and Rabbitts., 2003). scFvs have been extensively characterised as research and imaging tools and in therapeutic applications (Haylock et al., 2017). For example, a large panel of anti-TAU (a microtubule-associated protein involved in Alzheimer's and Parkinson's disease) intrabodies selected from a naïve human antibody library can provide as a useful imaging tool to study TAU function in degenerating neurons (Gallardo et al., 2019).

Intrabodies were the first non-antibody scaffold proteins that have been isolated against oncogenic Ras. Using IAC technology, anti-Ras scFvs with improved solubility and binding function *in-vivo* were shown to inhibit oncogenic HRas G12V mediated transformation of NIH 3T3 cells (Tanaka et al., 2007). Further studies using IAC technology established that single variable domains (iDab) are highly efficient as intrabodies. iDab6 intrabody was isolated by screening the libraries in yeast using HRas G12V as a bait protein. iDab6 has shown to specifically bind to oncogenic HRas with mutations at either amino acid 12 or 61 and impaired Ras-dependent tumourigenesis in mouse models (Tanaka et al., 2007). The details of the intrabody binding site on GTP-bound HRas was obtained by X-ray crystallography. The complementary determining regions (CDRs) of V_H domains of iDab6 intrabody interact with the switch I and switch II region of

GTP bound HRas. Most of the interactions between HRas and VH region of the antibody is via hydrogen bonds derived from the main and side chain of residues of CDRs. The ability of intrabody iDab6 to inhibit Ras-effector interactions was confirmed using biochemical assays using GST fusion protein pulldowns in the presence of increasing amounts of iDab6 (Tanaka et al., 2007). In addition to using intrabodies as target validation in disease models, small molecules were developed that target the same location in Ras and inhibit Ras-effector interactions. Altogether, these findings demonstrated the use of non-antibody binding proteins (nABPs) as an excellent approach to develop Ras inhibitors (Quevedo et al., 2018; Cruz-Migoni et al., 2019).

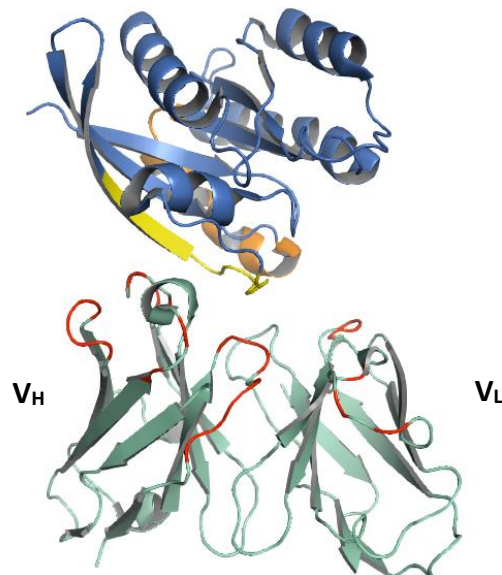


Figure 1.12 Co-crystal structure of HRas and intrabody iDab6 binder protein. iDab6-HRas protein complex (PDB: 5E95). Intrabody variable regions (red) from Variable heavy chain (V_H) of intrabody competitively binds to the conformationally variable regions of Ras, where its signalling effector molecules interact. Intrabody iDab6 scaffold and variable regions are highlighted in cyan green and red, respectively. Ras is shown in blue with the switch I (30-40) and switch II (61-75) regions highlighted in yellow, and orange respectively. V_L. Images were generated in PyMOL. V_H- variable heavy, V_L-variable light regions of iDab6.

6.1.1.2 Affibody

Affibodies are class of non-immunoglobulin binding proteins obtained via randomization of 13 solvent-accessible residues of a bacterial receptor domain Z, derived from staphylococcal protein A (Stahl et al., 2017). These contain three α helices, no disulphide bonds and are smallest synthetic binders (6 kDa) so far. Affibodies are selected via phage display libraries obtained by randomizing 13 residues on the first two α -helices of the three-helix bundle (Gebauer and Skerra., 2019). The potential of Affibodies for medical applications particularly as tracers in medical imaging as well as for receptor signal blocking and delivery of toxic payloads has been explored extensively (Frejd and Kim., 2017; Stahl et al., 2017).

Affibody variants specific for HRas and Raf1 were selected successfully via phage display, which displayed micromolar and nanomolar affinities, respectively (Grimm et al., 2010). Affibody molecules specifically binding to H-Ras or Raf1 (CRaf) were selected with a range of high nanomolar to low micromolar affinities (K_d) against both proteins. Affibody variants selected against HRas were shown to bind to a site that differed when HRas binds to Raf1. In contrast, affibody isolated against Raf1 was capable of inhibiting Ras-Raf interaction in a dose-dependent manner *in vitro*. (Grimm et al., 2010). In conclusion, affibody molecules can be used as tools for molecular recognition in diagnostic and therapeutic applications and have expanded the available approaches to target members of the MAPK pathway.

6.1.1.3 Monobodies

The Monobody scaffold is based on 10th type III domain of human fibronectin (Koide et al., 1998). The fibronectin structure has β sandwich fold similar to immunoglobulin domains, exhibiting exposed loops at one end (termed as BC, DE and FG) (Sha et al., 2017). These are similar to the CDR of antibody variable domains. Unlike conventional Ig domains, the monobody scaffold lacks the central disulphide bond that normally links β sheets. Monobodies were first generated via mutagenesis of the BC and FG loops; later, the DE loop was also included in mutagenesis (Figure 1.13) (Martin et al., 2018; Khan et al., 2020).

In a quest to identify novel strategies to inhibit Ras, monobody NS1 was isolated that selectively interacts with HRas ($K_d \sim 15$ nM) and KRas ($K_d \sim 65$ nM) but not NRas (Spencer-Smith et al., 2017). Moreover, NS1 potently inhibited KRas and HRas mediated signalling and oncogenic transformation both *in vitro* and *in vivo*, however, NS1 did not inhibit NRas or oncogenic proteins such as BRafV600E or MEK (Spencer-Smith et al., 2017). To understand the mechanism of inhibition of HRas mediated signalling by NS1, crystal structure of NS1 in complex with GDP loaded Ras was solved to 1.4 Å resolution. NS1 binds to the $\alpha 4, \beta 6, \alpha 5$ region of Ras distal to switch regions (Figure 1.13). This $\alpha 4$ - $\alpha 5$ region has been proposed as a dimerization interface in Ras proteins, which in turn, is required for activation of BRaf-CRaf heterodimerisation (Khan et al., 2019). Using electron microscopy (EM) spatial analysis as well as co-immunoprecipitation assay, the NS1 intrabody was found to reduce KRas plasma membrane localization and at the same time inhibit Raf activation (Spencer-Smith et al., 2019). In summary, these findings established the importance of targeting $\alpha 4$ - $\alpha 5$ dimerization interface as an approach to inhibit Ras-mediated signalling *in vivo* and provides an invaluable tool for studying Ras dimerization and nanoclustering (Janosi et al., 2012).

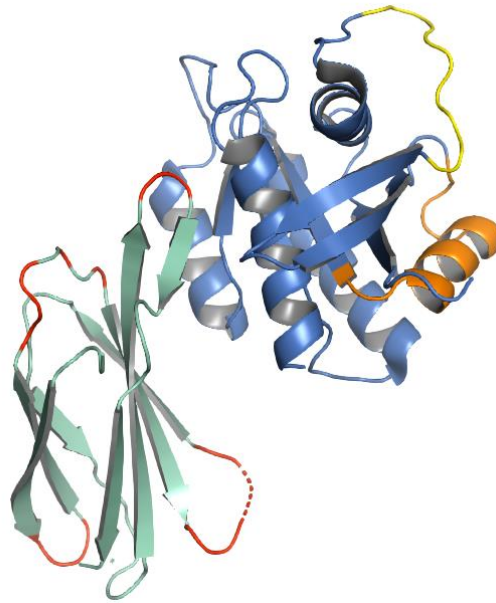


Figure 1.13 Co-crystal structure of HRas and monobody binder protein NS1 (PDB: 5E95). Monobody NS1 inhibits Ras by binding to an allosteric regulatory site. Monobody scaffold and variable regions are highlighted in cyan green and red, respectively. Ras is shown in blue with the switch I (30-40) and switch II (61-75) regions highlighted in yellow and orange, respectively. The image was generated in PyMOL.

6.1.1.4 DARPins

Designed Ankyrin Repeat Proteins (DARPins) are a novel class of binding molecules consisting of ankyrin repeat proteins built from tightly packed repeats usually having 33 amino acid residues. (Binz et al., 2004). Each repeat consists of β turn followed by two antiparallel α helices. Ankyrin repeat (AR) domains usually consist of 4-6 repeats, which are stacked onto each other, leading to a solenoid-shape structure with a hydrophobic core and large solvent-accessible surface (Figure 1.14) (Pluckthun.,2015). These characteristics were used to exploit AR domains for construction of libraries comprising of novel binding molecules. DARPins libraries thus comprise fixed and variable positions. The fixed positions are conserved framework residues acting as a scaffold for the six variable positions per repeat module that can be potentially engaged in interactions with the target. Because of their robustness and extreme stability, binding molecules have been selected from

synthetic DARPin libraries (Theoretical diversity library is 5.2×10^{15} or 3.8×10^{23} for two-module or three-module binders, respectively) via ribosome display or phage display. DARPins can be evolved to bind to various targets using ribosome display with dissociation constants (K_d) within the picomolar range (Boersma., 2018). As proof of concept, DARPins were selected to bind to ERK either in its nonphosphorylated (inactive) or doubly phosphorylated (active pERK) form (ERK2 $K_d=6.6$ nM and pERK2 $K_d=117$ nM). Using bioluminescence resonance transfer technology (BRET), the specificity of DARPins inside the cell was confirmed (Kummer et al., 2012). The potential of using DARPins as next-generation protein therapeutics is currently being evaluated in clinical trials, with VEGF A specific DARPin (Abicipar®) in phase III clinical trials for the treatment of advanced solid tumours and age-related macular degeneration (Rodrigues et al., 2018).

DARPins have also been used to target Ras. K27 (Figure 1.14 A) and K55 DARPins inhibit Ras and have shown to reduce both ERK and AKT activation. K27 preferentially binds to inactive GDP form of Ras ($K_d=4$ nM) whereas K55 favoured Ras-GTP (Guillard et al., 2017). DARPin K27 competes with SOS binding to Switch I region, and leaves both switch I and bound GDP in near identical conformation to that of nonliganded GDP bound Ras. DARPin K55 interacts with both switch I and II of GTP-bound KRas (G12V) and prevented interaction with Raf ($K_d=167$ nM) (Guillard et al., 2017). These two Ras inhibitory DARPins function by blocking different aspects of Ras functions, namely nucleotide exchange of GDP to GTP (K27) and blocking effector interaction (K55).

Recently, Rabbitts and colleagues isolated two DARPins K13 and K19 that specifically inhibit the KRas isoform by binding to $\alpha 3$ - $\alpha 4$ interface in the allosteric lobe (Figure 1.14 B). These DARPins blocked Ras dimerization as well as SOS mediated nucleotide exchange (Bery et al., 2019). Along with iDab6, NS1 monobody and Ras: Raf Affibodies, these findings further highlight the importance of Ras: Raf PPI for inhibition of Ras/effector interactions and downstream signalling pathways in cancer cells (Khan et al., 2020).

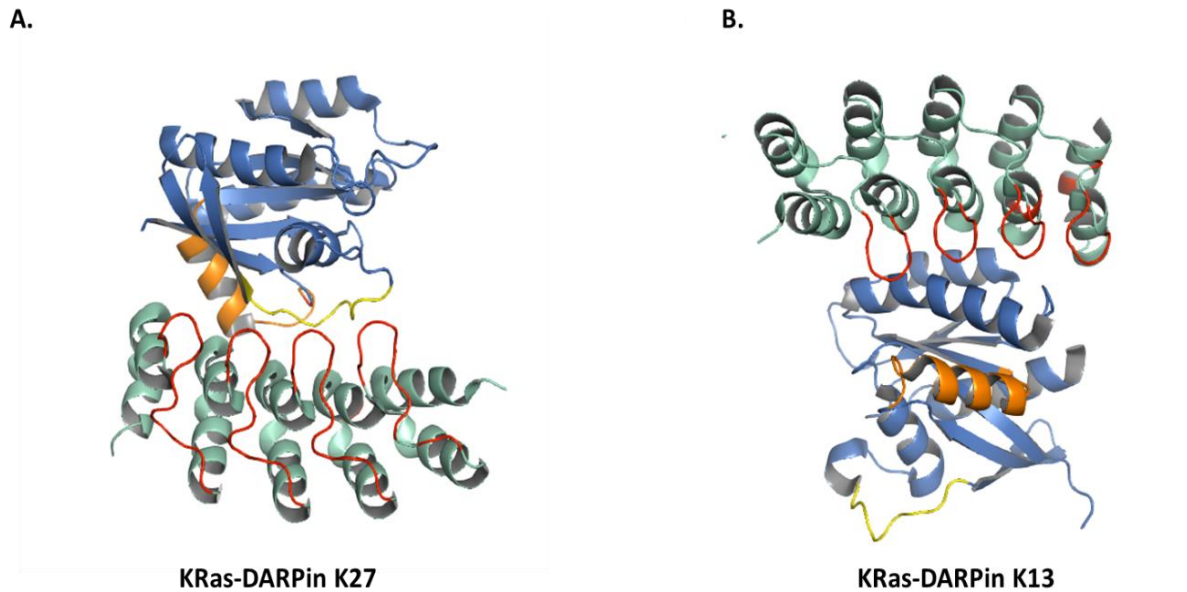


Figure 1.14 Co-crystal structures of Ras and DARPin binder proteins **A.** KRas and DARPin K27 complex (PDB: 52OS), with K27 DARPin binder inhibiting nucleotide exchange reaction of GDP to GTP by binding to a region overlapping with GEF SOS. **B.** KRas and DARPin K13 (PDB: 6H4H) showing inhibition by binding to an allosteric regulatory site away from switch regions of Ras. Ras is shown in blue with the switch I (30-40) and switch II (61-75) regions in yellow and orange respectively. DARPin scaffold and the variable regions of the DARPin binders are highlighted in cyan green and red, respectively. The images were generated in PyMOL.

7.1 Affimer Reagents

The non-antibody based protein scaffold used in this study is called an Affimer. Two types of Affimer scaffold have been generated, which are described in further detail below.

7.1.1 Type I Affimer scaffold

The type I scaffold is derived from human protease inhibitor Stefin A (Stadler et al., 2011) (Figure 1.14 A). It is 98 amino acid in length, single-chain protein, which interacts with its target via three distinct features, the amino terminus and two hairpin structures, namely loop1 and 2. This protein was chosen because protease inhibitor proteins are highly stable and use exposed peptide loops to bind to their targets, making them promising randomised protein scaffolds. Binding of stefin A to cathepsins (cysteine protease) was abolished by insertion of randomised peptides into loop regions (herein termed variable regions). This scaffold was termed Stefin A Quadropole Mutant –Tracy (SQT) (Stadler et al., 2011). The X-ray crystal structure of Stefin A, demonstrating the fold of Type I scaffold can be observed in Figure 1.15 A. Yeast-two hybrid libraries were constructed using this scaffold with insertions of randomised peptides either 10 amino acids in length in a variable region I (VR1) or 12 amino acids in length in variable region 2 (VR2). These libraries comprising 10^7 unique sequences were screened to identify specific binders to the POZ domain of B cell lymphoma protein (BCL6), and a peptide derived from penicillin-binding protein 2 (PBP2) which is specific to methicillin-resistant *Staphylococcus aureus* (Stadler et al., 2011). The SQT scaffold can also present peptides for interaction within human cells. The insertion of the Noxa BH3 alpha-helix into the SQT scaffold allows for specific interaction with anti-apoptotic protein Mcl-1 in human skin cancer cells. These results show that the SQT variant (Type-I Affimer scaffold) derived from Stefin-A is a robust and versatile scaffold that can present binding peptides for target interactions and is functional in both yeast and human cells.

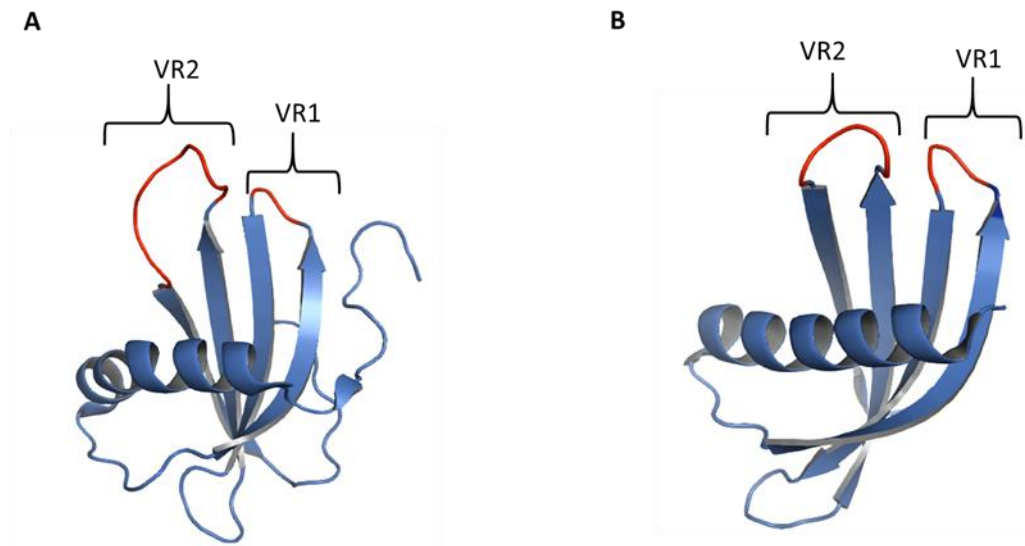


Figure 1.15 Structure of the Affimer scaffolds. Crystal structures of **A.** Affimer Type I (PDB 1NB5) scaffold based on human protease inhibitor Stefin A and **B.** Affimer type II (PDB 4N6U) scaffold based on plant-based phytocystatin sequence with variable regions indicated in red. Images generated in PyMOL.

7.1.2 Type II Affimer

The type II scaffold design, originally termed an Adhiron, is related in structure to Type I scaffold (Figure 1.15 B) (Tiede et al., 2014). It is based on the consensus sequence of 57 plant-derived phytocystatins. It was chosen for its small size (12kDa), high thermodynamic stability, high-affinity target binding as well as lack of disulphide and glycosylation sites. This scaffold encodes a four-strand β sheet core and central α helix and two randomised nine amino acid loop regions for specific molecular recognition (Carter., 2011; Tiede et al., 2014). An Affimer type II phage library of 1.3×10^{10} clones was created by the insertion of random amino acid codons in the two variable regions (Tiede et al., 2014). Since initial proof of concept studies, which isolated highly specific Affimers against yeast SUMO protein (Tiede et al., 2014) more than 350 successful screens have been carried out by Bioscreening Technology Group (BSTG) at University of Leeds, to allow identification of Affimers against biological targets particularly those of clinical interest. The extent to which Affimers can be used in applications such as dissection of intracellular

pathways, inhibition of extracellular receptor function, *in vivo* imaging, modulation of ion channel function, super-resolution microscopy, diagnostics and in drug discovery has been evaluated (Tiede et al., 2014; Tiede et al., 2017). For example, enzyme inhibitor switch sensors were developed by insertion of Affimer binding proteins, which disrupt the enzyme-inhibitor complex. These sensors are rapid wash free and sensitive assays in areas like therapeutic drug monitoring, health diagnostics and plant pathogen detection and can be provided as a platform for point-of-care and in-field diagnostics (Adamson et al., 2019). In addition, Affimer against glypican-3 (GPC-3), a promising new tumour marker for hepatocellular carcinoma (HCC) has been isolated by phage display. Affimer specific for GPC3 has been combined with monoclonal antibody to develop a new sandwich chemiluminescence assay (CLIA). This newly developed CLIA test has been shown to have high specificity and can be used as a sensitive immunodiagnostic kit to detect GPC3 in the serum of HCC patients (Xie et al., 2017). All the above examples demonstrate the use of Affimers as promising tools for label-free detection of biomarkers, offering improved specificity and affinity, as compared to traditional antibody diagnostic kits.

Affimers have been used as highly selective protein-based inhibitors that bind to FcγRIIIa, a subtype of immunoglobulin receptor family present in natural killer (NK) cells and macrophages. These receptors are a valid therapeutic target for the treatment of autoimmunity. The FcγRIIIa specific Affimer provides the ability to block IgG binding and abrogate FcγRIIIa mediated downstream effector function in macrophages (Robinson et al., 2018). Additionally, Affimers have also been used to gain insights into the interaction between HIF1α and p300, which play an important role in tumour metabolism by inhibiting the interaction with low micromolar IC₅₀ in the range 1-5 μM. This highlights the use of Affimers as tools to understand and modulate protein-protein interactions in disease (Burslem et al., 2017; Kyle et al., 2015).

Isoform-specific Affimers have been isolated against PI3K α , a heterodimeric protein comprising of p110 catalytic subunit and p85 regulatory subunit. This protein is a key molecule in the activation of the PI3K-Akt pathway and is mediated by oncogenic Ras. There are currently five variants of p85 regulatory subunit (p85 α , p85 β , p85 γ , p55 α , p50 α) out of which p85 α is highly expressed. Despite a high degree of sequence homology among the variants, a number of p85 α specific Affimers have been isolated by screening it against the N terminal SH2 domain of p85 α . These binders were then cross reacted against p85 β and p55 α subunits. None of these Affimers bound to C terminal p85/p55 SH2 domains, indicating the ability of Affimers to bind to particular isoform of heterodimeric protein (Tiede et al., 2017). All the above findings, therefore, demonstrated Affimers as valuable tools to study intracellular signalling.

Objectives

The overall aim of the project is to investigate the suitability of Affimer reagents as molecular biology tools to study Ras structure and function. Affimer reagents targeting Ras have been isolated previously, and preliminary experiments demonstrated the ability of these reagents to modulate Ras activity. This project aims to characterise the selected Affimers as a new tool to identify druggable binding sites in Ras. Firstly biochemical characterisation of KRas specific Affimer followed by structural characterisation of the Affimer-KRas protein complex was carried out to understand the mode of action of inhibition of KRas. This biochemical and structural understanding of Affimer action on Ras function could be used to inform small molecule drug design and development of novel anti-Ras therapeutics. If successful, this strategy can be applied to screen unique non-antibody binding proteins against other disease-related targets, which are currently considered 'undruggable'.

Chapter 2

Materials and Methods

2.1 Materials

2.1.1 General reagents

All reagents were supplied by Sigma Aldrich (Gillingham, Dorset, U.K) unless otherwise stated.

2.1.2 Bacterial strain genotypes

BL21 Star™ (DE3) *E.coli* cells were purchased from Invitrogen (Life Technologies, M.A, U.S.A) and were used for protein production. XL-1 Blue supercompetent *E. coli* cells were purchased from Stratagene (Agilent Technologies, CA, U.S.A) and were used for genetic engineering work and replication of plasmid DNA. The genotypes of each strain are shown in Table 2.1.

Table 2.1 Genotypes of bacterial strains used for this project.

<i>E. coli</i> strain	Genotype
BL21(DE3)	<i>ompT gal dcm lon hsdS_B(r_B⁻m_B⁻) λ</i> (DE3 [<i>lacI lacUV5-T7p07 ind1 sam7 nin5</i>] [<i>malB</i> ⁺] _κ - 12(λ ^S))
XL1-Blue	<i>endA1 gyrA96(nal^R) thi-1 recA1 relA1 lac glnV44</i> F'[Tn10 proAB ⁺ lacI ^q Δ(<i>lacZ</i>)M15]

2.1.3 Primers used for sub-cloning

Primers used for sub-cloning (sequences are shown in Table 2.2) and site-directed mutagenesis (sequences are shown in Table 2.3) were obtained from Sigma-Aldrich (Gillingham, Dorset, U.K). Primers were used in the amplification of Ras or Affimer DNA from parent vectors by polymerase chain reaction (PCR), for sub-cloning into destination vectors. For both Ras and Affimer, donor and recipient vectors is pET-11a (5677 bp). Plasmid pGST-thr-RAF1-RBD was purchased from Addgene (Cambridge, MA, U.S.A). The

recipient vector for this plasmid is pDest 521 (6770 bp). Vector maps can be viewed in Appendix A.

Table 2.2 List and sequence of primers used for subcloning.

Primer name	Primer sequence (5'-3')
KRas-forward	CGC GCT AGC ATG ACC GAA TAT TAA ACT GGT GG
KRas-reverse	CGT TGG CGG CCG CTT ATT TAG TTT GCG AAT TTC ACG
KRas 6 His forward	GCT AGC ATG ACC GAA TAT AAA CTG GTG G
KRas 6 His reverse	GCA TAT GCG GCC GCG CTT TAT GTT TGC GAA TTT CAC G
Affimer- His forward	ATG GAT CCG CCA CCA TGG CCG CTA CCG GTG TTC GTG
Affimer -His reverse	GTT TCG CCA ACC ACC GGA CCA ATA CTT CTA CTG CTA CTG TTC GTA GTA GTA GTA GTA ATC CCA TTC GCC GGC GAT TAC G
Affimer VR1 forward (P1)	ATG GCT AGC AAC TCC CTG GAA ATC GAA G
SOE forward primer (P2)	CCT GGA AGC TAA AGA CGG T
SOE reverse primer (P3)	CAC CGT CTT TAG CTT CCA GG
T7 Reverse primer (P4)	GCT AGT TAT TGC TCA GCG G
KRas M66A forward	GGA AGA ATA TAG CGC CGC CCG TGA TCA ATA CAT GC
KRas M66A reverse	GCA TGT ATT GAT CAC GGG CGG CGC TAT ATT CTT CC
RAF1-RBD R67A forward	GTT TTT CTG CCG AAT AAA CAA GCC ACC GTC GTC AAC GTT CG
RAF1-RBD R67A reverse	CGA ACG TTG ACG ACG GTG GCT TGT TTA TTC GGC AGA AAA AC
RAF1-RBD R67E forward	GTT TTT CTG CCG AAT AAA CAA GAG ACC GTC GTC AAC GTT CG
RAF1-RBD R67E reverse	CGA ACG TTG ACG ACG GTC TCT TGT TTA TTC GGC AGA AAA AC
KRas H95Q forward	GAA GAT ATC CAT CAG TAC CGT GAA CAG
KRas H95Q reverse	CTG TTC ACG GTA CTG ATG GAT ATC TTC
KRas H95L forward	GAA GAT ATC CAT CTC TAC CGT GAA CAG
KRas H95L reverse	CTG TTC ACG GTA TAG ATG GAT ATC TTC

Table 2.3 List and sequences of alanine mutant primers used for sub-cloning.

Primer name	Primer sequence 5' – 3'
K3-VR1.1 forward	GTT GTT AAA GCG AAA GAA CAG GCT TCT ATC GAC ATC TGG TAC GAC
K3-VR1.1 reverse	GTC GTA CCA GAT GTC GAT AGA AGC CTG TTC TTT CGC TTT AAC AAC
K3-VR1.2 forward	AAA GCG AAA GAA CAG CAT GCT ATC GAC ATC TGG TAC G
K3-VR1.2 reverse	CGT ACC AGA TGT CGA TAG CAT GCT GTT CTT TCG CTT T
K3-VR1.3 forward	GTT AAA GCG AAA GAA CAG CAT TCT GCT GAC ATC TGG TAC GAC TTC ACC ATG
K3-VR1.3 reverse	CAT GGT GAA GTC GTA CCA GAT GTC AGC AGA ATG CTG TTC TTT CGC TTT AAC
K3-VR1.4 forward	CGA AAG AAC AGC ATT CTA TCG CTA TCT GGT ACG ACT TCA CCA T
K3-VR1.4 reverse	ATG GTG AAG TCG TAC CAG ATA GCG ATA GAA TGC TGT TCT TTC G
K3-VR1.5 forward	CGA AAG AAC AGC ATT CTA TCG ACG CTT GGT ACG ACT TCA CCA TGT ACT A
K3-VR1.5 reverse	TAG TAC ATG GTG AAG TCG TAC CAA GCG TCG ATA GAA TGC TGT TCT TTC G
K3-VR1.6 forward	AGA ACA GCA TTC TAT CGA CAT CGC TTA CGA CTT CAC CAT GTA CTA CC
K3-VR1.6 reverse	GGT AGT ACA TGG TGA AGT CGT AAG CGA TGT CGA TAG AAT GCT GTT CT
K3-VR1.7 forward	CAG CAT TCT ATC GAC ATC TGG GCT GAC TTC ACC ATG TAC TAC CTG

K3-VR1.7 reverse	CAG GTA GTA CAT GGT GAA GTC AGC CCA GAT GTC GAT AGA ATG CTG
K3-VR1.8 forward	ATT CTA TCG ACA TCT GGT ACG CTT TCA CCA TGT ACT ACC TGA C
K3-VR1.8 reverse	GTC AGG TAG TAC ATG GTG AAA GCG TAC CAG ATG TCG ATA GAA T
K3-VR1.9 forward	TCT ATC GAC ATC TGG TAC GAC GCT ACC ATG TAC TAC CTG ACC CTG
K3-VR1.9 reverse	CAG GGT CAG GTA GTA CAT GGT AGC GTC GTA CCA GAT GTC GAT AGA
K3-VR2.1 forward	CTG TAC GAA GCG AAA GTT TGG GTT AAG GCT CTG AAC AAC AGT CAT ACC TAT AAA AAC
K3-VR2.1 reverse	GTT TTT ATA GGT ATG ACT GTT GTT CAG AGC CTT AAC CCA AAC TTT CGC TTCGTA CAG
K3-VR2.2 forward	GTA CGA AGC GAA AGT TTG GGT TAA GAA AGC TAA CAA CAG TCA TAC CTA TAA AAA CTT C
K3-VR2.2 reverse	GAA GTT TTT ATA GGT ATG ACT GTT GTT AGC TTT CTT AAC CCA AAC TTT CGC TTCGTAC
K3-VR2.3 forward	CGA AGC GAA AGT TTG GGT TAA GAA ACT GGC TAA CAG TCA TAC CTA TAA AAA CTT CAA AG
K3-VR2.3 reverse	CTT TGA AGT TTT TAT AGG TAT GAC TGT TAG CCA GTT TCT TAA CCC AAA CTT TCG CTT CG
K3-VR2.4 forward	AGC GAA AGT TTG GGT TAA GAA ACT GAA CGC TAG TCA TAC CTA TAA AAA CTT CAA AGA AC
K3-VR2.4 reverse	GTT CTT TGA AGT TTT TAT AGG TAT GAC TAG CGT TCA GTT TCT TAA CCC AAA CTT TCG CT
K3-VR2.5 forward	AGT TTG GGT TAA GAA ACT GAA CAA CGC TCA TAC CTA TAA AAA CTT CAA AGA AC
K3-VR2.5 reverse	GTT CTT TGA AGT TTT TAT AGG TAT GAG CGT TGT TCA GTT TCT TAA CCC AAA CT

K3-VR2.6 forward	CGA AAG TTT GGG TTA AGA AAC TGA ACA ACA GTG CTA CCT ATA AAA ACT TCA AAG
K3-VR2.6 reverse	CTT TGA AGT TTT TAT AGG TAG CAC TGT TGT TCA GTT TCT TAA CCC AAA CTT TCG
K3-VR2.7 forward	GGT TAA GAA ACT GAA CAA CAG TCA TGC TTA TAA AAA CTT CAA AGA ACT GCA GG
K3-VR2.7 reverse	CCT GCA GTT CTT TGA AGT TTT TAT AAG CAT GAC TGT TGT TCA GTT TCT TAA CC
K3-VR2.8 forward	AAG AAA CTG AAC AAC AGT CAT ACC GCT AAA AAC TTC AAA GAA CTG CAG GAG
K3-VR2.8 reverse	CTC CTG CAG TTC TTT GAA GTT TTT AGC GGT ATG ACT GTT GTT CAG TTT CTT
K3-VR2.9 forward	AAG AAA CTG AAC AAC AGT CAT ACC TAT GCT AAC TTC AAA GAA CTG CAG GAG TTC AA
K3-VR2.9 reverse	TTG AAC TCC TGC AGT TCT TTG AAG TTA GCA TAG GTA TGA CTG TTG TTC AGT TTC TT

Table 2.4 Details of antibody concentration, dilution factor and source.

(IB: Immunoblot).

Antigen	Species	Concentration (mg/ml)	Dilution factor	Source	Catalogue number
Ras	Rabbit	1.175	IB 1:1000	Abcam	EPR18713- 13
6x His (HRP)	Rabbit	0.100	IB 1:1000 ELISA 1:5000	Abcam	Ab1187
GST (HRP)	Rabbit	0.178	IB 1:5000	Genetex	GTX114099
Rabbit IgG	Goat	0.065	IB 1:10000	Cell Signalling Technology	7074S

2.1.4 Common buffers and solutions

- Tris buffered saline (1X TBS)- 50 mM Tris-Cl, 150 mM NaCl pH 7.6
- TBS- Tween (TBS-T): 1X TBS + 0.1 %Tween-20
- Phosphate buffered saline (1X): 137 mM NaCl, 2.7 mM KCl, 10 mM Na₂ HPO₄, 2mM KH₂PO₄, pH 7.4.
- Affimer Lysis buffer: 50 mM NaH₂PO₄, 300 mM NaCl, 20 mM Imidazole pH 7.4
- Affimer wash buffer: 50 mM NaH₂PO₄, 500 mM NaCl, 20 mM Imidazole pH 7.4
- Affimer elution buffer: 50 mM NaH₂PO₄, 500 mM NaCl, 300 mM Imidazole, 10% w/v glycerol pH 7.4
- Nucleotide exchange buffer: 20 mM Tris-Cl, 50 mM NaCl, 0.5 mM MgCl₂ pH 7.5
- GST fused protein lysis buffer: 125 mM Tris-Cl, 150 mM NaCl, 1mM DTT, 1% w/v Triton X-100 pH 7.4
- GST fused protein wash buffer: 125 mM Tris-Cl, 150 mM NaCl, 1mM DTT pH 7.4.
- GST fused protein elution buffer: 125 mM Tris-Cl, 150 mM NaCl, 1mM DTT, 1% w/v Triton X-100, 50 mM reduced glutathione pH 7.4
- Assay buffer: 125 mM Tris-Cl, 150 mM NaCl, 5 mM MgCl₂, 0.1% w/v Tween 20, 1 mM DTT (add DTT fresh before use) pH 8.0
- Blocking buffer: Casein blocking buffer 10X (Sigma-Aldrich), diluted 2X in PBST

2.1.6 Bacterial cell culture reagents

- LB media (Lennox-L-Broth base) (Invitrogen Life Technologies): 86.2 mM NaCl, 10g/L peptone, 5g/L yeast extract.
- 2TY media: 24 g/L yeast extract; 16g/L tryptone, 5g NaCl.
- LB agar (Lennox L agar) (Invitrogen Life Technologies): 10g/L SELECT peptone 140; 5g/L SELECT yeast extract, 5g/L sodium chloride, 12g/L SELECT agar.

- SOC media: 0.4% w/v glucose, 20 g/L tryptone, 5g/L yeast extract, 0.5 g/L NaCl.

2.1.7 SDS PAGE and western blot reagents

- Separating gel buffer: 1.5 M Tris-Cl; 0.4% w/v SDS; pH 8.9. Filter sterilised through 0.22µm filter.
- Stacking gel buffer: 0.4M Tris-Cl; 0.4% w/v SDS; pH 6.7. Filter sterilised through 0.22µm filter.
- SDS PAGE running buffer: 25 mM Tris-Cl; 0.19 M glycine; 0.1% w/v SDS; pH 8.3.
- SDS PAGE sample buffer (4X): 8% w/v SDS; 0.2 M Tris-HCl (pH 7); 20% glycerol; 1% bromophenol blue (BDH laboratories); 20% v/v β-mercaptoethanol added before use.
- Coomassie blue stain: 45% v/v methanol; 7% v/v acetic acid; 0.25% w/v Coomassie Brilliant Blue R-250 (Sigma-Aldrich).
- Destain solution: 25% v/v methanol; 7.5% v/v acetic acid.
- Transfer buffer (Bio-Rad): 25 mM Tris-Cl; 0.19 M glycine; 20% v/v methanol; pH8.3.
- Stripping buffer: 0.2 M glycine; 0,1% w/v SDS; 1% w/v Tween-20; pH 2.2.
- Transfer buffer (Bio-Rad): 100 mM Tris-Cl, 121 mM Glycine, 20% v/v methanol.
- Tris Buffer saline -Tween 20 (TBS-T): 10 mM Tris-Cl, 150 mM NaCl, 0.1 % Tween-20 at pH 7.5.

2.2 Methods

2.2.1 DNA protocols and molecular sub-cloning

2.2.1.1 Polymerase Chain Reaction (PCR)

The DNA sequences used during sub-cloning into various expression vectors were amplified by polymerase chain reaction (PCR). The reactions were performed in 200 μ l PCR tubes, using a G-Storm™ GS2 thermal cycler. Reactions were carried out with Phusion® High-Fidelity DNA polymerase (New England Biolabs; NEB, M.A, U.S.A) using the components supplied with the DNA polymerase. Reaction components and thermocycling conditions are detailed in Table 2.5 and Table 2.6. Following thermocycling, the template methylated DNA was digested by 10 U *Dpn I* (NEB) for 1 h at 37 °C. The PCR product was then purified using a NucleoSpin® Gel and PCR Clean-up kit (Macherey-Nagel), according to the manufacturer's instructions (see section 2.2.1.5).

Table 2.5- Composition of thermal cycling reaction mixture

Component	25 μ l Reaction	Final concentration
Sterile water	13.8 μ l	
5X Phusion HF buffer	5 μ l	1X
dNTP mix 25 mM	0.2 μ l	200 μ M each
DMSO	0.75 μ l	3 % v/v
Forward primer 10 μ M	2 μ l	0.8 μ M
Reverse primer 10 μ M	2 μ l	0.8 μ M
Phusion DNA polymerase	0.25 μ l	0.02 units/ μ l
Template DNA	1 μ l	

Table 2.6 – Condition of thermal cycling reaction.

Cycling step	Temperature	Time	Cycles
Initial denaturation	98 °C	30 seconds	1
Denaturation	98° C	20 seconds	
Annealing	54° C	20 seconds	30
Extension	72° C	20 seconds	
Final extension	72° C	10 min	1
Hold	4 ° C	Hold	1

2.2.1.2 Agarose gel electrophoresis

Nine microliters of the PCR amplified and *Dpn I* digested DNA was mixed with 1 µl of the 10x DNA loading dye (30 % w/v glycerol, 0.2 % w/v Orange G, H₂O, final concentration 1x) and 5 µl of samples were loaded onto a 2 % w/v agarose gel in Tris-acetate-EDTA (TAE) buffer (40 mM Tris-Cl; 20 mM acetic acid, 1 mM EDTA, pH 8.0), containing 1X SYBR® Safe DNA Gel Stain. Quick-Load® Purple 2-log DNA Ladder (NEB) was loaded in the first well. Electrophoresis was carried out in Mini-Sub® Cell GT apparatus (Bio-Rad, Hertfordshire, U.K) in TAE buffer at 100 V. DNA bands were visualised under UV light and imaged using an Amersham™ Imager 600 (GE Healthcare, Buckinghamshire). After the electrophoresis, DNA bands were excised from the gel using a scalpel. Extraction of the DNA was performed using a NucleoSpin® Gel and PCR Clean-up kit (Macherey-Nagel, Leicestershire, U.K) (see section 2.2.1.5).

2.2.1.3 Restriction digestion

The restriction digestion reactions were carried out in a total reaction volume of 50 µl containing 10 U restriction enzyme(s), 1 – 5 µg DNA and 1X CutSmart® Buffer (NEB) in nuclease-free water. The resulting fragments were purified using a NucleoSpin® Gel and PCR Clean-up kit (Macherey-Nagel, Leicestershire, U.K) (see section 2.2.1.5).

The recipient vector pET-11a was dephosphorylated to remove 5´ phosphate and prevent self-ligation. Dephosphorylation was carried out using Antarctic Phosphatase (heat-labile alkaline phosphatase) in a total reaction volume of 60 µl, containing 5 U Antarctic Phosphatase (NEB), 5 µg vector DNA and 1X

Antarctic Phosphatase Reaction Buffer (NEB) in nuclease-free water. After incubation for 15 min at 37 °C, Antarctic Phosphatase was heat-inactivated by incubation at 65 °C for 5 min.

2.2.1.4 DNA ligation

Ligation reactions were performed in a total volume of 20 µl, containing 25 ng vector DNA, 75 ng insert DNA, 1 U T4 DNA Ligase (Roche Basel, Switzerland) and 1X T4 DNA Ligase Buffer (Roche), in nuclease-free water. Ligation reactions were incubated at 4 °C overnight, followed by transformation of XL-1 Blue super competent *E. coli* cells.

2.2.1.5 DNA extraction and purification

DNA fragments were purified from enzymatic reactions such as PCR as well as agarose gels. DNA fragment from agarose gel was excised, and the weight of the gel slice was determined. For each 1g agarose gel, 1 ml of binding buffer NT1 from NucleoSpin® Gel and PCR Clean-up kit was added. The sample was incubated for 10-20 min at 50°C and vortexed until the gel slice was completely dissolved. NucleoSpin Gel and PCR clean up midi column were placed in 15 ml collection tube, and the sample was loaded. The column was centrifuged for 1min at 3000 x g for DNA to bind to the column. 4 ml of wash buffer NT3 was added to wash the silica membrane in the column and centrifuged again for 1 min at 3000 x g. After repeating this step, the column was spanned again for 10 min at 3000 x g to dry the silica membrane completely. DNA was eluted by placing the column in new 15 ml centrifuge tube, and 200 µl of nuclease-free water (NEB) was added and incubated at 70 °C for 5 min and centrifuged for 2 min at 3000 x g.

2.2.1.6 Transformation of *E. coli* bacterial strains with DNA

The appropriate competent cells for each construct were thawed at 4° C. 10 ng of DNA was aliquoted to a microcentrifuge tube and pre-chilled on ice, following which 10 µl of competent cells (per transformation) was added. The cell/DNA mixture was mixed and incubated at 4° C for 30 min, followed by heat

shock in a 42° C water bath for 45 seconds. Samples were then incubated for further 2 min on ice, before the addition of 190 µl of SOC media. The mixture was incubated at 37°C for 1 h with shaking at 230 rpm. 100 µl of the transformation mixture was plated onto Lennox L agar plate containing 100 µg/ml carbenicillin (LB-carb plate) and incubated overnight at 37°C.

2.2.1.7 Purification of plasmid DNA

The sub-cloned plasmid DNA was purified by QIAprep® Spin Miniprep Kit for the use of the plasmid in bacterial production. A single bacterial colony from LB-carbenicillin plate was inoculated into 5 ml of Lennox broth (LB media) containing 100 µg/ml carbenicillin (LB carb media) and incubated overnight at 37°C and 230 rpm. For minipreps, the overnight cultures were centrifuged at 4816 x g for 10 min at 4° C. Pelleted bacterial cells were resuspended in 250 µl buffer P1 (re-suspension buffer) and transferred to a microcentrifuge tube. 250 µl of buffer P2 (lysis buffer) was added and mixed thoroughly by inverting the tube 4-6 times until the solution becomes clear. 350 µl of buffer N3 (neutralisation buffer) was added as soon as possible and mixed thoroughly by inverting the tube 4-6 times. Following which the tube was centrifuged for 10 min at 13000 rpm. 800 µl of supernatant from the tube was then added to QIAprep® Spin column by pipetting and centrifuged for 1000 x g for 1 min. The column was washed with 0.5 ml PB buffer and centrifuged at the same specification mentioned above. The column was finally washed with 0.75 ml of Buffer PE twice and eluted by adding 25 or 50 µl of nuclease-free water.

2.2.1.8 Determination of DNA concentration

The concentration of purified DNA was measured by a NanoDrop™ Lite spectrophotometer. The instrument was blanked with nuclease-free water before taking measurements of the DNA samples. The absorbance at 260 nm has been used to calculate the DNA concentration using the Beer-Lambert Law (Beer., 1852; Lambert., 1760) ($A_{260} = \epsilon cl$, where ϵ is the extinction coefficient, c is the DNA concentration in ng/µl, and l is the path length in cm).

2.2.1.9 DNA sequencing

Sub-cloning was confirmed by DNA sequencing. The purified plasmid DNA was diluted to 100 ng/ μ l, and sequencing was performed by Genewiz (Essex, U.K) using the primers detailed in Table 2.7.

Table 2.7- Primers used for DNA sequencing of plasmids

Plasmid	Primer name	Primer DNA sequence (5'-3')
pET-11a	T7	TAATACGACTCACTATAGGG
pGEX 6P-2	5GEX	GGGCTGGCAAGCCACGTTTGGTG

2.2.1.10 Construction of K3 VR1 and K3 VR2 mutants

To generate Affimer K3 Δ VR1 and K3 Δ VR2, residues of VR1 and 2 were replaced with three residues of alanine from the control Affimer variable regions using splice overlap extension. Affimer K3 variable region (VR) 1 was amplified using Phusion DNA polymerase with 1 μ l of Affimer K3 DNA, Affimer K3 VR1 forward and reverse primers (Table 2.2) and reaction components outlined in Table 2.5. The same approach used for control Affimer VR2 DNA sequence but using control Affimer DNA and Affimer VR2 forward and reverse primers instead. The PCR products were purified by PCR purification kit and subjected to splice overlap extension (as detailed in sec.2.2.1.1, but without any primers used), to anneal the fragments together. This was followed by PCR with Affimer forward and reverse primers using Phusion DNA polymerase. The same approach was followed for obtaining K3 Δ VR2 mutants. The spliced product was digested with *NheI* and *NotI* overnight at 37°C. The spliced product was purified and subcloned in pET-11a vector digested with *Nhe-I* and *Not-I*. DNA was ligated as per section 2.2.14 and transformed in XL-1 blue supercompetent cells for culturing and extracting DNA by miniprep. The DNA was sent for sequencing to confirm the ligation.

2.2.1.11 Alanine scanning by site directed mutagenesis

Primers were designed using primer design guidelines as per QuikChange site directed mutagenesis kit by Agilent® (C.A, U.S.A). Variable regions of Affimer K3 were substituted to alanine (shown in Table 2.3). The PCR reactions contained 1 KOD polymerase buffer, 0.2 mM dNTP, 2 mM MgSO₄, 0.3 μM of forward and reverse primers, 10 ng DNA template and 1 U KOD Hot start DNA polymerase in a total volume of 50 μl. The reaction mixtures were then subjected to thermal cycling parameters as per Table 2.8. Following thermal cycling, PCR products were digested with *DpnI* for 1 h at 37°C. XL-1 blue supercompetent cells were transformed with *Dpn-I* treated samples as outlined in section 2.2.1.5. Sub cloned plasmid DNA was extracted using a QIAprep spin miniprep kit. Mutagenesis was confirmed by sequencing (Genewiz, Essex, U.K).

Table 2.8- Cycling conditions for site directed mutagenesis protocol.

Cycle step	Temperature	Time	Cycles
Initial denaturation	98°C	2 min	1
Denaturation	98°C	20 seconds	
Annealing	68°C	10 seconds	30
Extension	70°C	3.5 min	
Final extension	70°C	5 min	1

2.2.1.12 Site directed mutagenesis of KRas and RAF1-RBD

The same method was followed, as mentioned in section 2.2.1.10 with the exception being KRasM66A, RAF1RBD R67A and R67E primers were used as template DNA (see table 2.2).

2.2.2 Protein analysis methods

2.2.2.1 Protein concentration determination

The concentration of purified protein was measured using Nanodrop™ Lite spectrophotometer. The instrument was blanked using appropriate sample buffer before reading the absorbance of the sample. The sample protein concentration was determined by measuring absorbance at 280 nm using Beer-Lambert Law ($A_{280} = \epsilon \cdot c \cdot l$ where ϵ = extinction coefficient, c = protein concentration in mg/ml and l = path length in cm.). The extinction coefficient was calculated from the protein sequence using ExPASy ProtParam software (Wilkins et al., 1999).

Additionally, protein concentration was determined using Bicinchoninic acid (BCA) assay. A Pierce™ BCA kit was used, as per manufacturer's instruction in microplate format, in which sample to working reagent ratio is 1:8 (working range 20-2000 µg/ml).

2.2.2.2 SDS-PAGE

Purified proteins or whole cell lysates were resuspended in 4X SDS sample buffer and incubated at 95°C for 5 min. Samples were loaded on 15% w/v SDS-Polyacrylamide resolving gel and 7.5% w/v stacking gel and run at 150 V for 60 min in SDS running buffer. PageRuler™ pre-stained protein ladder (10-180 kDa) was used as molecular weight marker. Gels were stained for 15 min in Coomassie brilliant blue and de-stained overnight using a destaining solution. Coomassie brilliant blue gels were imaged using an Amersham™ Imager 600 (Laemmli., 1970).

2.2.2.3 Immunoblotting

Proteins subjected to SDS-PAGE were transferred to a nitrocellulose membrane in 1X transfer buffer using Turbo Trans blot (Bio-Rad). Membranes were incubated in 5% w/v skimmed milk (Sigma) in TBS-T for 1 h on a rocker at room temperature. Membranes were then incubated with primary antibodies

(Table 2.4) in 5% w/v skimmed milk powder overnight at 4°C and washed three times with TBS-T for 15 min each time before incubation with HRP conjugated secondary antibodies (Table 2.4) for 1 h. The membranes were then washed three times in TBS-T followed by detection using Immunoblot forte Western HRP substrate (Millipore, Watford, U.K). Images were taken in Amersham™ Imager 600 (GE Healthcare). Quantification of proteins was performed using densitometry on Image J and normalised using Alanine Affimer as a loading control for Ras/Raf binding assays.

2.2.3 Protein production

2.2.3.1 Affimers

Affimers sequences were subcloned in the pET-11a vector and expressed in *E. coli* BL21 star™ DE3 cell line. After transformation, a single bacterial colony was used to inoculate a 7 ml LB carbenicillin (100 µg/ml) media and grown at 37°C and 230 rpm. Following which, 5 ml of the overnight culture was added to 50 or 400 ml of LB-carbenicillin media and grown at 37° C, 230 rpm until O_{600nm} reached 0.6~0.8. Protein expression was induced by adding 0.1mM IPTG to the cultures and incubated at 25° C on shaking incubator at 150 rpm. Cells were harvested by centrifugation at 4816 x g for 20 min. For 400 ml cell culture, cells were lysed in a buffer containing 50 mM Na₂HPO₄, 150 mM NaCl, 20 mM Imidazole, 10% w/v glycerol pH 7.4 supplemented with 0.1 mg/ml lysozyme, 0.1% w/v Triton X-100, 1X Halt protease inhibitor cocktail and 10U/ml Benzonase for 20 min at 4°C. The lysate was heat denatured at 50°C for 20 min, followed by centrifugation at 4816 x g for 20 min and 12,000 x g for further 20 min. The clear soluble lysate was incubated with 400 µl of Ni²⁺-NTA resin assuming the binding capacity of the beads was 40 mg/ml of purified protein, based on expected protein yields and resin binding capacity. Excess Affimer was removed by extensive washing with 50 mM Na₂HPO₄, 300 mM NaCl and 20 mM Imidazole pH 7.4. His tagged Affimers were eluted with 50 mM Na₂HPO₄, 150 mM NaCl and 300 mM Imidazole and 10% w/v glycerol pH 7.4

Proteins were dialysed overnight at 4°C in 1X PBS and 10% w/v glycerol using Slide- A-Lyser™ cassettes, 7K MWCO. Protein concentration was measured at A₂₈₀ using Nanodrop® lite spectrophotometer and calculated using Beer-Lambert Law. Protein purity was analysed by Coomassie Staining and 15% w/v SDS-PAGE. All Affimer sequences used in this project is shown in Appendix B.

2.2.3.2 KRas/KRas His tag

Plasmids encoding N-terminally His-tagged and C-terminally biotin acceptor protein (BAP)-tagged KRas was synthesised by GenScript. Piscataway (USA) was used to design KRas with no tag (KRas WT) and with 6 times histidine tag (KRas 6-His). The KRas WT DNA sequence was amplified by PCR (as detailed in section 2.2.1.1) with KRas forward and reverse primers in case of KRas with no tag and KRas 6His forward and reverse primers for KRas 6-His (Table 2.2). The PCR products were digested with *NheI* and *NotI* restriction enzymes at 37°C overnight (as described in section 2.2.1.3). The digested products were purified using Qiagen Gel and PCR Clean up kit (Qiagen) and ligated into pET-11a vector, which was also digested with *NheI* and *NotI* restriction enzymes (as detailed in section 2.2.1.4). These recombinant plasmids were produced in *E. coli* BL21 Star™ DE3 cell line. A single bacterial colony from LB-carbenicillin plate was used to inoculate a 7 ml LB-carbenicillin culture overnight at 37°C and 230 rpm. Then 500 ml LB- carbenicillin media was inoculated with 5 ml of overnight culture and grown at 37°C and 230 rpm to an OD₆₀₀ between 0.6–0.8. 0.1 mM IPTG was added to the culture and further grown overnight at 25 °C and 150 rpm. The cells were harvested by centrifugation at 4816 x g for 15 min. Cells were lysed in 50 mM Tris-Cl, 150 mM NaCl, 20 mM Imidazole, 5 mM MgCl₂, 5% w/v Glycerol, pH 7.5 supplemented with 0.1 mg/ml lysozyme, 0.1% w/v Triton X-100, 1x Halt protease inhibitor cocktail and 10 U/ml Benzonase for 20 min at 4 °C. The lysates were clarified by centrifugation at 4,816 x g for 20 min, 12,000 x g for a further 20 min, then incubated with 500 µl Ni²⁺-NTA resin at 4 °C for 1 h. Unbound proteins were removed by washing with 50 mM Tris-Cl, 300 mM NaCl, 20 mM Imidazole, 5 mM MgCl₂, 5% w/v Glycerol, pH 7.5. His-tagged

KRas protein was eluted with 50 mM Tris-Cl, 150 mM NaCl, 300 mM Imidazole, 5 mM MgCl₂, 5% w/v Glycerol, pH 7.5 and was quantified using BCA assay. Protein purity was analysed by Coomassie staining on 15% w/v SDS-PAGE. KRas sequence is shown in Appendix B.

2.2.3.3 SOS^{cat}

Human SOS1 catalytic domains (SOS1^{cat}) gene sequence (residues 564-1059) with an N-terminal His-tag was subcloned in kanamycin resistant pET-11a vector and expressed in *E. coli* BL21 StarTM DE3. 500 ml LB carbenicillin (100µg/ml) culture was induced with 0.5 mM IPTG and grown overnight at 25 °C and 150 rpm. Cells were harvested by centrifugation at 4816 x *g* for 15 min at 4°C. Cell pellets were lysed in 20 mM Tris-Cl pH 8, 300 mM NaCl, 20 mM imidazole, 5% w/v glycerol supplemented with 1% w/v Triton-x100, 1x halt protease inhibitor cocktail, 0.1 mg/ml lysozyme and 10 U/ml Benzonase nuclease. The cell lysate was centrifuged at 12,000 x *g* for 20 min, and the cleared supernatant was added to pre-washed Ni-NTA resin. SOS^{cat} was eluted using 20 mM Tris-Cl pH 8, 500 mM NaCl, 300 mM imidazole, 5% w/v glycerol and dialysed into 50 mM Tris-Cl pH 7.5, 100 mM NaCl. SOS^{cat} sequence is shown in Appendix B.

2.2.3.4 Affimer-KRas complex

The KRas wt DNA sequence (without His- and BAP-tag) from expression vector pET-11a was amplified by PCR (as detailed in section 2.2.1.1). The PCR products were digested with *Nhe I* and *Not I* restriction enzymes at 37°C overnight (as described in section 2.2.1.3). The digested products were purified using Qiagen Gel, and PCR Clean up kit (Qiagen) (as detailed in section 2.2.1.5) and ligated with pET-11a vector which was also digested with *Nhe I* and *Not I* restriction enzymes (as detailed in section 2.2.1.4). Ligated DNA was transformed into XL-1 Blue super-competent cells (see 2.2.1.6), and DNA was extracted by using mini-preparation (refer to section 2.2.1.7). Extracted DNA was sent for sequencing to confirm successful ligation. The correctly sub-cloned DNA was transformed into *E.coli* BL21 StarTM DE3 cell line for protein production, as described in section 2.2.3.2. Affimer was

produced and purified, as outlined in section 2.2.3.1. Ten milligrams of purified Affimer was mixed with excess KRas lysate and incubated on a roller for 2-3 h. Four hundred microliters of pre-washed Ni²⁺-NTA resin was added to Affimer-KRas lysate mixture and incubated on a roller overnight at 4 °C. Unbound proteins were removed by washing in 50 mM Tris-Cl, 150 mM NaCl, 5 mM MgCl₂, 1 mM DTT, 20 mM Imidazole, 5% w/v glycerol, pH 7.5. Affimer-KRas complex was eluted with 50 mM Tris-Cl, 150 mM NaCl, 5mM MgCl₂, 1mM DTT, 300 mM Imidazole, 5% w/v glycerol, pH 7.5. The eluted proteins were analysed by Coomassie staining on 15 % w/v SDS-PAGE. Affimer-KRas complex was further purified into 10mM Tris-Cl, 50 mM NaCl, 0.5mM TCEP, pH 8 by size exclusion chromatography, using HiPrep 16/60 Sephacryl S-100 column (GE Healthcare). They were analysed by Coomassie staining on 15 % w/v SDS-PAGE. The purified complex was concentrated using Vivaspin 6 5K MWCO centrifugal concentrator (Sartorius) to 12 mg/ml as determined by the BCA protein assay.

2.2.3.5 GST-thr-Raf1RBD protein expression

The GST-tagged Ras binding domain (RBD) of Raf1 in pGEX vector (Addgene, M.A, U.S.A) was used to transform BL21 StarTM DE3 cells for protein production. A single bacterial colony from LB-carbenicillin plate was used to inoculate a 5 ml LB media with 100 µg/ml carbenicillin overnight at 37°C 230 rpm. Then 500 ml LB-carbenicillin media was inoculated with 5 ml of overnight culture and grown at 37°C and 230 rpm to an OD₆₀₀ between 0.6–0.8. 0.5 mM IPTG was then added to the culture and further grown at 37°C at 230 rpm for 4 h. Cells were harvested by centrifugation at 4816 x g for 20 min. Cell pellets were lysed in 50 mM Tris-Cl, 150 mM NaCl, 1 mM DTT, 1% w/v Triton X-100, pH 7.5 supplemented with 1mg/ml lysozyme, 1x HaltTM protease inhibitor cocktail and 3U/ml Benzonase for 30-60 min at 4°C. The lysates were cleared by centrifugation at 4,816x g for 20 min then 12,000 x g for a further 20 min and the cleared cell lysates were used for subsequent assays.

2.2.4 Ras nucleotide loading

Before nucleotide loading, 60 μM Ras protein was desalted into nucleotide loading buffer (25 mM Tris-Cl, 50 mM NaCl, 0.5 mM MgCl_2 pH 7.5) using a Zeba™ spin desalting column (Thermo Fisher) equilibrated with buffer according to the manufacturer's instructions. MANT-GDP or GTP was added in 20-fold excess over Ras as well as 1 mM DTT and 5 mM EDTA in a final volume of 130 μl and incubated at 4 °C for 1 h. After incubation MgCl_2 was added in a 2-fold excess over EDTA and incubated for a further 30 min at 4 °C. Ras-mGDP or Ras-GTP was then desalted using a Zeba spin column into nucleotide exchange (NE) buffer (20 mM HEPES pH 7.5, 150 mM NaCl, 10 mM MgCl_2). Nucleotide loading was confirmed by native mass-spectrometry (refer section 2.3.3).

2.2.5 Guanine nucleotide exchange assay

Nucleotide exchange buffer (section 2.1.4) was supplemented with 0.4 mM GTP and 0.5 μM SOS^{cat} for experiments involving KRas. The Affimers were diluted with this buffer to make 20 μM stock solutions and quantified using BCA assay. Following which serial dilutions of the Affimers was carried out by diluting each new concentration of Affimer 2-fold with nucleotide exchange buffer supplemented with SOS^{cat} and GTP. A 1 μM stock of the KRas bound to fluorescent GDP analogue MANT-GDP (mGDP) protein was made by diluting the stock KRas-mGDP (20 μM) in nucleotide exchange buffer supplemented with 2 mM DTT. Solutions were incubated at 37°C for 10 min prior to the assay. The reaction was initiated by addition of Affimer/ SOS^{cat} /GTP solution to Ras-mGDP/DTT containing solution. Changes in fluorescence of KRas-mGDP were measured by a fluorescence spectrometer (Tecan Spark) in a Corning black, flat-bottomed, non-binding 384 well plate using 340/450 nm excitation/emission filter, every minute for 90 min. The data was then normalised to Ras mGDP-only control and fit a single exponential decay using Origin Pro software. The derived rates were normalised to Ras-Sos and Ras-mGDP only samples and fit to Hill equation ($y = \text{START} + (\text{END} - \text{START}) / (1 + 10^{(x - \text{IC}_{50})/n})$) from which the IC_{50} values were calculated (Kanie and Jackson., 2018).

2.2.6 Ras-Raf interaction assay

Glutathione magnetic agarose beads (Thermo Scientific) were blocked with 2x blocking buffer (Sigma) overnight at 4° C. Beads were then washed with Binding/Wash (B/W) buffer (125 mM Tris-Cl, 150 mM NaCl, 5 mM MgCl₂, 1 mM DTT, 0.1% w/v Tween-20, pH 8.0) and incubated with Raf-RBD-GST soluble cell lysate and GST lysate (negative control) for 1 h at room temperature on a roller. At the same time, 1 µg of KRas-GTP (in B/W buffer) was incubated with 60 µg/100 µl of Affimers (in PBS) or PBS (no Affimer control) for 1 h at room temperature on a roller. Beads were washed 3x with B/W buffer and mixed with KRas-Affimer solutions. The pulldown was performed on KingFisher Flex™ robotic platform, programmed to incubate Raf-RBD-GST bound beads with KRas-Affimers for 1 h at room temperature. This was followed by 4x washes with B/W buffer, 15 sec each and elution of pulled down proteins into SDS-PAGE sample buffer. Proteins were then analysed by western blot with anti-GST and anti-Ras antibodies (Table 2.4).

2.2.7 Affimer-Ras interaction assay

His Mag Sepharose™ Ni beads (GE healthcare) were blocked with 2X blocking buffer overnight at 4°C. Beads were incubated with 20 µg of Affimer K3/mutant K3 for 1 h at room temperature on a roller. After incubation beads were washed with Binding/Wash (B/W) buffer (125 mM Tris-Cl, 150 mM NaCl, 5 mM MgCl₂, 1 mM DTT, 0.1% w/v Tween-20, pH 8.0) 3X times and mixed with 100 µl of KRas lysate (no tag). The pulldown was performed on KingFisher Flex™ robotic platform, programmed to incubate Affimer bound beads with KRas WT / mutant KRas for 1 h at room temperature. This was followed by 4x washes with B/W buffer, 15 sec each and elution of pulled down proteins into SDS-PAGE sample buffer supplemented with 500 mM Imidazole. Proteins were then analysed by western blot with anti-Ras and anti-His antibodies (Table 2.4).

2.2.8 Protein crystallisation

2.2.8.1 Initial screening of Affimer K3-KRas

Crystallisation experiments were initiated with commercial sparse matrix screens, JCSG Core I-IV (Qiagen, Manchester, U.K). Using the NT8 drop setter robot (Formulatrix, M.A, U.S.A), the Affimer-KRas complex in 10 mM Tris-Cl, 50 mM NaCl, 0.5 mM TCEP, pH 8 at a protein concentration of 12 mg/ml was mixed in 1:1, 2:1 and 1:2 ratio of protein to a unique set of conditions from sparse matrix screens mentioned above. The sitting-drop vapour diffusion technique was utilised. The plates were sealed and stored at room temperature. Crystal formation was monitored with the Rock Imager (Formulatrix) using visible light. Also, the absorption of aromatic residues at 280 nm (UV) was employed in order to differentiate protein crystals from salt crystals.

2.2.8.2 Additional preliminary screening for Affimer K3-KRas

Additional crystallisation experiments were carried out with commercial crystal screens, Crystal screen 1 and 2 (Hampton, CA, U.S.A) and Wizard Classic 3 and 4 (Rigaku, WA, U.S.A). Using NT8 drop setter robot (Formulatrix), the Affimer-KRas complex in 10 mM Tris-Cl, 50 mM NaCl, 0.5 mM TCEP, pH 8 at a protein concentration of 24 mg/ml was mixed in 1:1, 2:1 and 1:2 ratio of protein to a unique set of conditions from sparse matrix screens mentioned above. The sitting-drop vapour diffusion technique was utilised. The plates were sealed and stored at room temperature. Crystal formation was monitored with the Rock Imager (Formulatrix) using visible light. In addition, the absorption of aromatic residues at 280nm (UV) was employed in order to differentiate protein crystals from salt crystals. Crystals were obtained in 2 M $(\text{NH}_4)_2\text{SO}_4$ pH5.6, 0.2 M K Na Tartrate and 0.1 M Trisodium citrate. Crystals were frozen in 75% w/v mother liquor and 25% w/v ethylene glycol.

2.2.8.3 Crystal diffraction and structure determination

X-ray diffraction data were collected using beamline ID30A-1 at the European synchrotron radiation facility, on a wavelength of 0.966 Å and at 100 K. The structure of KRas-K3 complex was solved by molecular replacement using Protein Data Bank (PDB) codes 4OBE for the KRas and 4N6T for the Affimer with the program Phaser (McCoy., 2007). Structures were refined using REFMAC5 (Murshudov et al., 2011), followed by iterative cycles of a manual model building using COOT (Emsley and Cowtan., 2004). Data collection and refinement statistics are summarized in Table 2.9. Data collection, processing and structure determination were carried out by Dr Chi Trinh.

Table 2.9 X-ray crystallographic data collection, processing and refinement statistics for Affimer K3-KRas complex.

Data set	AffimerK3-KRas
Source	ESRF ID30A-1
Wavelength (Å)	0.966
Resolution range (Å) *	54.09–2.06 (2.11–2.06)
Space group	$P2_1$
Unit-cell parameters (Å)	$a=73.1, b=39.5, c=113.1$ $\alpha=90.0^\circ, \beta=106.9^\circ, \gamma=90.0^\circ$
No. of observed reflections	113731
No. of unique reflections	38740
Redundancy	2.9 (3.0)
Completeness (%) *	99.7 (99.9)
$\langle I/\sigma(I) \rangle^*$	6.2 (1.3)
R_{merge}	0.09
$R_{\text{pim}} (\%) \text{ \textyen}^*$	6.3 (29.1)
Resolution range for refinement (Å)	54.16-2.06
R, R_{free}	0.236, 0.278 0.242, 0.284
R_{free} test set	1946 reflections (5.04%)
Wilson B factor (Å ²)	33.0
Anisotropy	0.532
L test for twinning	$\langle L \rangle = 0.50, \langle L ^2 \rangle = 0.34$
Estimated twinning fraction	0.013 for h, -k, -h-l
Average overall B factor (Å ²)	46.0
$F_0 F_c$ correlation	0.94
Total number of atoms	0.4298
Ramachandran analysis, the percentage of residues in the regions of plot (%) ‡	
Favoured region	95%
Outliers	0.4%
PDB code	6YXW

Values given in parentheses correspond to those in the outermost shell of the resolution range.

$$\S R_{\text{merge}} = \frac{\sum_{hkl} \sum_i |I_i(hkl) - \langle I(hkl) \rangle|}{\sum_{hkl} \sum_i I_i(hkl)}$$

* $R_{\text{p.i.m}}$ is the precision-indicating (multiplicity-weighted) R_{merge} relative to I^+ or I^- .

† R_{free} was calculated with 5% of the reflections set aside randomly.

‡ Ramachandran analysis using the program Molprobit. (Chen et al., 2010)

2.3.1.4 Initial screening of Affimer K3 apo

Crystallisation experiments were initiated with commercial sparse matrix screens, JCSG Core I-IV (Qiagen) and Morpheus screen (Molecular Dimensions, Sheffield, U.K). Using the NT8 drop setter robot (Formulatrix), the Affimer K3 in 10 mM Tris-Cl, 50 mM NaCl, 0.5 mM TCEP, pH 8 at a protein concentration of 80 mg/ml was mixed in 1:1, 2:1 and 1:2 ratio to a unique set of conditions from sparse matrix screens mentioned above. The sitting-drop vapour diffusion technique was utilised. The plates were sealed and stored at room temperature. Crystal formation was monitored with the Rock Imager (Formulatrix) using visible light. In addition, the absorption of aromatic residues at 280nm (UV) has been employed in order to differentiate protein crystals from salt crystals. Crystals were obtained in 0.1 M HEPES pH7.5 containing 30% v/v PEG 300 and 0.2M MgCl₂. Crystals were frozen in 75% w/v mother liquor and 25% w/v ethylene glycol.

2.3.1.5 Crystal seeding of Affimer K3 apo

Small, non-three-dimensional crystals are picked from initial JCSG screens. Seed stock is prepared by transferring a stack of crystals to micro seed bead tube, in which protein solution (20 mg/ml) used previously, for crystallisation screening is added. Once vortexed, three serial dilutions of seed stock were prepared in the protein solution. These serially diluted samples are used for crystal seeding using optimisation block (0.1 M Na phosphate citrate, 40% v/v PEG 300) prepared previously from JCSG screens. The plates were sealed and stored at room temperature. Crystal formation was monitored with the Rock Imager (Formulatrix) using visible light. In addition, the absorption of aromatic residues at 280 nm (UV) has been employed in order to differentiate protein crystals from salt crystals.

2.3.1.6 Crystal diffraction and structure determination of K3 Affimer

X-ray diffraction data were collected using beamline i24 at the Diamond synchrotron radiation facility, on a wavelength of 0.8 Å and at 100 K. The structure of K3 Affimer was solved by molecular replacement using Protein Data Bank (PDB) code 4N6T for the Affimer with the program Phaser (McCoy., 2007). Structures were refined using REFMAC5 (Murshudov et al., 2011) followed by iterative cycles of the manual model building using COOT (Emsley and Cowtan., 2004). Data collection and refinement statistics are summarized in Table 2.9. Data collection, processing and structure determination were carried out by Dr Chi Trinh.

2.3.1.7 Circular Dichroism (C.D) spectroscopy analysis

Far UV spectra were performed on Chirascan circular dichroism (C.D) spectrophotometer (Applied Photophysics, Surrey, U.K) at 20° C, using 1 mm path length cuvette and a scan speed of 5 nm/min. The spectra (190-260 nm) were recorded using 200 µl protein solution (at a concentration of approximately 0.2 mg/ml) and averaged over 3 repeats with a buffer (20 mM sodium phosphate) baseline subtracted. Dichroweb software (Whitmore and Wallace., 2004) was used for C.D and deconvolution analysis.

2.3.1.8 Native mass spectrometry

The KRas protein samples with and without GppNHp (non-hydrolysable GTP) were sent to the mass spectrometry facility in the University of Leeds. To confirm the mass of the KRas protein in its native/folded state bound to GppNHp, 1 mg/ml of protein was buffer exchanged in 200 mM ammonium acetate pH 7.5 and analysed by nano-electrospray ionisation mass spectrometry. Quadrupole orbitrap mass spectrometer was used for transmission of high *m/z* ions (Q-Exactive Plus, ThermoScientific). Ions were generated with a nanospray voltage of 1.5 kV; these were passed through the heated capillary tube (250 °C) into the mass spectrometer. Ions were trapped briefly (4 µs) in the source region to aid desolvation with a desolvation voltage

of -150 V. Ions then passed through the multipoles and quadrupole which was operated at wide transmission window (m/z 350-5000) to the c-trap from where packets of ions were injected into the orbitrap cell for mass analysis. The instrument was operated by Tune software version 2.10 provided with the instrument. Mass calibration up to m/z ~12000 was performed using 2mg/ml CsI clusters in IPA: water. Data was processed using Xcalibur Qual Browser v4.0.27.19 and UniDec v2.7.1.

Chapter 3

Biochemical characterisation of Ras specific Affimer

3.1 Introduction

Ras is a small GTPase that acts as a molecular switch in a variety of signalling pathways and is involved in various functions including regulation of cell proliferation, differentiation and survival (Young et al., 2009). Ras oscillates between inactive GDP bound (Ras-GDP) and active GTP bound form of Ras (Ras-GTP). Ras-GTP interacts with multiple effector proteins including Raf and PI3 kinases, leading to activation of cell proliferation and survival (Prior et al., 2012). Aberrant Ras signalling due to mutation results in tumorigenesis. For instance, single base missense mutation mostly occurring at codon 12, 13 and 61 results in impairment of GAP induced GTP hydrolysis of Ras. These mutations cause Ras to stabilise active GTP bound form leading to uncontrolled cell growth (Pei et al., 2018). Ras mutations occur in 30% of all human cancers and are well-established cancer drivers. There are three different isoforms of Ras namely, HRas, KRas and NRas and among them KRas is the most frequently mutated Ras isoform, accounting for 86% of all Ras mutations. Mutations in KRas are prevalent in cancers with high mortality rates which include pancreas (95% prevalence), colon (35% prevalence) and lung cancers (17% prevalence) (Omerovic et al., 2008; Stephen et al., 2014).

Despite Ras being an attractive pharmacological target, there are challenges in inhibiting Ras using current small molecule-based drug discovery techniques (Ostrem and Shokat., 2016; Stephen et al., 2014; Dang et al., 2017). The challenges include a lack of accessible pockets to which drug could bind with high affinity. Different strategies to directly inhibit Ras has met with recent success with the development of pharmacological agents that specifically target KRas^{G12C} mutant protein. This has led to a first direct Ras inhibitor to enter phase I clinical trials (O'Bryan., 2019). KRas^{G12C} mutation is present in 15% of all lung cancer and 32% of colon cancer patient samples (Sondka et al., 2018). However, G12C mutation accounts for only 11% of all KRas mutations. Development of small-molecule inhibitors against other KRas

mutations such as G12D (33.4%) and G12V (22.8%) using conventional screening have not been successful so far (O'Bryan., 2019).

To identify druggable pockets in KRas for small molecules to bind to, Affimer reagents that bind to KRas have been isolated (see preliminary results). Here, biochemical characterisation of Affimer K3 via a range of techniques like nucleotide exchange assays, circular dichroism, co-immunoprecipitation indicated that both variable regions in Affimer K3 are essential for binding and inhibition of KRas. Mutation of two variable regions of K3 to alanine revealed that most residues present in only one of the variable region has been shown to be involved in inhibition of KRas activity, while the second variable region could be involved in stabilisation of intramolecular interactions of K3 Affimer and trapping KRas in an inactive conformation. Taken together, these results suggest that Affimer K3 can be used as a tool to identify druggable binding pocket in “difficult to drug” KRas oncoprotein.

3.1.1 Preliminary results

In order to identify KRas binding reagents, the Affimer phage library (1.3×10^{10} clones) (Tiede et al., 2014) was screened against WT KRas-GDP. After multiple rounds of panning, ninety-six randomly selected clones were isolated that bound to KRas irrespective of nucleotide state and were tested via phage ELISA (Figure 3.1). The majority of isolated Affimers displayed little or no binding to control (Streptavidin only). Out of ninety-six clones, seven unique Affimer sequences were identified. The amino acid sequences of variable regions of these seven unique Affimers and number of appearances (defined as a number of occurrences of the clone) is shown in Table 3.1. This, therefore, demonstrated that Affimer can bind to both active and inactive conformations of KRas. The screening work was carried out by Dr. Christian Tiede.

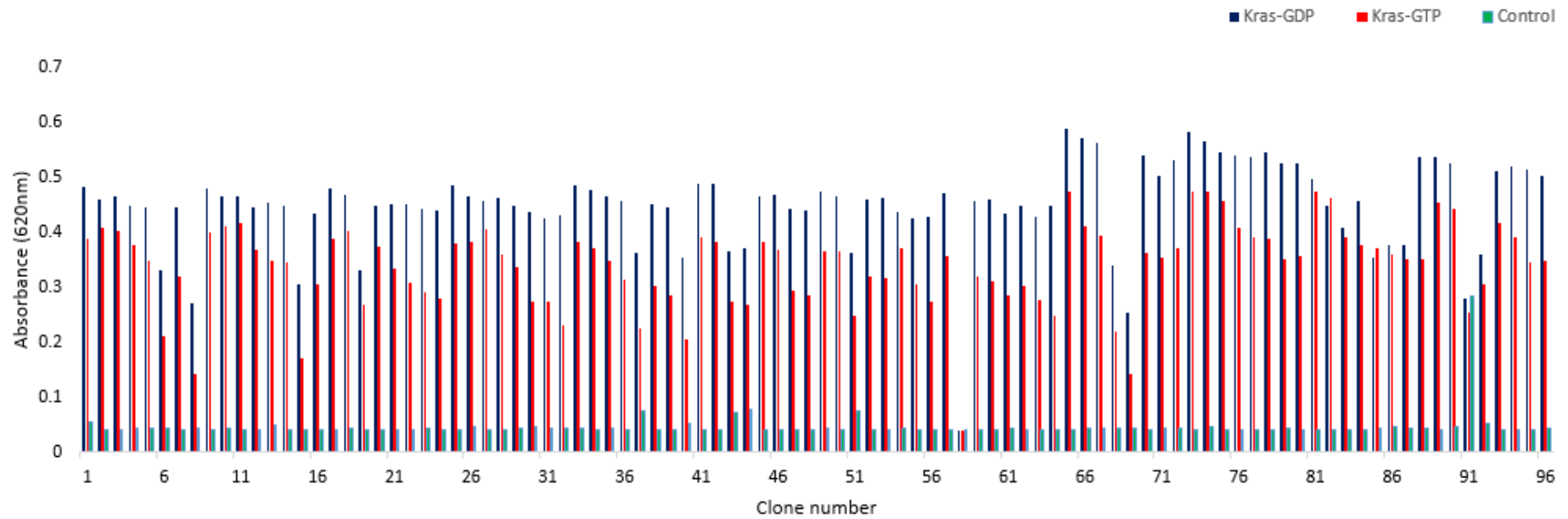


Figure 3.1 Phage ELISA for 96 Affimer clones isolated against KRas wild type. Bacteriophage expressing one Affimer clone was incubated with biotinylated wild type KRas GDP and GTP immobilised on streptavidin-coated plates. Plates were washed 3 times with 1xPBST, and the bound phage was detected with HRP conjugated anti-phage antibody and absorbance was measured at 620 nm. Streptavidin only wells were used as control.

Table 3.1 Amino acid sequences of variable regions and the number of appearances of seven unique Affimers against KRas wild type.

Affimer	Variable region 1	Variable region 2	Number of appearances
K3	HSIDIWYDF	KLNNSHTYK	80
K6	HFTPWFQRN	RIMVTDKMR	2
K37	FFYLWLAPG	AANSPMYHE	1
K19	QYNPWFQTN	VIHGTRWGN	5
K68	YPNPWYQVN	NMRVDMIVH	1
K69	WHFDYQQYN	RQLRMGSMN	1
K91	WDFSAWWKY	RNRYFKFPN	1

To identify the ability of Affimers to inhibit nucleotide exchange reaction- a process involved in the activation of Ras, nucleotide exchange assay was carried out (Figure 3.2). This assay is useful for screening small molecular inhibitors for drug discovery and high throughput targeting of KRas^{G12C} (Ostrem et al., 2013). For this assay, KRas was loaded with fluorescent N-Methylantraniloyl guanosine-5'-diphosphate (MANTGDP/mGDP). MANTGDP binds to KRas in the presence of EDTA. EDTA chelates magnesium ions, which form coordination bonds with β and γ phosphate of GTP and with GTPase (Kanie and Jackson., 2018). KRas-mGDP was incubated with GEF SOS^{cat}, excess of unlabelled GTP and a fixed concentration of Affimer. SOS^{cat} catalysed nucleotide exchange was monitored by a decrease in fluorescence intensity of mGDP upon nucleotide release of mGDP from KRas. The reaction was monitored for 90 minutes, and data was normalised to Ras only control to account for well to well variability and fit to a single exponential decay model (Kanie and Jackson., 2018).

The observed results demonstrated the ability of seven unique Affimers (as shown in Table 3.1) to inhibit SOS^{cat} mediated nucleotide exchange reaction in a time-dependent manner. Affimer K3, K6 and K37 displayed the most potent inhibition of the reaction with fluorescence intensity (FI) between 1-0.95 very close to WT KRas-mGDP control (black square dots) (this work was carried out by Kevin Tipping). While Affimer K19, K68 showed a modest effect with FI values between 0.7-0.75 and Affimer K69, K91 demonstrated the weakest inhibition with FI values at 0.4 very close to SOS^{cat} control (red circle dots) (Figure 3.3). This FI values suggests that three Affimer clones, namely K3, K6, K37, have the most potent inhibition of nucleotide exchange reaction due to consistently high fluorescence values similar to WT KRas-mGDP control over a 90-minute time interval. These three Affimers were carried forward for additional biophysical and structural characterisation.

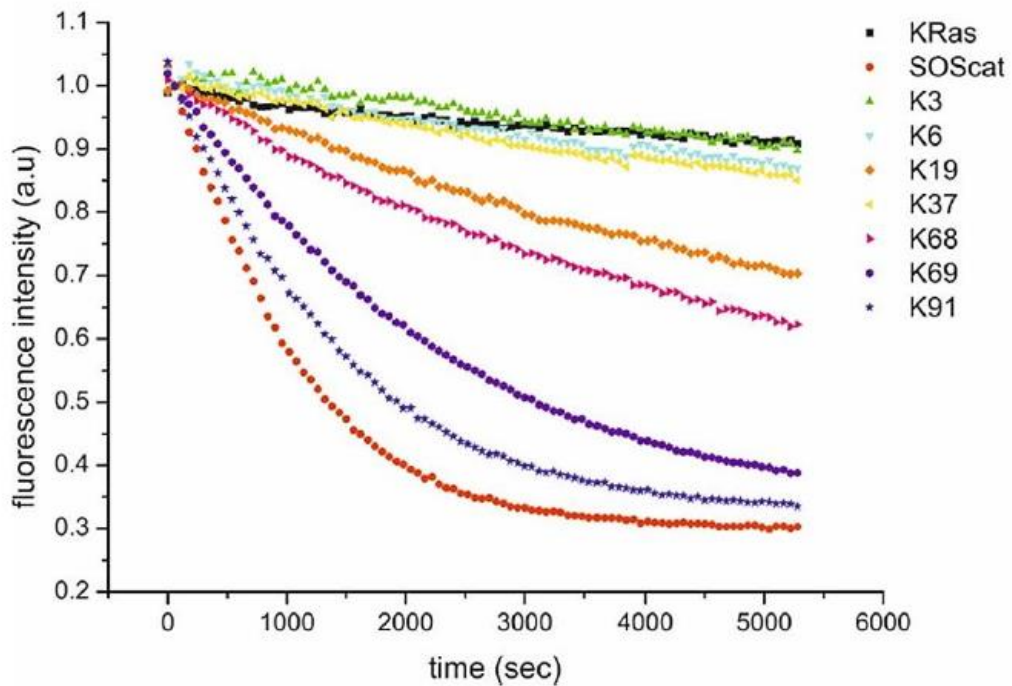


Figure 3.3 KRas binding Affimers inhibited SOS catalysed nucleotide exchange reaction. Wild type KRas protein, loaded with fluorescent nucleotide mGDP (Black squares) exhibits a constant high FI value of 1 and used as a positive control. Another control is a mixture of KRas-mGDP and SOS^{cat} (red circles), in which there is nucleotide release of mGDP and binding of GTP indicating a consistent decrease in FI value over time. Different KRas binding Affimer clones (coloured shapes) are evaluated with FI values between these two controls. FI values were measured every 60 seconds for 90 minutes. Each Affimer inhibited nucleotide exchange reaction with different potencies (Haza., 2019).

Since Ras isoforms have a high degree of sequence homology and activate a common set of upstream and downstream effectors (Castellano and Downward, 2011), WT HRas was tested with KRas binding Affimers in the nucleotide exchange assay. It was observed that Affimer K3, K6 and K37 were also capable of inhibiting nucleotide exchange of HRas. Affimer K6 and K37 did not show any isoform specificity as evidenced by similar inhibitory potencies towards WT HRas as toward WT KRas (Table 3.2). Interestingly, significantly lower inhibition of HRas ($IC_{50} \sim 2.6 \mu M$) in comparison to KRas ($IC_{50} \sim 145 nM$) was observed with K3. This suggests that K3 displayed potent inhibition of KRas in an isoform-specific manner.

Table 3.2 – Calculated IC₅₀ values of K6 and K37 Affimers for KRas and HRas WT. Values were calculated from Hill equation, to which data were fitted and represent the average of three biological repeats (n=3). Error bars ± represent standard error of the mean (SEM).

Affimer	IC ₅₀ values (nM)	
	KRas WT	HRas WT
K3	144± 94	2585± 335
K6	594 ± 271	389 ± 187
K37	697 ± 158	626 ± 320

To analyse the effect of Affimers on three most frequently mutated KRas mutations such as KRas^{G12D} (35%), KRas^{G12V} (24%) and KRas^{Q61H} (13%), nucleotide exchange assay was carried out as previously described. Affimer K3 showed similar inhibitory potencies towards WT KRas and G12D and G12V mutants, but it is significantly less effective at inhibiting nucleotide exchange on Q61H mutant. Additionally, Affimer K3 showed higher IC₅₀ values than K6 and K37 Affimer to inhibit G12D and G12V mutants. This, therefore, indicated K3 not only displayed isoform specificity but also capable of inhibiting KRas mutants. Altogether, these findings have established the ability of Affimers to modulate Ras activation by nucleotide exchange. This work was carried out by Katarzyna Haza.

Table 3.3 – Calculated IC₅₀ values of K3, K6 and K37 Affimers for oncogenic KRas mutants. Values were calculated from Hill equation, to which data were fitted and represent the average of three biological repeats (n=3). Error bars represent ± SEM.

Affimer	IC ₅₀ value (nM)		
	KRas G12D	KRas G12V	KRas Q61H
K3	144 ± 40	176 ± 115	3005 ± 865
K6	185 ± 46	571 ± 148	532 ± 165
K37	356 ± 161	640 ± 253	1075 ± 651

3.2 Results

To further characterise and understand binding and inhibition of KRas by K3 Affimer, nucleotide exchange assay and a range of biophysical techniques were used.

3.2.1 Affimer K3 inhibits SOS^{cat} mediated nucleotide exchange

For examining the inhibitory function of Affimer on KRas, nucleotide exchange assay was carried out using KRas, SOS^{cat} and Affimer K3. Protein expression and purification of Affimer K3 and KRas was carried out in *E. coli* BL21 (DE3) StarTM competent cells and purified using Ni²⁺ ion affinity chromatography (Ni²⁺-NTA) as described in section 2.2.3.1 and 2.2.3.2. Eluted fractions were analysed by SDS-PAGE and Coomassie staining, which indicated purification of proteins with a molecular weight of 12 kDa for Affimer (Figure 3.4 A) and 21 kDa (Figure 3.4 B) for KRas, respectively. In the case of Affimer, $A_{280\text{ nm}}$ was measured using a Nanodrop spectrophotometer (section 2.2.1.8) for each elution, and these values were used to calculate protein concentration using Beer-Lambert Law. For KRas, BCA assay was carried out to estimate the total protein concentration in elution buffer (refer section 2.1.4). The typical yields of purified proteins ranged from 20-30 mg/L culture for Affimer K3 and 1-5 mg/L for KRas.

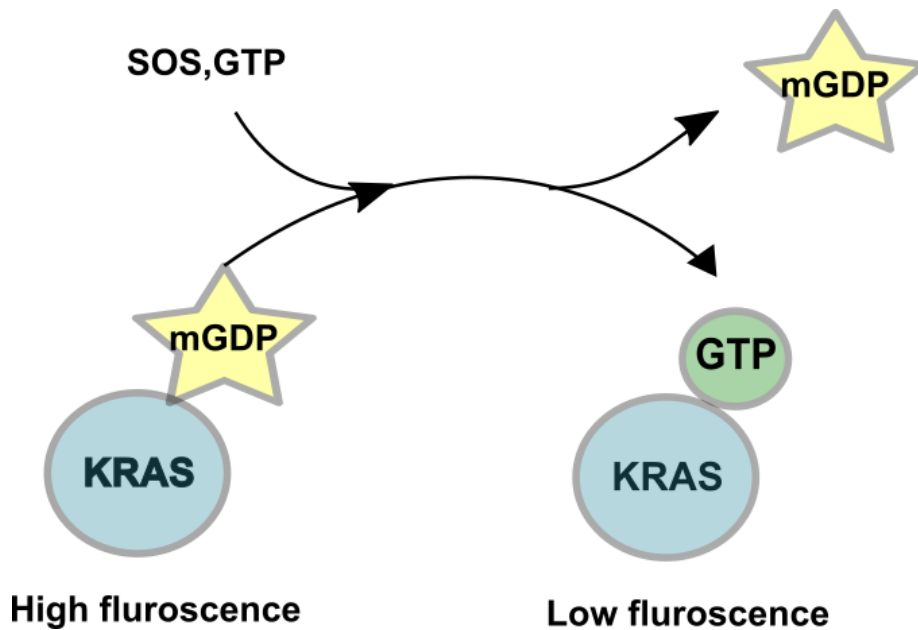


Figure 3.2 Diagram of nucleotide exchange assay. KRas (blue), loaded with fluorescent MANTGDP/mGDP (yellow) was incubated with GEF SOS and excess of unlabelled GTP (green). Over 90-minute time interval, nucleotide exchange was monitored as evidenced by a decrease in fluorescence intensity upon nucleotide release of mGDP from KRas, followed by binding to GTP.

However, in case of SOS^{cat} , conditions for protein production were different from Affimer and KRas and is described in section 2.2.1.6. The recombinant proteins were purified from bacterial cell lysates using nickel ion affinity chromatography. Eluted fractions were analysed by SDS PAGE and Coomassie staining, which indicated purification of proteins with a molecular weight of 59.2 kDa for SOS^{cat} (Figure 3.4 C). For determination of SOS^{cat} protein concentration, a BCA assay was carried out. The typical yields of purified SOS^{cat} ranged from 4-10 mg/L culture.

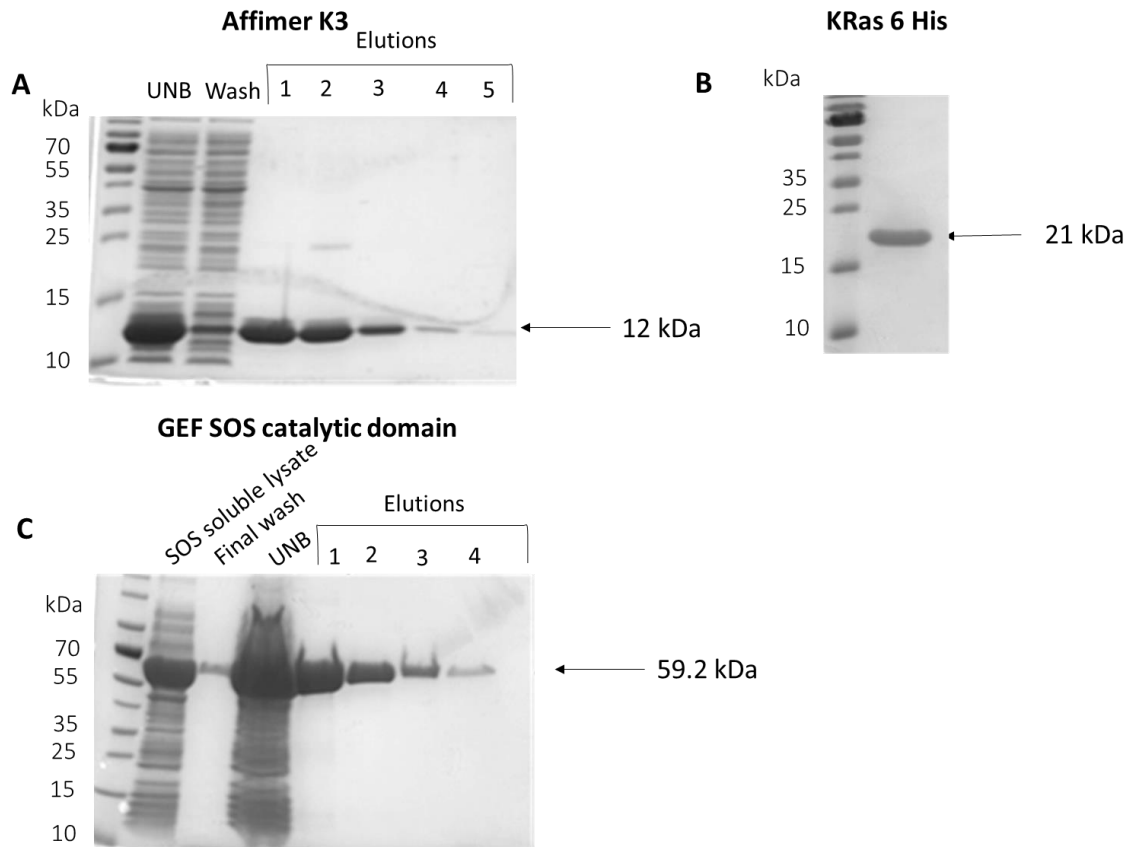


Figure 3.4 Production and purification of Ras, Affimer K3 and SOS for nucleotide exchange assay **A.** Following IPTG induced expression in *E. coli* BL21 StarTM DE3 cells, Affimer K3 (12 kDa) was purified by His-tag affinity chromatography and eluted proteins were identified by coomassie staining, which indicated 95% or more purity of the samples. **B.** Following IPTG induced expression in BL21 StarTM DE3 cells, the whole-cell lysate was analysed by Coomassie staining, which demonstrated efficient expression of KRas (20.5 kDa) **C.** SOS1 catalytic domain (SOS^{cat}) (59.2 kDa) was produced and purified as mentioned in A. and analysed by Coomassie staining, which indicated efficient purity for downstream assays.

To understand the effectiveness of Affimer K3 as a potent inhibitor of nucleotide exchange of WT KRas, a range of Affimer K3 concentration from 5 nM to 10 μ M was titrated against 1 μ M KRas. Dose-dependent inhibition of nucleotide exchange reaction was observed with the highest Affimer concentration displaying the highest level of inhibition. From the obtained dose-response curve, the concentration of Affimer K3 required for 50% inhibition of the reaction was calculated to be 200 ± 6 nM (Figure 3.5). The

value calculated by Katarzyna Haza was 144 ± 94 nM for K3 WT (Table 3.2). However, the variability within the sample is high i.e. $+94$ nM.

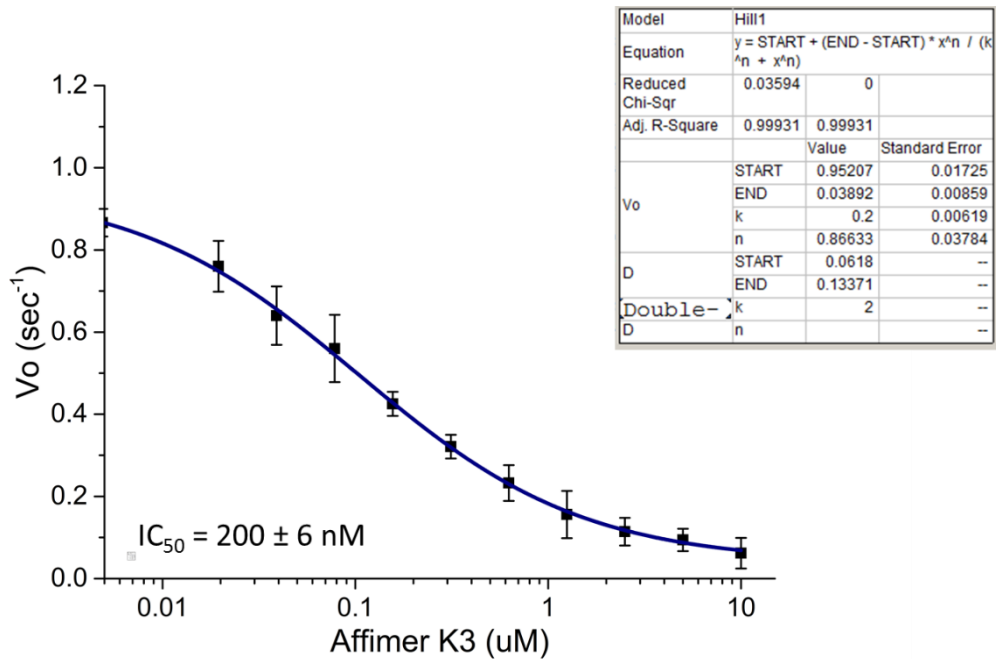


Figure 3.5 Affimer K3 inhibits nucleotide exchange on wild type KRas. Dose-response curved for Affimer K3 demonstrating inhibition of nucleotide exchange of wild type KRas. The initial nucleotide exchange reaction was plotted against Affimer concentrations of 5 nm-10 μ M and fitted to Hill model, which was used to calculate IC_{50} values. The result is representative of three biological replicates ($n=3$). IC_{50} of K3 Affimer was found to be 200 ± 6 nM.

3.2.2 Affimer K3 inhibits the interaction of Ras with Ras binding domain of CRaf

One of the strategies to block Ras function involves inhibiting Ras-effector interactions with a number of previously reported Ras inhibitors demonstrating impairment of this interaction (Keeton et al., 2017). Therefore, the capabilities of Affimers to inhibit Ras-Raf interaction were also investigated. This was done by pulldown assay as described in section 2.2.3.4, with recombinant Ras binding domain (RBD) of CRaf (McGee et al., 2018). Since K3, K6, and K37 Affimers have been identified as the potent inhibition of nucleotide exchange reaction; these were further investigated for Ras-Raf inhibition.

Before the Ras-Raf inhibition assay, KRas was loaded with GppNhp (a poorly hydrolysable GTP analogue), and its binding to KRas was verified using native mass spectrometry (refer section 2.3.3) (Leney and Heck., 2017). Deconvolution of native mass spectra of WT KRas (20536 Da) (Figure 3.6 A) and KRas loaded with GppNhp (21031 Da) was compared. The spectra show a mixture of both wild type as well as GppNhp bound KRas (Figure 3.6 B). There is a shift of 495 Da indicative of the molecular weight of GppNhp minus the phosphate group. To analyse the effect of Affimer K3, K6 and K37 on KRas-Raf interaction, immunoprecipitation assay was performed as described in section 2.2.6. Affimer containing alanine residues in the variable regions and Dynabeads™ only sample were used as controls (Figure 3.7 A).

The 'no Affimer' and 'alanine Affimer' sample successfully pulled down KRas-GTP with RBD-GST (Figure 3.7A). GST only sample was used as a negative control since Raf1-RBD has a GST tag. A band representing KRas was not present on the gel, indicating specific binding to RBD, and not to the GST tag. Pre-incubation of K3 with KRas blocked the KRas-RBD interaction almost completely, as demonstrated by a faint band on the gel in comparison to the amount of KRas-GTP obtained using alanine Affimer (Figure 3.7 B). Affimer K6 and K37 also significantly impaired this interaction, although much less extent than K3. These findings suggest that Affimer K3 has a dual mode of inhibition of KRas i.e. it inhibits nucleotide exchange to GTP and at the same time inhibits downstream effector such as Ras, trapping KRas in inactive GDP bound state.

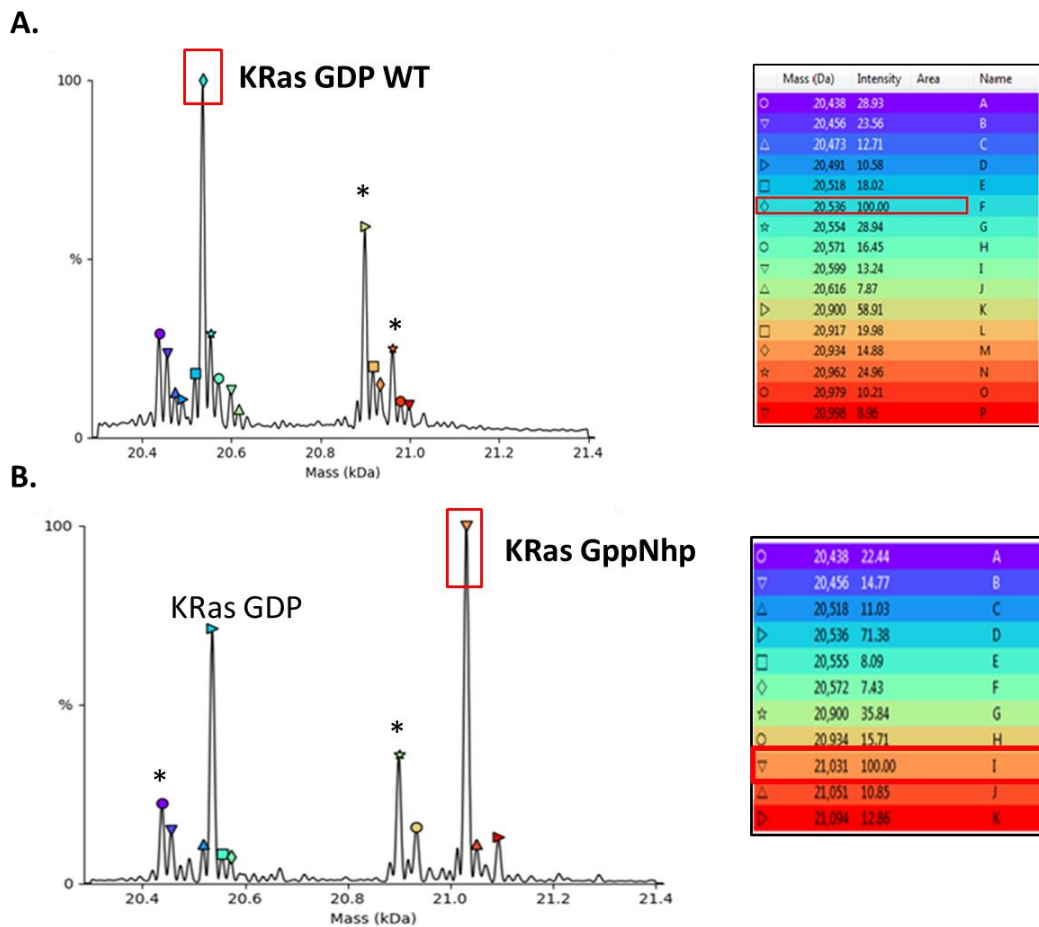


Figure 3.6 Deconvolution of native mass spectra. Deconvolution of electrospray ionisation mass spectrometry (ESI-MS) showing the presence of **A.** KRas WT and **B.** GppNhp (non-hydrolysable GTP) bound to KRas. Highlighted red boxes show mass (Da) of WT Ras (M.W-20536 Da) and GppNhp bound Ras (M.W- 21031Da), indicating a shift in spectra when GppNhp is added to KRas. Asterisk (*) indicates bound sodium and magnesium adducts. Based on mass/charge (m/z) ratio, different symbols have been assigned to differentiate each peak with the lowest mass (kDa) assigned blue and highest red.

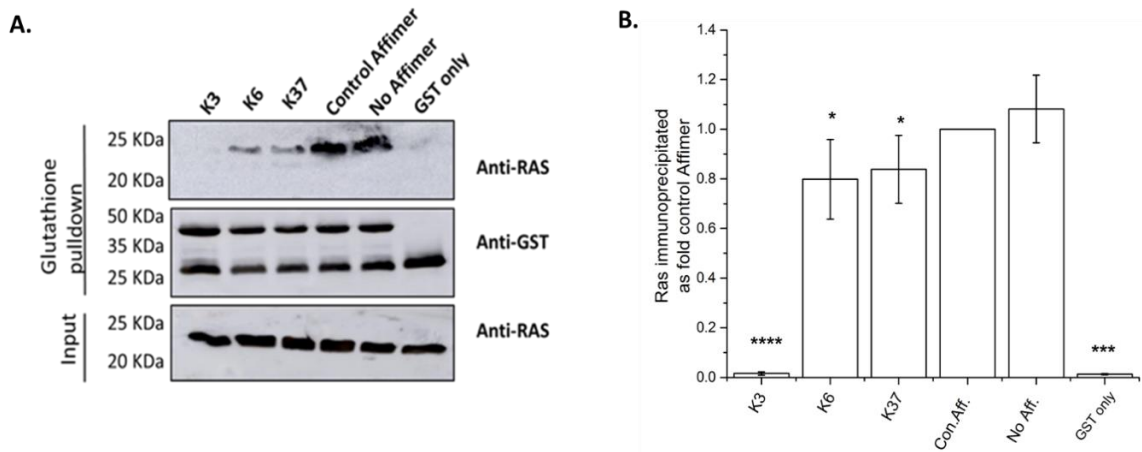


Figure 3.7 Immunoprecipitation of KRas with GST Raf1RBD is inhibited by Ras binding Affimers. GST tagged Raf1RBD was added to KRas-GTP, which was pre-incubated with Affimers. RBD-GST was precipitated on glutathione Dynabeads and pulled down proteins were analysed by western blot with anti-Ras and anti-His antibodies. **A.** Western blot analysis of precipitated proteins were analysed using anti-Ras and GST antibodies both before (input) and after pull-down assay (output). Alanine Affimer is used as a control. Affimer K3, K6 and K37 significantly inhibited KRas-RBD interaction, as demonstrated by reduced pull-down of KRas-GTP in comparison to no Affimer sample. GST only was used as a negative control. **B.** For densitometry analysis, relative KRas-GTP levels from the pull-down assay were normalised to levels of Alanine Affimer (control Affimer). Negligible or very low amounts of Ras are present for KRas, which is at a similar level to GST only control. Results are representative of three biological replicates (n=3). Error bars denote \pm SEM. Error bars are \pm SEM. p<0.05 (*), p<0.01 (**), p<0.001 (***) and p<0.0001 (****). Con.Aff = Control Affimer; No Aff. =No Affimer.

3.2.3 Both variable regions of Affimer K3 are involved in binding and inhibition of KRas

To investigate which variable region of K3 Affimer are essential for binding and inhibition of KRas, each variable region (VR1 and VR2) was replaced by three alanine residues, producing two variants of K3 - K3 Δ VR1 and K3 Δ VR2. These mutants have been created by a technique called splicing by overlap extension (SOE) as described in section 2.2.1.10 (Thornton., 2016). Four PCR products were used to make the constructs (Figure 3.8A). The first PCR product contained the K3 sequence encoding the VR1, the second PCR product contained alanine Affimer VR2 sequence. The third PCR product contained alanine VR1 sequence, while the fourth PCR product contained K3 VR2 sequence. These PCR products of approximately 190 (PCR I/III) and 200 bp (PCR II/IV) length (Figure 3.8B), were then subjected to SOE as described in chapter 2.2.1.10, to splice the two fragments together (PCR I+II and III+IV). Agarose gel analysis indicated a single band in which two products of 390 bp in size were conformed, indicating successful splicing of two PCR fragments (Figure 3.8B). The product encoding K3 Δ VR1 and of K3 Δ VR2 was ligated in pET11a bacterial expression vector (refer section 2.2.1.6). The replacement of K3 Δ VR1 and Δ VR2 in each plasmid DNA was confirmed by sequencing.

K3 Δ VR1 and K3 Δ VR2 mutant proteins were produced and purified as described in section 2.2.3.1 and ability to bind and inhibit KRas interactions were evaluated using pulldown assays (refer section 2.2.9). Either, wild type Affimer K3, K3 Δ VR1 or K3 Δ VR2 mutant proteins were immobilised on Pierce[®] Ni-NTA magnetic Agarose beads and incubated with soluble KRas protein (no tag). After washing the beads, the eluted Ras-Affimer complex were analysed by western blotting to visualise the presence of Ras using an anti-Ras antibody and Affimer using an anti-His antibody. The wild type K3 Affimer pulled down KRas as demonstrated by a thick band when stained with Ras antibody (Figure 3.9). In contrast, no bands were observed for K3 Δ VR1 and K3 Δ VR2, therefore indicating no binding to KRas. Likewise, Alanine Affimer (control

Affimer) did not pull down KRAs, indicating any pulled down proteins is due to specific interaction with KRAs (Figure 3.9).

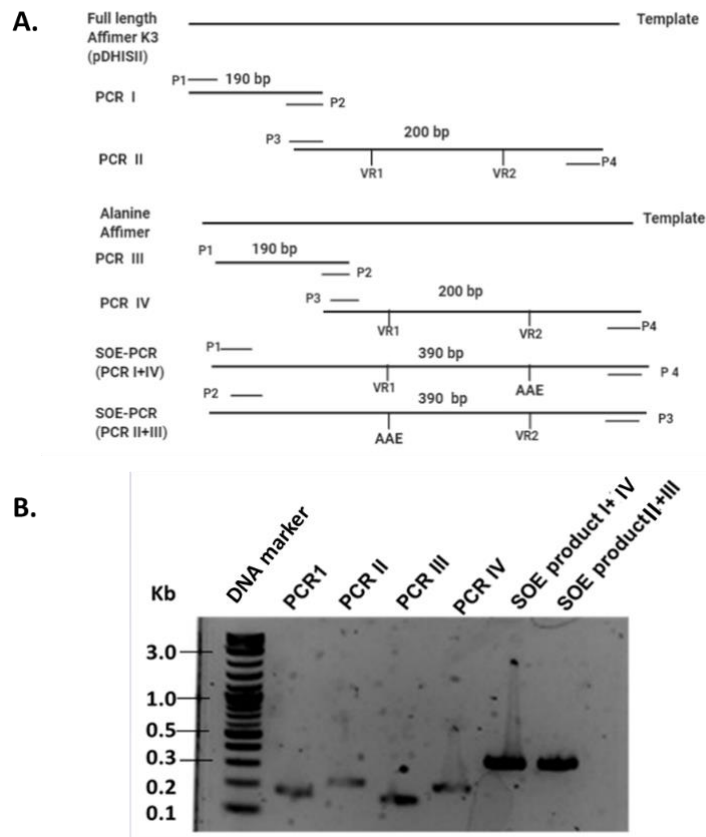


Figure 3.8 Cloning strategy to create mutants with deleted Affimer K3 variable region 1 or 2. A. Schematic diagram outlining two templates – Full-length K3 Affimer and Alanine Affimer with amplification of VR1 of K3 and Alanine Affimer VR2 and vice versa and splice overlap extension product of two PCR products I + IV and II+III. Primers P1, P2, P3 and P4 sequences are mentioned in table 2.2 **B.** Agarose gel analysis of the four PCR products demonstrating four bands of approximately 190 and 200 bp in size. Splice overlap extension of I+IV and II+III generate two PCR clones encoding K3 Δ VR1 and K3 Δ VR2 mutants respectively of approximately 390 bp in size. This indicates successful splicing of the PCR products. PCR1= P1+P3, PCR2=P2+P4 using K3 Affimer sequence as template, PCR3= P1+P3, PCR4= P2+P4 using Alanine Affimer sequence as template.

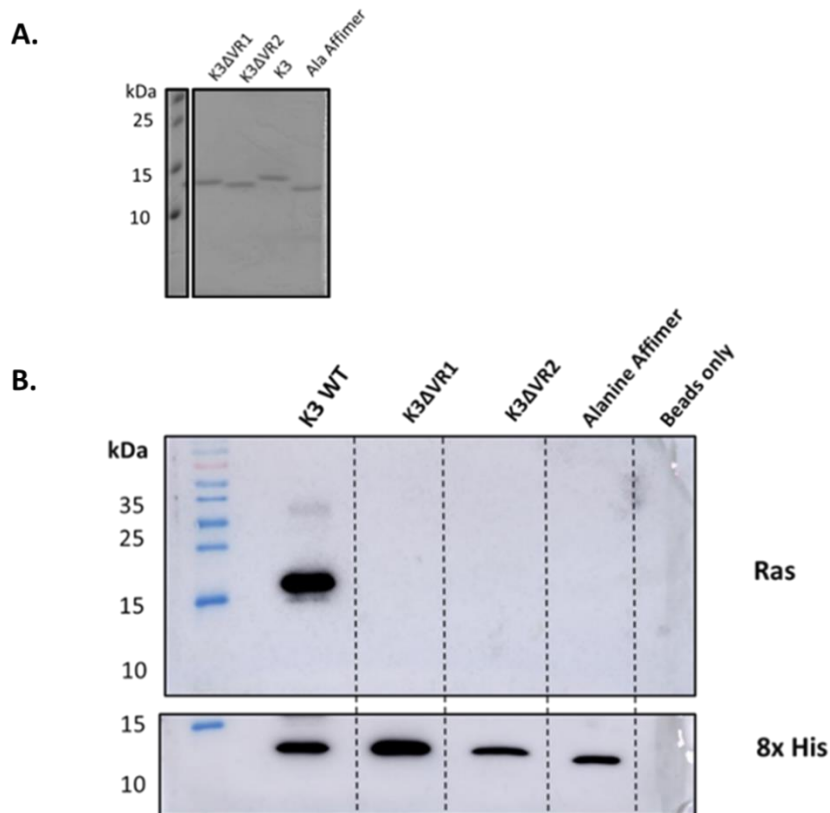


Figure 3.9 Binding studies of Affimer K3, K3 Δ VR1 and K3 Δ VR2 on KRas.
A. 15% SDS-PAGE analysis of K3 Δ VR1, K3 Δ VR2, K3 and Alanine Affimer proteins prior to binding studies **B.** Pierce® Ni-NTA agarose magnetic beads were pre-incubated with 8x His tagged Affimer K3 and deleted VR1 and VR2 mutants. The KRas-Affimer complex was precipitated and pulled down proteins were analysed by western blot with anti-Ras and anti-8x His antibodies. Results are representative of three biological replicates (n=3).

Next circular dichroism (CD) was carried out to check the stability and folding after substitution of variable regions to alanine residues (K3 Δ VR1 and K3 Δ VR2). Secondary structure of mutant Affimer K3 proteins, as well as wild type K3 protein used in the pulldown assays, were analysed by CD in far UV spectra (190-240 nm). CD spectra of individual mutant proteins and wild type when overlapped shows mean residue ellipticity (MRE) variation around 2 ± 1 % (Figure 3.10). MRE is a unit specific for proteins and accounts for molar ellipticity of individual amino acid residues instead of whole protein, allowing for easy comparison of proteins with different molecular weights (Greenfield., 2006). This, therefore, indicates that structural integrity of Affimer mutants is stable even after substitution of alanine in each variable region.

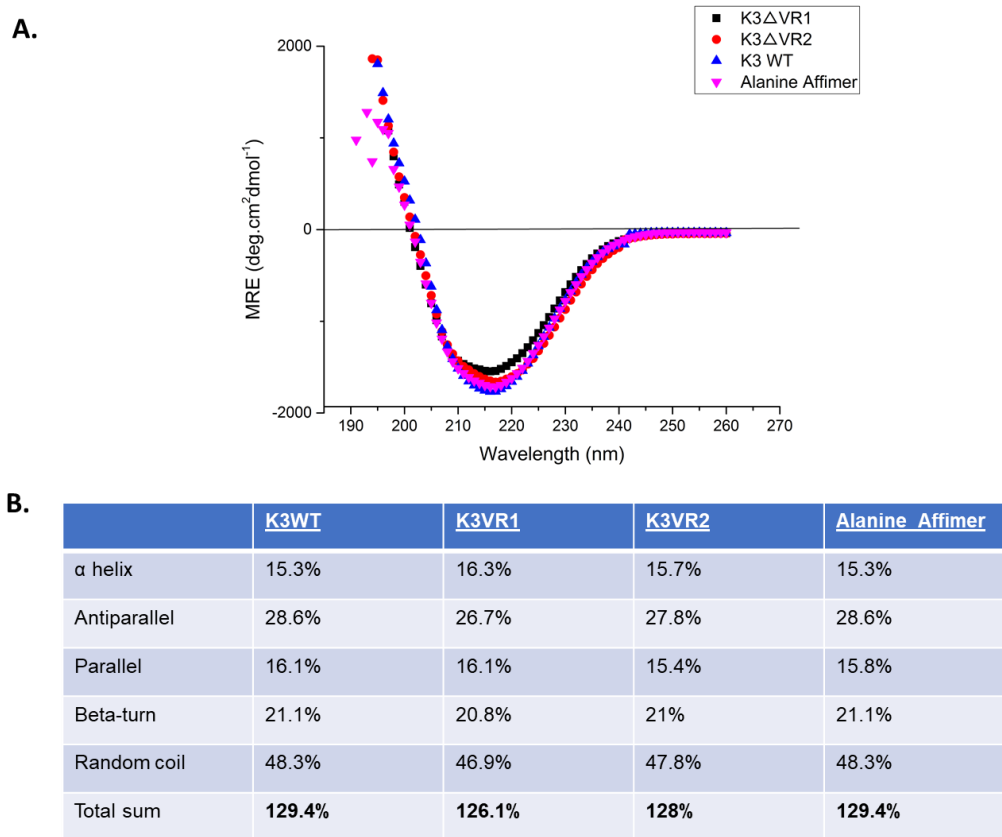


Figure 3.10 Circular dichroism analysis of K3 WT, K3ΔVR1 and K3ΔVR2

A. Circular dichroism spectra (far ultraviolet region [190-240 nm]) of purified K3 WT, K3ΔVR1 and K3ΔVR2 proteins (see Figure 3.9A) at 0.2 mg/ml concentration in 20mM sodium phosphate buffer solution. The molar ellipticity values of spectra showed similar ellipticity values indicating no change in the structural integrity of proteins. **B.** Deconvolution of CD spectra suggests 15-16% α helix, antiparallel β sheets around 27-28%, which is similar to spectra observed with Adhiron scaffold. Overall variation in spectra between mutants and wild type K3 Ras was found to be around 2%. Results are representative of three biological replicates (n=3). Deconvolution and CD analysis were carried out using Dichroweb software.

Next, the functional effect of VR1 and VR2 deletion of K3 was tested using the nucleotide exchange assay (as described in section 2.3.1). In this assay, Affimer protein concentration was calculated as per section 2.2.2 and confirmed by running 0.2 mg/ml of each Affimer protein on an SDS PAGE gel

(Figure 3.11 A). Incorrect protein concentrations can lead to a significant difference in the association rate constant (k_a) and affinity (K_D), which can eventually affect inhibitory concentration (IC_{50}) (Pol, 2010). Fluorescence intensity (F.I) (a.u) of K3 and KRas mGDP was 1, indicating complete inhibition of nucleotide exchange activity. However, FI values for mutant K3 Δ VR1 and K3 Δ VR2 were around 0.65-0.7 at the same level as SOS^{cat} (Figure 3.11 B). The assays showed the inability of K3 Δ VR1 and K3 Δ VR2 to inhibit nucleotide exchange on KRas, even when the highest Affimer K3 concentration of 50 μ M was used. Altogether, these findings established that both VR1 and VR2 of Affimer K3 are expected to bind and inhibit KRas (Figure 3.8).

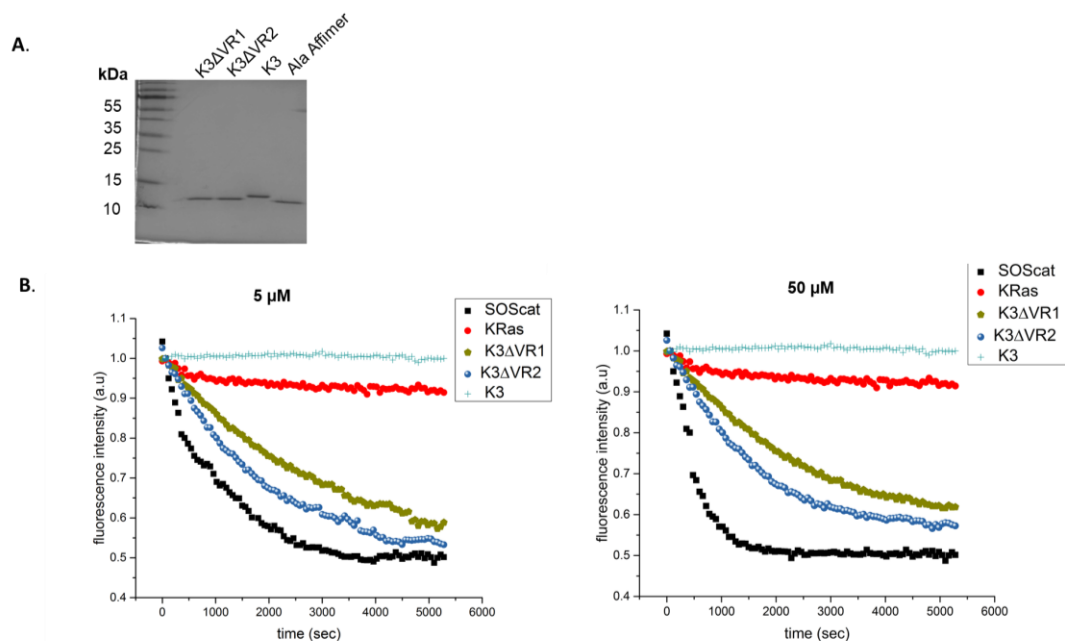


Figure 3.11 Nucleotide exchange assay for K3WT, K3 Δ VR1 and K3 Δ VR2

A. Protein expression and purification of K3 WT, K3 Δ VR1 and K3 Δ VR2 was carried out and was run on a 15% SDS-PAGE indicating correct protein concentration. **B.** Nucleotide exchange assay on WT Affimer K3 and K3 Δ VR1 and K3 Δ VR2 with protein concentration ranging from 5 μ M and maximum 50 μ M show that both VR1 and VR2 are essential for KRas binding. Results are representative of two biological replicates (n=2).

3.2.4 Identification of Affimer K3 residues involved in binding and inhibition of KRas

One of the major goals in understanding cellular processes is a detailed understanding of how protein-protein interactions work (De Las Rivas and Fontanillo., 2010). The three-dimensional protein structures provide information about their binding epitopes. However, they do not elucidate the functional roles of individual residues within the epitope that make energetic contributions to the binding interaction (Weiss et al., 2000). One strategy for the elucidation of functional epitopes to understand protein structure and function is site-directed mutagenesis. Alanine scanning mutagenesis is the most widely used technique in systematically mapping functional binding epitopes (Weiss et al., 2000). The substitution of variable regions to an alanine residue removes all the side chain atoms past the β carbon. The effects of individual alanine mutations can be used to infer the role of individual side chains (Gauguin et al., 2008).

QuikChange site-directed mutagenesis was used to replace each of the Affimer K3 variable residues to alanine, to determine the contributions to the binding interaction with KRas (Kunkel., 1985). The QuikChange method allows efficient site-directed substitution, deletion or insertion in a one-step procedure (Kunkel., 1985). The mutagenesis was performed as described in section 2.2.2 by Dr Katarzyna Haza. Mutagenesis was confirmed by sequencing, which demonstrated successful substitution of each residue.

Affimer K3 alanine mutants were produced and purified, as described in section 2.2.2 (see Figure 3.12).

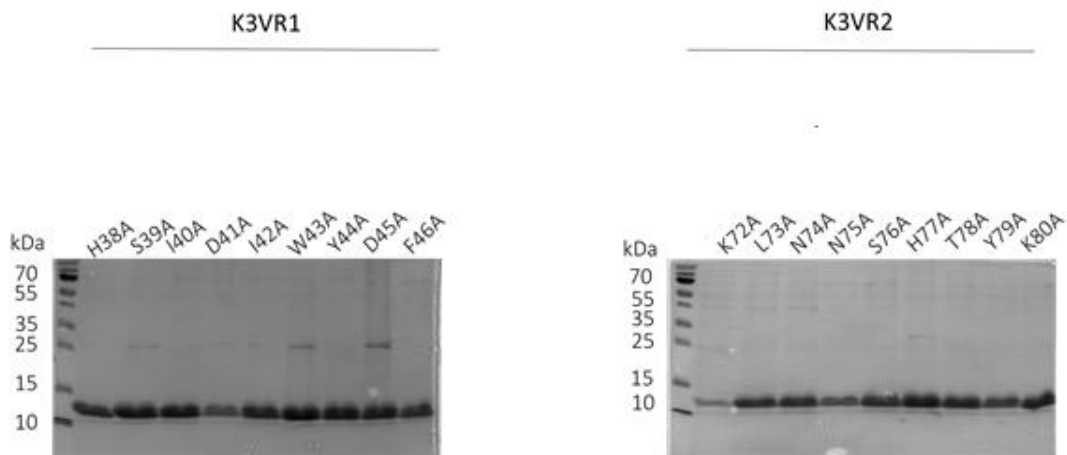


Figure 3.12 Expression and purification of K3 alanine mutants. Following IPTG induced production in BL21 Star™ DE3 cells K3 variable region 1 (VR1) alanine mutants and K3 variable region 2 (VR2) mutants were purified by His tag chromatography. These were eluted in imidazole buffer and dialysed in 1x PBS buffer and analysed by Coomassie staining, which indicated 90% or more purity of samples.

To identify which residues are involved in binding and inhibition of KRas, Ras-Affimer immunoprecipitation assay was performed. As visualised in Figure 3.13 VR1 residues I40, D41, I42, W43, Y44 and D45 when mutated to alanine had the most significant effect on binding to KRas as seen by no presence of Ras on western blot. This, therefore, demonstrated that these residues are mostly involved in binding and inhibition of KRas. Mutations of residues L73 and K80 to alanine had a moderate effect on binding to KRas, suggesting that these could be involved in facilitating the binding of Affimer K3 to KRas. These findings correlated with K3 Δ VR1 and K3 Δ VR2 mutants' findings in section 3.2.4, suggesting that both VR1 and VR2 of Affimer K3 are involved in binding.

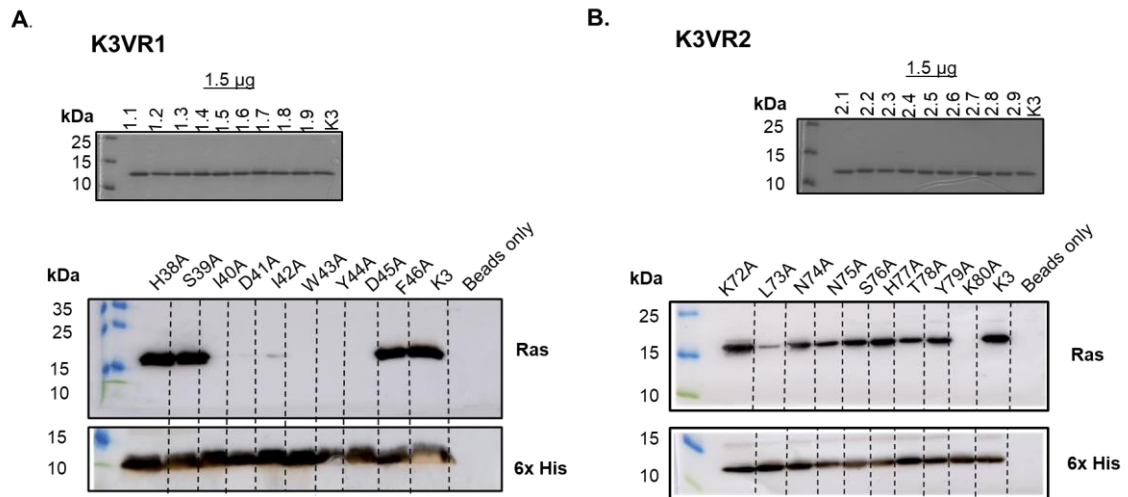


Figure 3.13 Effect of Affimer K3 variable regions alanine mutants on the ability to bind to KRas. **A.** After calculation of Affimer alanine mutant concentration, equal quantities of mutant proteins of K3VR1 were run on a gel to verify correct protein concentration. K3VR1 alanine residues have been labelled 1.1-1.9. For Ras-Affimer interaction assay, Pierce® Ni²⁺-NTA agarose magnetic beads were pre-incubated with Affimer K3 residues of VR1 substituted to alanine with KRas (no-tag). The Ras-Affimer complex was precipitated and pulled down proteins were analysed by western blot with anti-Ras and anti-His antibodies **B.** K3VR2. The same protocol was followed as mentioned in A except that Affimer K3 residues of VR2 were substituted with alanine. Results are representative of three biological replicates (n=3).

To further identify the functional effect of residues in both VR1 and VR2 of Affimer K3, the alanine mutants were tested in the nucleotide exchange assay with wild type KRas as control Affimer (Figure 3.14). Complete inhibition of nucleotide exchange reaction is characterised by a low initial rate (V_0). K3 WT has low V_0 of 0.18 and reaction rate of alanine mutants >0.18 is indicative of inability to inhibit the exchange reaction. Mutations of residues L73 and K80 in VR2 significantly impaired the ability to inhibit the nucleotide exchange reaction. However, the most profound effects were observed with residues I40, D41, I42, W43, Y44 and D45, which completely abolished the inhibitory effect of Affimer K3 (Figure 3.14). This demonstrated that these residues are critical for effective inhibition of nucleotide exchange. Additionally, the functional effects of these residues correlated with the binding assay of Ras-Affimer complex, as demonstrated in Figure 3.13.

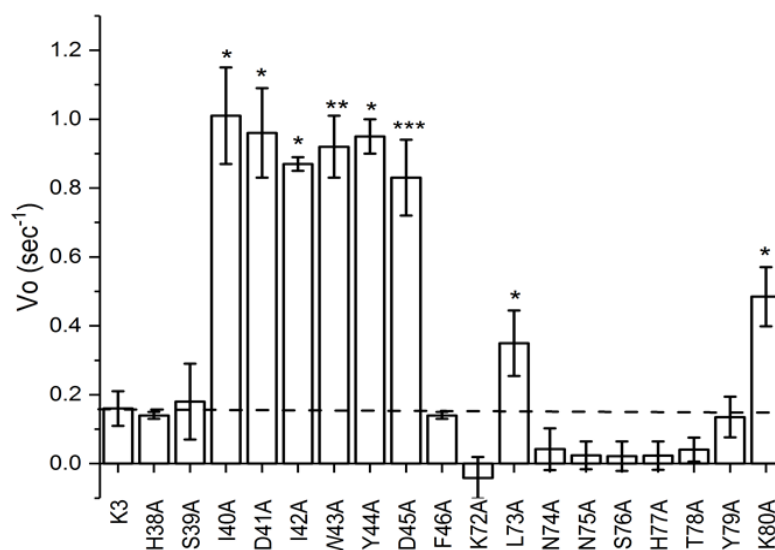


Figure 3.14 Functional effects of Affimer K3 variable regions alanine mutants on inhibition of nucleotide exchange to active GTP state. Affimer K3 wild type and alanine mutants were assayed at 10 μ M in a nucleotide exchange reaction with wild type KRas-mGDP and initial reaction rates for each protein were plotted. The dashed line indicated the reaction rate of wild type Affimer K3. Results are representative of three biological replicates (n=3). Error bars are \pm SEM. $p < 0.05$ (*), $p < 0.01$ (**), $p < 0.0001$ (****).

3.3 Discussion

Ras proteins are binary molecular switches and play a key role in regulating signal transduction. Ras mutations are oncogenic drivers of many human cancers, yet there are no approved Ras-targeted cancer therapies. The perceived ‘undruggability’ of Ras has led to tremendous interest in new targeting approaches. Affimers are a novel class of alternative binding proteins that behaves similarly to antibodies by binding with high affinity and specificity to its target molecule (Tiede et al., 2017). Affimer technology has been developed by our lab to isolate Affimer reagents against recombinant proteins, peptides and small molecules by phage display technology. The Affimer library (1.3×10^{10} clones) has been previously screened, and seven unique KRas-binding clones have been isolated. In the preliminary experiments, these Affimers were shown to bind to KRas, irrespective of nucleotide bound form

(Figure 3.1). This mode of binding is similar to previously reported anti-Ras monobody NS1. The NS1 monobody binder was found to be insensitive to the nucleotide state of Ras and did not promote nucleotide release or block nucleotide exchange on HRas. Structural studies provided an explanation for this as NS1 monobody binds to an allosteric site away from switch I and II regions of Ras (Spencer-Smith et al., 2017). However, in contrast, KRas binding Affimers have shown to inhibit nucleotide exchange to active GTP bound state (Figure 3.3). This, therefore, indicates that Affimer tends to bind to a region distant to allosteric lobe where monobody NS1 binds. Structural studies involving X-ray crystallography of Affimer K3-KRas complex and comparison of binding site with another KRas binding Affimer K6 (discussed in detail in chapter 4) can provide conclusive answers.

One of the strategies to inhibit the function of Ras is to prevent its activation by GEF SOS. This can be achieved by blocking nucleotide exchange to GTP and thereby reducing the amount of active Ras (Gysin et al., 2011). KRas labelled with fluorescently tagged GDP nucleotide (mGDP) have been used to measure the effects of nucleotide exchange. Out of seven KRas binding Affimers K3, K6 and K37 were identified as the most potent inhibitors, with IC_{50} values ranging from 200 to 697 nM for wild type KRas (Table 3.2). Likewise, Affimers' IC_{50} values were significantly better than stabilised peptides SAS-SOS1 ($IC_{50}=5-15 \mu\text{M}$) (Hillig et al., 2019) and HBS3 (25 μM). Notably, Affimers displayed 1000-fold better inhibitory potency than small-molecule Ras inhibitor DCAI ($IC_{50}=155 \mu\text{M}$) and recently discovered pan-Ras inhibitor 3144 which has IC_{50} in low micromolar range 17.8 μM (Welch et al., 2017). However, DARPin K27 binding protein binds to KRas GDP and inhibits nucleotide exchange with IC_{50} of 2.4 nM. Other DARPins like K13 and K19 (Bery et al. 2019) also inhibit nucleotide exchange with IC_{50} of 127 and 7.16 nM respectively. This could be due to large interaction surface area of DARPins, which covers the entire SI/SII pocket.

Ras isoforms K, H and NRas are ubiquitously expressed and display 90% sequence identity. However, they play specific roles in physiological and pathological processes (Castellano and Santos., 2011). Therefore, isoform-specific Ras inhibitors are highly desirable. Since 85% of Ras driven cancers

carry KRas mutations, much of the focus has been in the development of KRas specific inhibitors. Interestingly, Affimer K3 demonstrated isoform selectivity, as it displayed lower inhibitory activity towards HRas ($IC_{50}=2585 \pm 335$ nM) as compared to KRas (144 ± 94 nM) (Haza et.al 2019). Additional experiments with the third isoform NRas would be beneficial to confirm isoform specificity of K3 Affimer. However, it could not be carried out due to issues in production of soluble NRas protein (data not shown).

Recently many small molecule inhibitors have been developed that target KRas^{G12C} mutant specifically (Khan et al., 2020). These small molecules covalently attached to KRas mutant cysteine residue, and do not bind to wild type KRas protein. However, Affimer K3 has shown to inhibit KRas G12D (IC_{50} 144 ± 40 nm) and G12V (IC_{50} 176 ± 115 nm) as well as wild type KRas protein. Additionally, K3 Affimer has shown to have 20-fold lower inhibition for KRas^{Q61H} mutant in comparison to G12D and G12V. This could be because G12 mutations are more predominant in KRas and HRas, while Q61 mutations are predominant in NRas (Cox et al., 2014). Above all, these findings signify that Affimer K3 can bind to both mutant and wild type KRas *in vitro*.

Another strategy to target Ras is to develop inhibitors that are capable of inhibiting the interaction of Ras proteins with their effectors, which drive and sustain malignant transformation and tumour growth (Keeton et al., 2017). While many Ras targeting scaffold proteins were shown to inhibit Ras-Raf interaction (Martin et al., 2018; McGee et al., 2018; Spencer-Smith et al., 2017; Tanaka et al., 2007), the ability to block nucleotide exchange simultaneously with Ras- effector binding has been reported in case of DARPin K13 and K19 *in-vivo*. DARPin K13/K19 besides inhibiting Ras dimerization by binding to α -3/ α 4 region of Ras, also perturb nucleotide exchange and Ras-effector interactions. K3 Affimer also inhibits nucleotide exchange as well as Ras effector interactions. Three of the seven KRas binding Affimers significantly impaired Ras-RBD-Raf1 binding with K3 displaying the most potent inhibition (Figure 3.3). Densitometry analysis revealed a 90-fold reduction in immunoprecipitated Ras when K3 is used for Ras-Raf inhibition as compared to 20-fold reduction when K6/K37 Affimer is used. This could be due to the

difference in binding modes and the extent of perturbation of Ras-Raf interaction.

To identify which variable peptide regions of Affimer K3 are essential for binding and inhibition of KRas, variable regions (VR1 and VR2) of K3 were deleted, and mutants were created via overlap extension polymerase chain reaction. These mutants were analysed via Affimer-Ras immunoprecipitation assay. The assay showed that both deleted VR1 and VR2 are essential for binding and stabilisation of Ras-Affimer K3 complex (Figure 3.7).

There is a possibility that deletion of variable regions VR1 and VR2 to generate K3 Δ VR1 and K3 Δ VR2 mutants used during pulldown assay above can affect Affimer scaffold protein folding. To verify the structural integrity of deleted loop mutants of Affimer K3, the secondary structure of the proteins was analysed via circular dichroism (CD) in the far UV spectrum. CD spectra provide an experimentally very convenient means of detecting structural changes in proteins, which can be examined in different spectral regions (S.M Kelly et al., 2005). The secondary structure of Affimer was examined by CD and revealed a high ratio of β sheet to α helix and random coil (Teide et al., 2014). Mean residual ellipticity (MRE) spectrum of mutants and wild type Affimer K3 overlapped completely with deconvolution software (Dichroweb[®]) estimating 2% variation in total percentage of helical content of Affimer K3, alanine and mutants. This variation indicates little to no conformational change or misfolding of Affimer K3 protein scaffold.

Mutation of each amino acid in variable regions of Affimer K3 to alanine via Affimer-Ras pulldown assay identified that the majority of VR1 amino acids are involved in binding to KRas (Figure 3.10). This finding correlated with nucleotide exchange activity of the alanine mutants, with residues I40, D41, I42, W43, Y44 and D45 when substituted to alanine, completely abolished the inhibitory effect of Affimer K3 (Figure 3.11). Also, L73 and K80 of VR2 might be involved in stabilising the Affimer K3 structure, since only first and last amino acids in VR2 are involved in binding to KRas and majority of residues are not involved in binding to KRas. The importance of VR2 is further

evidenced by nucleotide exchange activity of L73A and K80A with reaction rate (V_0) two-fold higher than K3 WT.

In conclusion, data presented in this chapter demonstrated KRas binding Affimers as potent inhibitors of nucleotide exchange activity, with K3 binder showing isoform specific selectivity towards wild type KRas and clinically relevant mutants like G12D and G12V. Moreover, dual inhibition of Ras activation and effector interaction showed K3 as the most potent inhibitor, with K3 VR1 involved in binding and inhibition of KRas. Overall, all these findings demonstrate the use of Affimers to target 'difficult to drug' KRas with ability to bind to wild type and mutant KRas proteins *in vitro*.

Chapter 4

Structural characterisation of Affimer-KRas complex

4.1 Introduction

The effectiveness of drug discovery process is dependent on the correct identification of targets involved in pathology of disease, followed by successful selection, optimisation and development of candidate drugs (Marsden et al., 2014). Antibodies have become an essential tool in drug discovery process and have been used for target identification, validation and in design of lead compounds (Rhodes and Trimmer, 2008) (Figure 4.1). This is because of specific binding characteristics which include specificity and affinity to the target protein, coupled with their amenability to protein engineering. The use of antibodies for target validation in the case of extracellular and cell surface targets have been well established (Naylor and Beech, 2013; Phillips and Signs, 2005). However, antibodies have limited access to intracellular targets due to their large size (>150 kDa) and the reducing environment of cytoplasm can lead to destabilization of disulphide bonds and aggregation (Marsden et al., 2014). This limitation has been addressed by using other antibody formats or alternative affinity tools for intracellular target validation. The examples of affinity tools include nanobodies, DARPins, monobodies etc. Nanobodies have been used to study the mechanism of adrenergic receptor agonist isoprenaline on β_2 adrenoreceptor, revealing the role of agonist in G protein activation in plasma membrane as well as early endosome formation (Irannejad et al., 2013). This example shows the application of antibody alternatives to fill the knowledge gap in understanding how the modulation of target has effect on cell function.

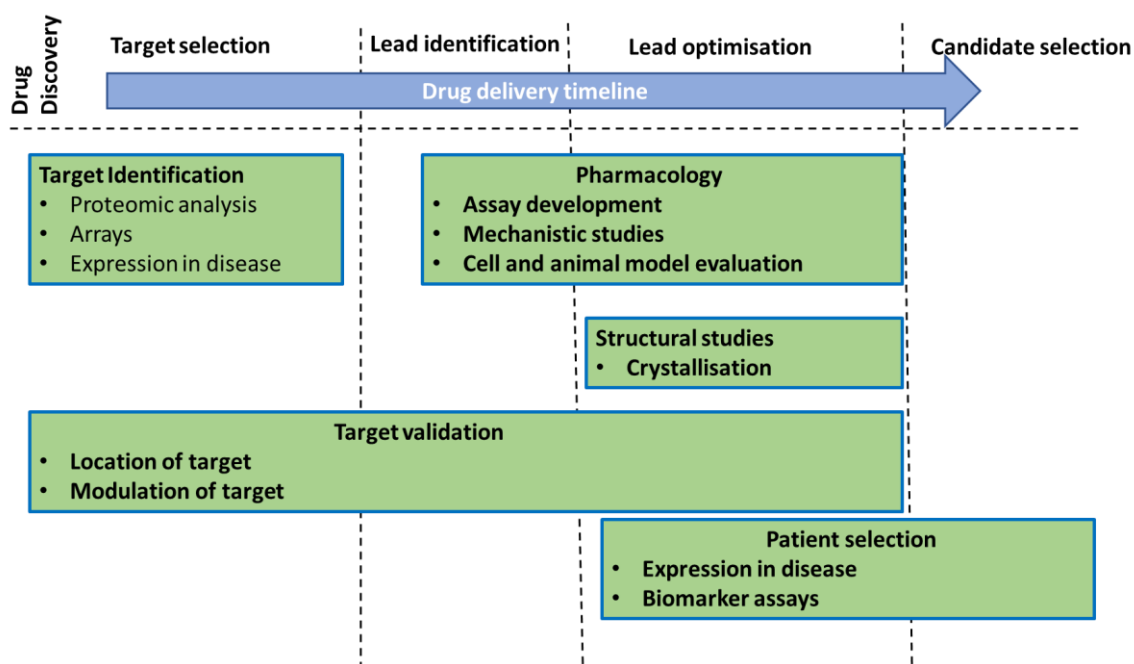


Figure 4.1 Timeline of drug discovery process and steps involved in identification of lead compound. Antibodies/antibody alternatives are key tools in research and are applied throughout drug discovery process. Adapted from (Marsden et al., 2014).

With the rapid rise in rational drug design, biophysical techniques have been employed to study potential drug sites before lead optimisation and candidate selection. X-ray crystallography is an especially important biophysical technique that has been used for lead site identification. Using X-ray crystallography for de-novo drug design, several compounds have reached clinical trials that target disease-relevant signalling proteins such as BCL-2 (Navitoclax for treatment of myelofibrosis), MDM2 (KRT-232 for treatment of glioblastoma), and BET (OTX -015 for treatment of solid tumours/lymphoma) (Mabonga and Kappo, 2019).

Engineered proteins have vast potential as leads for synthetic inhibitors of protein-protein interactions (Wuo and Arora, 2018; Miles, J. et al., 2020). These modulators of PPIs can be used as probes to understand cellular biology and can serve as starting points in drug discovery. Engineered proteins can be used as molecular recognition tools to identify interface residues or hot spots that contribute most of the binding energy. These hot spots are important targets for the development of small molecule inhibitors. The presence of

critical ionic residues in engineered proteins may aid in the development of inhibitors with high affinity and specificity (Wuo and Arora, 2018). Scaffold proteins that display smaller interaction interfaces such as anti-Ras monobody NS1 (interaction surface area of 568 Å²) or Affimers binding to SUMO proteins or Bcl family proteins (interface area in the range of 610-720 Å²) are likely to aid in small molecule inhibitor design (Hughes et al., 2017).

Previously, we have isolated Affimers that bind to KRas, out of which Affimer K3 showed most potent inhibition of SOS^{cat} mediated nucleotide exchange. Further biochemical characterisation of Affimer K3 shows the involvement of both variable regions in binding and inhibition of KRas. To further understand molecular details of Affimer K3-KRas binding, the atomic structure of KRas bound to Affimer K3 was solved to resolution of 2.1Å. To screen for crystallisation conditions, a high concentration of Affimer K3 in complex with KRas protein was used to set up factorial crystallisation trials. Additionally, Affimer K3 only crystal structure was also solved to resolution of 1.8 Å in order to understand the dynamic nature of VR2 of K3.

4.2 Results

4.2.1 Generation of Affimer K3-KRas complex.

X-ray crystallography was used to understand the mechanism of Affimer K3 binding to KRas. A high-resolution atomic structure of Affimer K3 bound to KRas is needed. For this a stable and homogeneous complex of Affimer K3-KRas is required. The initial step was to re-clone KRas without the biotin acceptor peptide (BAP) and 6x His affinity tags since fusion tags are known to hinder crystal growth (Smyth et al., 2003). The KRas sequence was amplified using PCR from a bacterial expression plasmid and cloned into pET11a plasmid (see section 2.2.3.4) (Haza, K.Z et al., 2020). The successful cloning was confirmed by sequencing. KRas protein was then produced in *E. coli* BL21 StarTMDE3 cells, as described in section 2.2.3.2.

Affimer K3 was first purified via Ni^{2+} -NTA chromatography and then was incubated with excess of *E. coli* cell lysate containing KRas protein (no tag). Following incubation, AffimerK3-KRas complex was then captured by Ni^{2+} -NTA resin for purification (see section 2.2.3.4). After washing the resin, the purified protein complex was eluted and analysed by 15% w/v SDS-PAGE and stained using Coomassie blue. Two bands of approximately 18 and 12 kDa corresponding to KRas and Affimer K3 were observed, indicating efficient purification of Affimer K3-KRas complex (Figure 4.2).

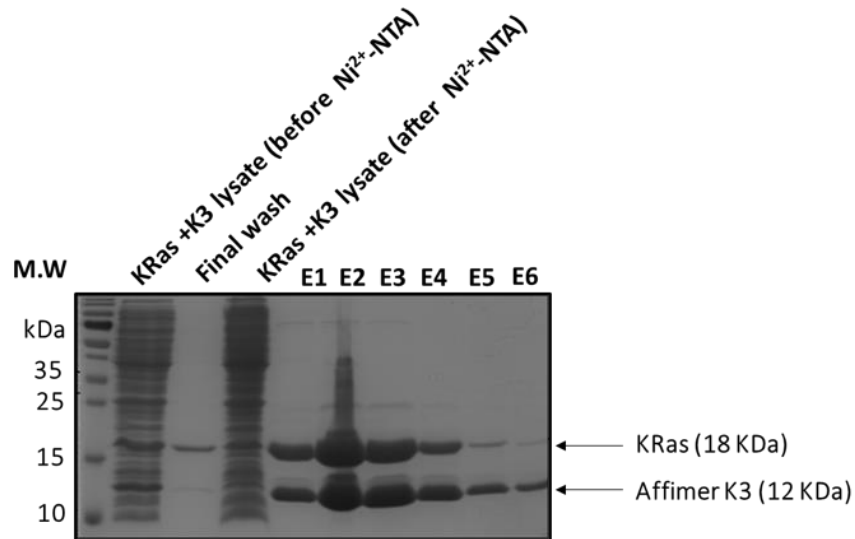


Figure 4.2 Purification of Affimer K3-KRas complex. Purified Affimer K3 protein (with 6x His tag) was mixed with KRas *E. coli* bacterial cell lysate and incubated overnight. The complex was purified by Ni^{2+} -NTA chromatography. The eluted fractions E1-E6 were analysed by 15% SDS-PAGE and stained using Coomassie blue. Eluted fractions showed two strong bands at 18 and 12 kDa indicating successful formation of KRas-Affimer K3 complex.

The eluted complex was further purified by size exclusion chromatography to remove any impurities from the cell lysate and to separate any Affimer not in a complex with KRas; this also demonstrates that the purified proteins were in a stable complex. Protein samples from the peak region (40-65 ml) as seen in A_{280} elution trace, were collected in 2 ml fractions and analysed using 15% SDS-PAGE gel (Figure 4.3 A). Once again, two bands of approximate molecular weight of 18 and 12 kDa, corresponding to KRas and Affimer K3

were observed, confirming the purification of Affimer K3-KRas complex (Figure 4.3 B). The eluted fractions were pooled and concentrated to 24 mg/ml total protein concentration and quantified by bicinchoninic acid assay (BCA).

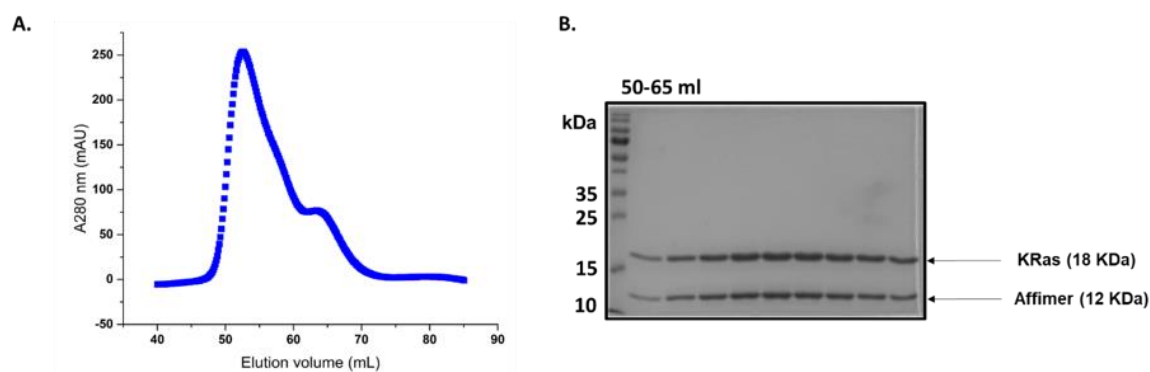


Figure 4.3 Size exclusion chromatography (SEC) of Affimer K3-KRas complex obtained after Ni²⁺-NTA chromatography **A.** Following Ni²⁺-NTA chromatography of Affimer K3-KRas, SEC using Hiprep® Sephacryl 16/60 column was carried out. Y axis of chromatogram is measure of intensity of absorbance in milli absorbance units (mAU) and X axis is indicated by elution volume (ml) **B.** Eluted fractions were analysed via 15 % w/v SDS-PAGE gel and Coomassie stained to verify the presence of purified K3-KRas complex.

4.2.2 Crystallisation of Affimer K3-KRas complex

Once a high concentration of homogenous, purified protein sample of Affimer K3-KRas was obtained, a set of screening conditions, called sparse matrix screens, was used for obtaining protein crystals. This is a high throughput crystallisation screening method that covers large areas of chemical space to hopefully obtain well diffracting crystals (Luft et al., 2011). The screening conditions are selected based on successful crystallisation attempts and published PDB entries (Jancarik and Kim, 1991). Crystallisation experiments for the AffimerK3-KRas protein complex were initiated using commercial sparse matrix screen JCSG screen I-IV. A total of 384 crystallisation conditions in the JCSG core suites offer a broad sampling of crystallisation space (Newman et al., 2005). Sitting drop vapour diffusion technique was employed as described in section 2.2.8.1. Crystal formation was monitored using an automated imaging system Rock Imager® (Formulatrix). Crystallisation

conditions were screened using different imaging methods such as visible light, ultraviolet (UV) light and second harmonic generation spectroscopy (SHG) imaging. In UV imaging, the absorption of light by aromatic residues at 280 nm was employed to confirm the presence of protein crystals. Also, second-order nonlinear optical imaging of chiral crystals (SONICC) was used which is based on combination of second harmonic generation (SHG) and UV Two photon excited fluorescence (UV-TPEF). This technology helps identifies crystals present in precipitate and can detect nano and microcrystals $< 1\mu\text{M}$ (Kissick et al., 2011).

In the initial screening using JCSG screen I-IV, crystals of Affimer K3-KRas started appearing within 8-13 days in 2 conditions only (Figure 4.4). Protein crystals grew as a cluster of needle-shaped crystals. UV + SHG imaging demonstrated that observed particles are indeed protein crystals. In addition, crystals were picked and sent to the Diamond Light source facility to confirm that these were protein crystals. The diffraction pattern showed sharp spots near the centre in concentric circles, but it gave a very poor resolution of 7.3 Å.

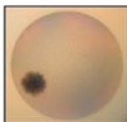
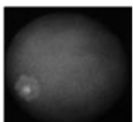


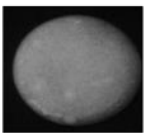

Screen	Well	Visible	UV imaging	SHG imaging	Condition
JCSG screen II	D3				0.05 M LiSO_4 (Salt), 0.1 M Tris-Cl pH 7 (Buffer), 50% w/v PEG200 (Precipitant). 8 days
JCSG screen II	F2				0.1 M Na Phosphate Citrate pH 4.2 (Buffer), 40% v/v PEG 300 (precipitant). 13 days.

Figure 4.4 Summary of initial crystallisation conditions obtained via JSCG screens. Screen plate names as well as well number in which crystals appeared are mentioned. The images of crystals in visible, UV and SHG imaging along with their conditions and duration of crystal appearance have been listed

4.2.3 Optimisation of initial crystal hit from JCSG screen II

Since the initial crystals obtained showed poor diffraction, the conditions were optimised to obtain crystals of sufficient quality. Optimisation of crystal hit from JCSG screen II (0.05 M LiSO₄, 0.1M Tris-Cl pH 7.0 and 50% v/v PEG 200) was carried out by varying pH of the buffer (pH 6.0-9.0) and precipitant concentration (40-55% v/v PEG 200) and keeping the salt concentration (0.1 M Tris-Cl) constant. Unfortunately, no crystals were observed even after varying the original crystal conditions.

4.2.4 Crystallisation using additional sparse matrix screens

Since optimisation of conditions from JCSG screens did not yield any good quality protein crystals other random sparse matrix screens for crystallisation of Affimer K3-KRas protein complex were used. These include Wizard™ classic screen III and IV (Rigaku®), Salt Rx screen (Hampton®) and crystal screen HT (Hampton®). Wizard classic screens have been proven to be ideal starting points for biological macromolecules. The Wizard classic formulations include a large range of precipitants, buffer and salts covering a broad range of crystallisation space with pH range from pH 4.5 to pH 10.5. In the case of Wizard screen III and IV, crystals of Affimer K3-KRas started appearing in 5-8 days in two different conditions (Figure 4.5). Since the crystals obtained were either needle shaped or microcrystals, optimisation of both the conditions of Wizard screens (See Figure 4.5) was carried out. Unfortunately, very few crystal hits with poor crystal quality was obtained.

Crystal screen HT is a sparse matrix screen consisting of 48 unique reagents from two crystal screens 1 and 2 in deep-well block format (Jancarik and Kim, 1991). In case of crystal screen HT, best crystal hit was obtained after 21 days in condition containing 2 M ammonium sulphate (precipitant), 0.1M Tri-sodium Citrate pH 5.6 (buffer) and 0.2 M potassium sodium tartrate (salt). These crystals (Figure 4.5) were around 20 µM-50 µM in diameter, which were large enough to diffract X-rays. These crystals were cryo-protected for data

collection in a solution containing 75% w/v mother liquor (liquid remaining after the solution has crystallised out) and 25% w/v ethylene glycol.

No crystals were observed when using Salt Rx screen.

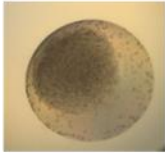
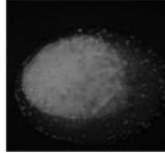

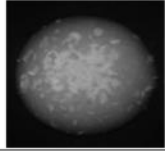
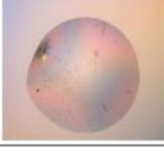
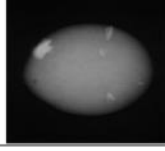
Screen	Well	Days	Visible	UV imaging	Conditions
Wizard screen III and IV	F6	5 days			25% w/v PEG 1500 (Precipitant) 0.1 M SPG pH 8.5 (buffer)
Wizard screen III and IV	F2	8 days			40% PEG 400 (precipitant), 0.1 M Tris-Cl pH 8.5 200mM LiSO ₄ (Additive)
Crystal screen HT	F2	21 days			2 M (NH ₄) ₂ SO ₄ (precipitant), 0.1 M Na ₃ Citrate pH 5.6 (Buffer), 0.2 M K Na Tartrate (Salt)

Figure 4.5 Summary of crystallisation conditions for Affimer K3-KRas complex crystals. Screen plate names as well as well number in which crystals appeared are mentioned. The images of crystals in visible and UV imaging along with their conditions have been listed. Conditions obtained from crystal screen HT was selected because the crystal size was good enough for X-ray diffraction and data collection.

4.2.5 Binding of Affimer K3 to KRas revealed a druggable SII/ α -3 pocket

X-ray diffraction data for KRas-K3 crystal obtained from the Crystal screen HT was collected at European Synchrotron Radiation Facility (ESRF) using ID30A-1 beamline. Data collection, processing and structure determination was performed as described in section 2.2.8.3 and was carried out by Dr Chi Trinh.

The crystal structure of Affimer K3-KRas bound to wild type GDP was solved at 2.1 Å resolution. The co-crystal structure revealed Affimer K3 interacting with switch II region (SII) (amino acids 60-76) of KRas (Figure 4.6). Affimer K3 residues 40-45 in VR1 has shown to be crucial for interaction with KRas. This interaction was correlated with pulldown and nucleotide exchange assays carried out previously, in which residues I41, D42, I43, W44, Y45, and D46,

when mutated to alanine, did not bind and inhibit KRas (see section 3.2.4). Binding of Affimer K3 to KRas revealed a novel Ras conformation with large druggable pocket between switch II and α -3 helix. The hydrophobic pocket identified by K3 was found to have a total buried surface area of 790.6 Å² which was calculated using PDB-e-PISA [EMBL-EBI] server (Krissinel and Henrick, 2007).

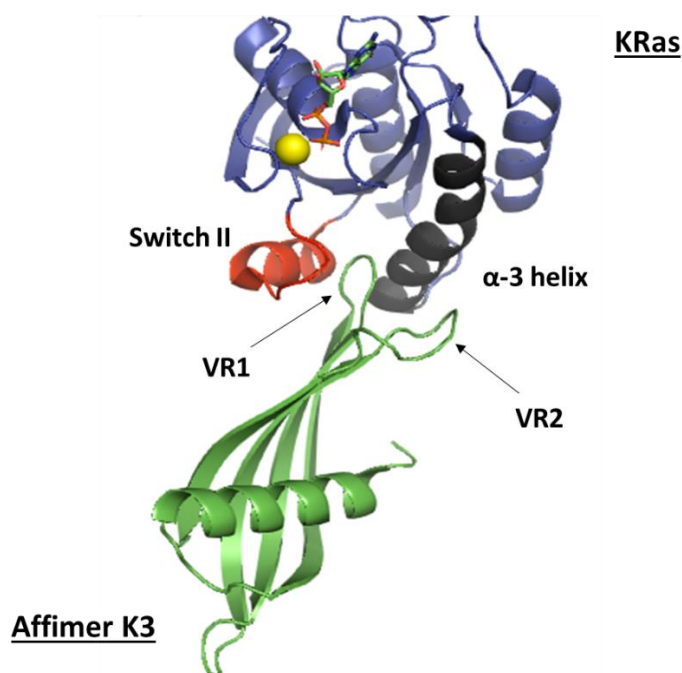


Figure 4.6 Co-crystal structure of KRas with Affimer K3. K3 Affimer VR1 (green) binds to pocket between Switch II (red) and α -3 helix (dark grey) of KRas (blue). Magnesium is shown as yellow sphere and GDP is shown as green sticks. Arrows indicated VR1 and VR2 of Affimer K3. Image was generated in PyMOL.

With Affimer K3 VR1 bound to the SII region, the D42 residue of K3 brings the SII region close to the α -3 by generating a hydrogen bond between R68 of SII and Q99 of α -3. Affimer K3-KRas complex formation is further strengthened by hydrogen bonds between side chain oxygen of D46 residue in K3 Affimer with the main chain nitrogens of Q99 and R102 in α -3 (Figure 4.7 A). This is further complemented by OH group on the side chain of Y45 of K3 forming hydrogen bonds with side chain oxygen of E62 of SII. This hydrogen bonding network creates a large binding interface, in which residues of Affimer K3

namely I41 and I43 form hydrophobic interactions with V103, M72 and V9 of KRas respectively (Figure 4.7 C). The pocket created by hydrophobic interactions is further stabilised by W44 indole side chain orienting itself to form hydrogen bonds with H95 present in α -3 such that it is packed against residues of Q61, D92 and Y96 (Figure 4.7 B).

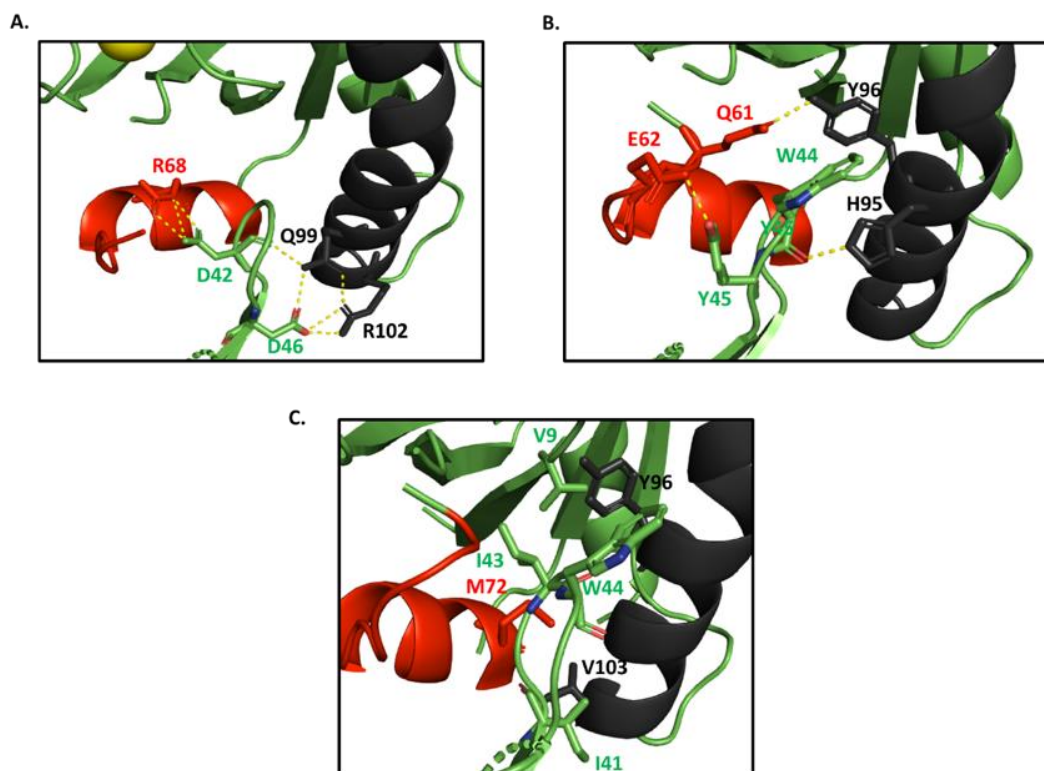


Figure 4.7 Intermolecular interaction between Affimer K3-KRas **A.** Affimer K3 residues D42 and D46 (highlighted in green) bind strongly to R68 of SII α -3 (red) and Q99 and R102 of α -3 (dark grey) bringing the two α helices in proximity. **B.** The intermolecular interactions mentioned in A is further strengthened by interaction by W44 side chain and Y45 (green) burying into hydrophobic pocket and forming hydrogen bond with H95 of α -3 (dark grey) and E62 of SII (red). **C.** Hydrophobic interactions between Affimer K3 residues and KRas. H-bonds are shown in yellow dashed lines.

The interaction between K3 and KRas described above caused a significant conformational shift in the SII region of KRas. Most notably, SII α -2 helix moves 4.3 Å away from α -3 as compared to KRas WT GDP (PDB-40BE) (Figure 4.8 A). This conformational shift generates a new network of intramolecular hydrogen bonds in KRas. When K3 binds, the D42 of K3 Affimer binds to R68 of SII via a salt bridge interaction. This interaction shifts the R68

residue into an orientation necessary to create a hydrogen-bonding network between E37 of Switch-I (SI) and S65, A59 and G60 of SII. Additionally, the side chain of Y71 of the SII α -2 helix flips to form a hydrogen bond with D54 of the β 3 strand (Figure 4.8 B) thereby stapling the SII region to the SI site. This hydrogen bond network has not been observed in WT KRas GDP (PDB: 4OBE) or WT KRas GppNHp (PDB: 6GOD).

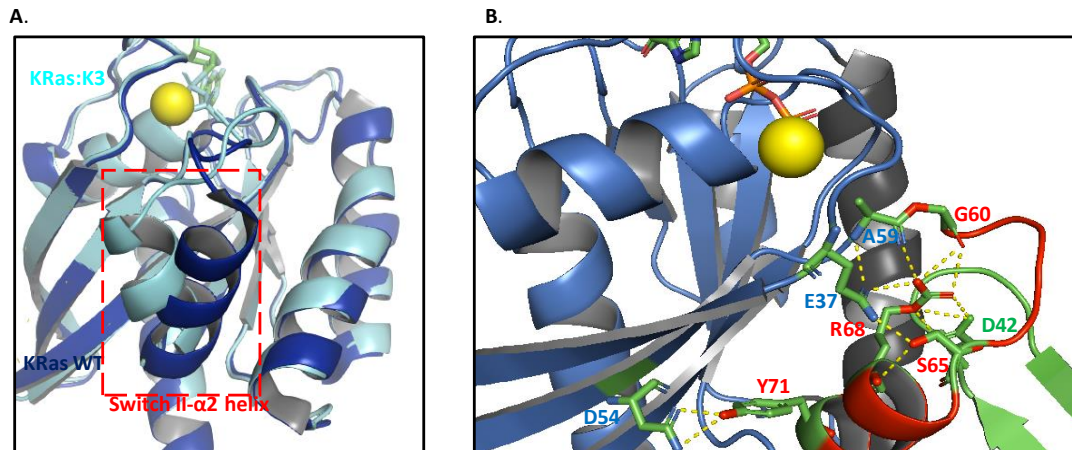


Figure 4.8 Conformational shift and hydrogen bonding network facilitated by binding of K3. **A.** KRas WT (blue) (PDB: 4OBE) structure was fixed and overlaid with KRas-K3 Affimer complex (cyan). This overlay shows a conformational shift in Switch II when Affimer K3 binds between α -2 and α -3 helix region of Ras **B.** Interaction of D42 residue of Affimer K3 (green) with R68 residue (red) in SII via salt bridge interaction. Hydrogen bonding network between E37 (blue) of SI and G60, S65 (red) of SII region. This hydrogen bond network has not been observed in KRas WT. H-bond is shown as yellow dashed lines, K3 Affimer (green), KRas (blue).

4.2.6 Crystal structure of Affimer K3 reveals a dynamic VR2 loop

We have previously observed that both VRs of Affimer K3 are involved in binding and inhibition of KRas (see section 3.2.3). It was observed that VR2 residues L73 and K80 have shown to be involved in binding and inhibition of KRas (see section 3.2.4). However, in case of Affimer K3-KRas crystal structure, we observed that VR2 is not involved in binding to KRas. This could be attributed to the dynamic nature of VR2. Thus, to investigate the Affimer K3 protein structure dynamics, crystallisation of Affimer K3 only was carried out.

Protein expression of Affimer K3 was carried out as per section 2.2.3.1. The eluted Affimer was purified by nickel ion affinity and then size exclusion chromatography. Two narrow and one broad peak were seen in $A_{280\text{nm}}$ elution trace (Figure 4.9 A). The elution profile shows that Affimer K3 can exist in different oligomeric states i.e it could exist in dimer or trimeric or even higher oligomeric states when present in high concentrations. The eluted fractions from all three peaks were collected and analysed using 15 % w/v SDS-PAGE gel and stained using Coomassie. For peak 1 and 2, we observed trimer/dimer at 24 kDa and for peak 2 purified monomeric K3 protein was obtained (Figure 4.9 B). The eluted fractions containing monomeric K3 was pooled and concentrated and quantified via BCA assay to 20 mg/ml total protein concentration.

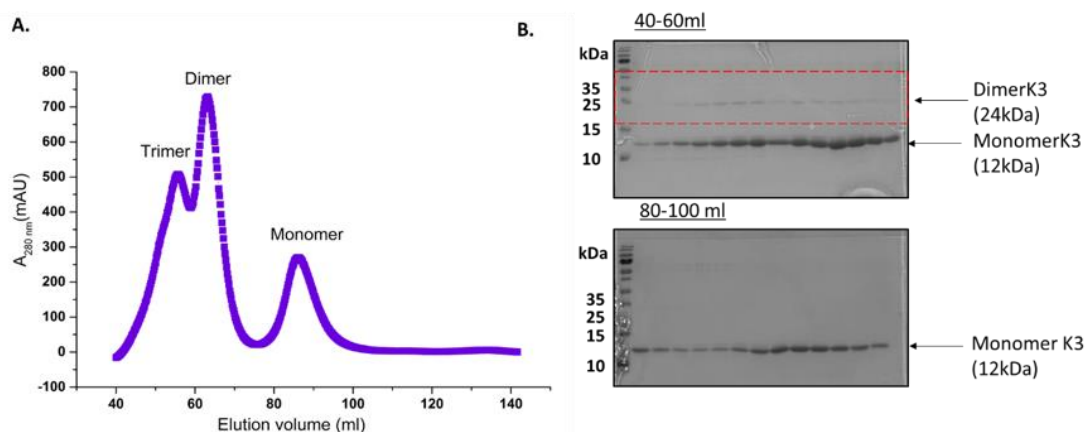


Figure 4.9 Elution profile of K3 Affimer. **A.** Analysis by Size exclusion chromatography of K3 Affimer shows three oligomeric states first is trimer or tetramer followed by dimer and monomeric form. Affimer K3 was eluted in fractions using Hiprep® 16/60 Sephacryl S-100 column (GE Healthcare®). Chromatography was carried out using 10 mM Tris, 50 mM NaCl pH 7.5 buffer with flow rate of 0.8 ml/min and the volume of protein injected was 1.5 ml **B.** Elution fractions from dimeric (red dashed box) and monomeric states of K3 were run on 15%SDS-PAGE gel and Coomassie blue stained.

After optimisation of Affimer K3 crystal conditions, single large three-dimensional protein crystals were obtained. However, multiple lattices were observed in the crystals, therefore indexing failed. Subsequently, the protein concentration was increased to 80 mg/ml, which is the highest possible concentration of Affimer K3 obtained without precipitation of purified soluble protein solution. JCSG screens I-IV and Morpheus screen (Molecular dimensions®) were used. Morpheus screen contains 96 conditions covering a range of pH, PEGs and low molecular weight ligands which promote initial crystal formation and lattice stability (Gorrec, 2009). Sitting drop vapour diffusion technique was employed as described in section 2.2.8.1. Crystal formation was monitored using an automated imaging system Rock Imager® (Formulatrix). This time 6 promising crystal were obtained: 3 from the JCSG screens and 2 from the Morpheus screen within 3 days (Figure 4.10). Protein crystals from 3 crystal hits (total of 12 crystals) were collected immediately after 3 days and frozen in liquid nitrogen at -80° C. Crystals were sent to

Diamond synchrotron for data collection and structure determination (beamline-i24).



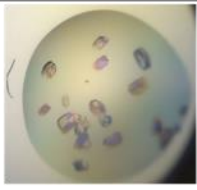
Screen	Well	Visible imaging	Conditions
JCSG core II (1:2)	C3		30% v/v PEG 300 0.1 M HEPES 7.5 0.2 M MgCl ₂
JCSG screen III	C6		0.2 M CaCl ₂ (Salt) 0.1 M HEPES 7.5 pH (Buffer) 28 %v/v PEG 400 (Precipitant)
JCSG screen II	C7		40 %v/v PEG 300 (Precipitant) 0.1 M Na Cacod 6.5 pH (Buffer) 0.2 M Ca Acet (Salt)

Figure 4.10 Summary of crystal conditions of Affimer K3 only. Screen plate names as well as well number in which crystals of Affimer K3 appeared are mentioned. The visible images of protein crystals along with the conditions are shown.

4.2.7 Crystal structure of Affimer K3

X-ray diffraction data of K3 Affimer crystal obtained from JCSG screen II and screen III (30% v/v PEG 300, 0.1 M HEPES pH 7.5, 0.2 M MgCl₂ and 40% v/v PEG 300, 0.1 M Na cacodylate pH 6.5, 0.2 M Ca acetate) was collected at Diamond synchrotron using i24 beamline. Data collection, processing was carried out by Dr Chi Trinh.

Affimer K3 protein crystals diffracted to 1.8 Å resolution. The asymmetric unit consists of a dimer of Affimer K3 directed at each other (Figure 4.11 A). Both Affimer K3 molecules within the lattice showed little intermolecular interactions due to the crystal packing. The electron density around the VR2 was found to be relatively weak, with poor main chain connectivity density for residues 74-83. This suggests that K3 Affimer VR2 is flexible. Average B factor of all atoms was found to be 46.0 Å² (Figure 4.11 B). B factor is a term used to define the

extent of atomic oscillations that are possible around the equilibrium positions in the crystal structure (Carugo, 2018). For the known structures in the highest resolution range (0.0–1.5 Å), the average B-factor is only 25 Å², while it is 80 Å², in the lowest resolution range (3.3–4.0 Å) (Carugo, 2018). In case of VR2, high B factor with average value of 54.42 Å² was observed. This is indicated by putty tube representation with colour variation from blue to green (narrow tube, “cold”, low B factors) then orange to red (wider tube, “hot”, high B factors). In case of the K3 VR1, low B factor with an average value of 22 Å² was observed. This was indicated by a narrow tube with blue to green colour variation (Figure 4.11B). Therefore, B factors establish that VR2 is more dynamic than the rest of structure.

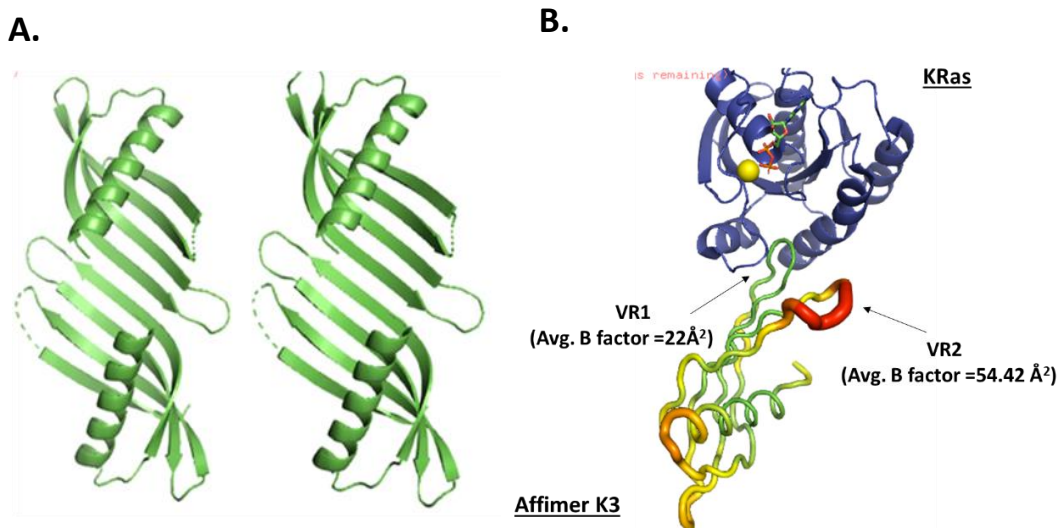


Figure 4.11 Crystal structure of Affimer K3. **A.** Asymmetric unit of Affimer K3 shows each Affimer directed at each other. Variable regions with missing VR2 shown in dotted lines **B.** Affimer K3 is shown in putty tube representation, with VR2 shows high B factors (64 Å²) as indicated by red and wide tube. VR1 shows low B factors (22 Å²) with narrow tube and is blue in colour. KRas is shown in blue.

4.3 Discussion

There have been significant strides in development of antibody/antibody alternatives as tools to allow rapid identification and characterisation of small molecules with optimised functionality. This progress has been possible due to the availability of structural data provided by X-ray crystallography and other structural biology techniques such as NMR and cryo-EM. Many cancer drug targets which had been considered as 'undruggable' such as transcription factors like MYC and NF κ B have had their protein structures solved and deposited in PDB database (Dang et al., 2017). This has led to development of inhibitors that are currently in clinical trials (Villanueva, 2019). The second major category of undruggable proteins is the Ras family of small GTPases. Despite 30 years of research, no drug has reached the market. The main reason was due to lack of druggable pockets for small molecules to bind with high affinity and specificity (Stephen et al., 2014). Findings from our lab have suggested that engineered binding proteins like Affimers can be used as tools to modulate PPI, identify druggable pockets and aid in the design of small-molecule inhibitors (Haza et al., 2020; (Robinson et al., 2018)

In this chapter, X-ray crystallography was used to solve the atomic structure of the KRas-AffimerK3 complex to understand the mechanism of inhibition of KRas. From the crystal screening and optimisation of Affimer K3-KRas it was observed that more crystals were produced when formulations contained low molecular weight PEG concentration or high molar concentrations (>2M) of ammonium sulphate or phosphate as precipitant. Once crystals of KRas-K3 protein complex were obtained, atomic structure of protein complex was solved to 2.1 Å resolution. It was observed that Affimer K3 binds to SII region of KRas (60-75aa), establishing K3 Affimer as an allosteric inhibitor of Ras.

When Affimer K3 binds to KRas, a hydrophobic pocket is revealed adjacent to SII and α -3. This pocket is created due to its molecular interactions with SII resulting in a conformation unfavourable for binding of the helical hairpin loop of SOS1. A similar hydrophobic pocket has also been observed using cyclic peptide KRpep2d, binding to KRas^{G12D} mutant (see appendix C). However, the major difference is that K3 binding involves residue H95, which is a unique

residue in the G domain of KRas, whereas the isoform specificity of KRpep2d has not been studied (Sogabe et al., 2017). Additionally, the peptide has shown to be not sufficiently efficacious for *in-vivo* studies. The pocket revealed by Affimer K3 binding is previously unseen conformer of SII-P. This pocket has been termed the SII/ α 3 pocket as it coincides with cryptic groove identified computationally (Grant et al., 2011). This SII-P has been recognised by covalent KRas^{G12C} inhibitors such as ARS-853 and 1620 which are currently in clinical trials (Janes et al., 2018; Ostrem et al., 2013).

Gentile and colleagues used fragment-based drug discovery method, namely tethering, to identify disulphide-based fragment 2C07. Fragment 2C07 binds to both nucleotide states of KRas (GDP and GTP) and expands the SII-P into a new groove away from nucleotide termed the SII groove (SII-G) (Gentile et al., 2017). SII-G is located between the central β sheet and α -2 and α -3 helices, the same cryptic groove to which Affimer K3 binds. The authors further noted that for non-covalent binding to SII-P, a substituted phenolic ring is required for coupling to a sub-pocket formed by V9, R68, D69 and M72 (Gentile et al., 2017). Affimer K3 fulfils this requirement with the aromatic ring of W44 extending into this sub-pocket. Therefore, the SII/ α -3 pocket shares this sub-pocket present in SII-G.

Additionally, Lu *et al.* observed multiple conformations of switch II when ARS series of compounds bind to SII-P using hydrogen/deuterium exchange mass spectrometry (Lu, et al., 2017). This suggests that SII-P binders are capable of an engaging range of KRas conformations. Here, when K3 binds to KRas, the α -2 helix is distal from the α -3 helix, indicating an open conformation (Figure 4.12 A). In the case of AMG510, a more closed conformation is observed, where the α -2 helix is semi-distal to the α -3 helix (Figure 4.12 C) (Lanman et al., 2020; Canon et al., 2019). Affimer K3 stabilised an open switch II conformation as compared to a closed conformation seen with AMG510. This binding of Affimer K3 to KRas facilitates a new network of hydrogen bonding interactions between SI/SII and SII/ α 3 helix that is not present in KRas^{G12C} AMG510 structure (PDB: 6OIM). In case of ARS 1620, binding of the most potent ARS compound that targets KRas^{G12C} leaves the helices proximal to each other as seen in KRas WT (Figure 4.12 B) (PDB 5V9U) (Janes et al.,

2018). These differences suggest that there may be an extended pocket area for small molecules based on the K3 pharmacophore i.e. there is potentially more affinity and selectivity that could be built into small molecules.

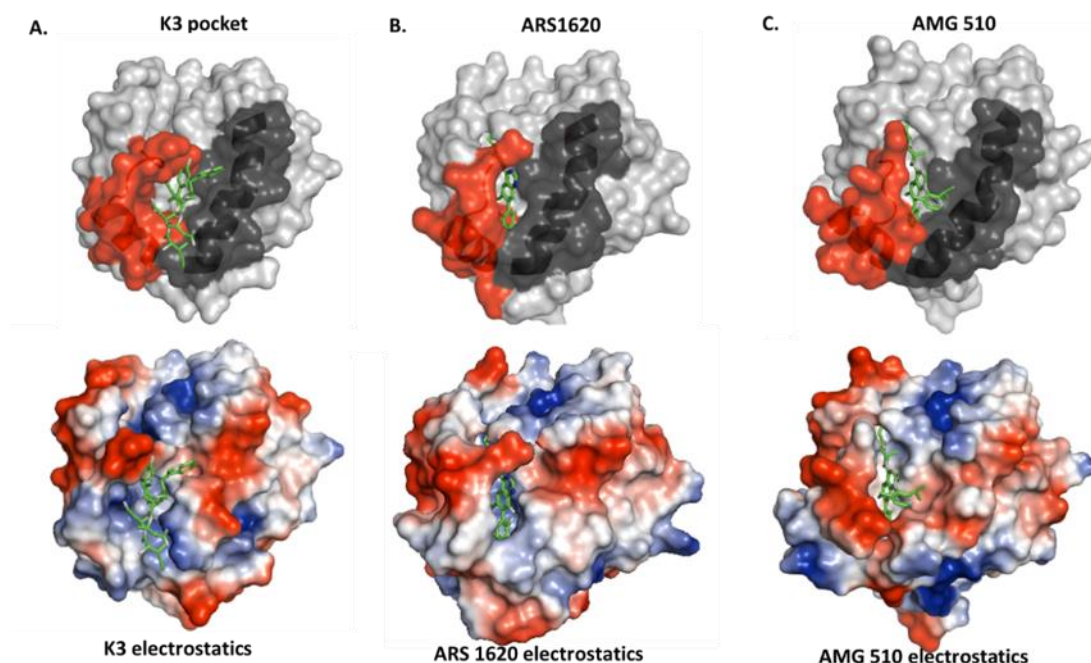


Figure 4.12 Comparison of surface shape and electrostatics of small molecules with K3 Affimer. Alteration in conformation of SII region (red) and α -3 helix (black) and corresponding alteration in electrostatics (bottom row) is shown **A.** Affimer K3 residues 41-45 when bound to KRas: GDP crystal structure indicate an open conformation (left panel). **B.** KRas^{G12C} compound ARS 1620 when bound to KRas^{G12C} (middle panel) shows a closed conformation where the α -2 helix is semi-distal to the α -3 helix **C.** AMG510 compound when bound to KRas^{G12C} (right panel) shows a half open conformation. Blue-positive potential, red-negative, white-neutral.

The biochemical data in Chapter 3 provides evidence that both VR1 and VR2 of Affimer K3 are involved in binding and inhibition of KRas (see section 3.2.4). But in the Affimer K3-KRas crystal structure, we observe that there are intramolecular interactions between VR2 residues K71 and K72 form hydrogen bonds with N75 and K80 residues of VR2 (Figure 4.13). These interactions could explain the importance of VR2 in stabilising KRas-Affimer K3 complex, as in absence of this interaction there is very weak to no binding of Affimer to Ras (see Figure 3.9). The molecular interactions between K3 Δ VR1/VR2 and

KRas WT can be further verified by using SPR. Additionally, VR2 has shown to have high B factor, indicating the flexible nature of VR2. Affimers have also been shown to bind to Ras intracellularly and inhibit downstream signalling, all three Affimers (K3, K6 and K37) showed inhibition of ERK1 phosphorylation using KRas expressing mouse embryonic fibroblasts (MEFs) (Haza, K.Z et al., 2020).

In conclusion, the data presented in this chapter demonstrates the use of non-antibody binding scaffolds with a relatively small binding interface to identify novel conformers of target protein. Affimer proteins can identify druggable regions on protein surfaces as evidenced by modulation of BCL2 family of proteins (Miles, J.A. et al., 2019). In this study, Affimer K3 selects a unique conformation to reveal a large druggable pocket in KRas. This pocket has been previously identified by AMG 510 and ARS 1620, but K3 exhibits different surface electrostatics due to an open conformation of the SII region. It will be interesting to use this α 3/SII pocket as a template for the development of novel Ras binding molecules. Additionally, the differences in the conformation when K3 binds to KRas indicates an extended pocket area for small molecules based on K3 pharmacophore.

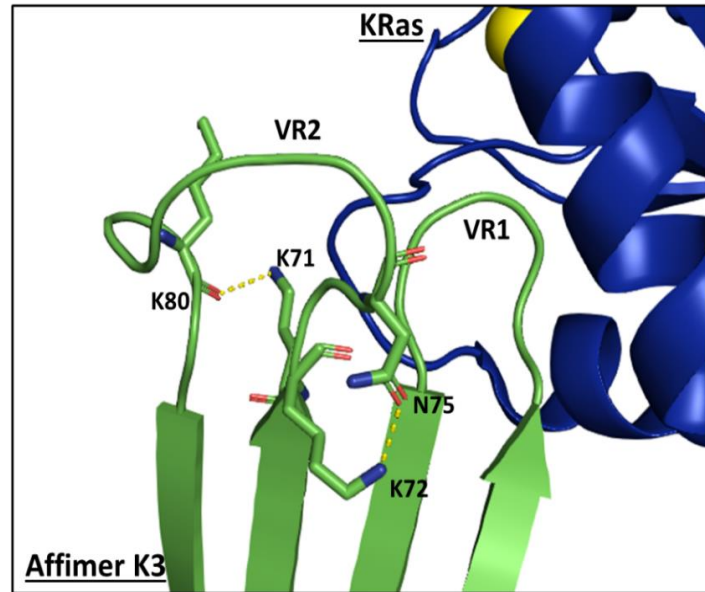


Figure 4.13 Intramolecular interactions of Affimer K3. Intramolecular interactions between residues of VR2 of Affimer K3 (green) are highlighted. H-bond interactions between variable regions' residues were generated in PyMOL and are shown as yellow dotted lines. KRas is shown in blue, GDP-yellow.

Chapter 5

Understanding Affimer K3 specificity towards KRas

5.1 Introduction

The Ras family of small GTPases consisting of HRas, NRas, KRas4A and KRas4B have shown to have a high degree of amino acid sequence similarity with differences observed mostly in C terminal hypervariable regions (Watzinger et al., 1998). In case of Ras GTP binding domain (G domain), there are 17 residue positions in the allosteric lobe that differ in at least one of the isoforms. Most of these residues are clustered in the nucleotide binding pocket as well as helix3. Out of the 17 residues 9 are unique to NRas, 7 are unique to HRas and 5 are unique to KRas. Interestingly, only 2 amino acids differ in all three Ras isoforms, this include H95 in helix 3 and R122 in loop8. Therefore, there is a need to generate Ras isoform specific protein binders to understand Ras isoform and mutation specific signalling differences (Baker, 2015; Waters et al., 2017). Here in this project BSTG group isolated Affimers that specifically target the G domain of KRas, which represents 85% of all Ras family mutations (Moore et al., 2020). Affimer K3 inhibits SOS1 mediated nucleotide exchange and Ras/Raf interaction by binding between SII and α -3 helix of KRas (Chapter4). Structural analysis identified W44 side chain of K3 to form hydrogen bonding with H95 on α -3 helix. H95 and E107 are two unique residues in the KRas isoform. To evaluate the specificity of Affimer K3 towards KRas, as observed in biochemical and cellular data (Haza et al., 2020), site directed mutagenesis and pulldown assay was carried out in this chapter to verify the binding and inhibition.

5.2 Results

5.2.1 Affimer K3 preferentially binds to KRas isoform

In Chapter 4, it was shown that the W 44 residue of Affimer K3 forms a hydrogen bond with H95-residue present in α -3 helix of KRas (Chapter 4, Figure 4.7). H95 is one of the unique residues present in KRas and not in HRas and NRas isoform. Therefore, we introduced mutations at position H95 by replacing His (H) with Q and L (found at residue 95 in HRas and NRas respectively). This was carried out using site directed mutagenesis. The plasmids DNA were sent for sequencing to verify whether they have point mutation (Figure 5.1).

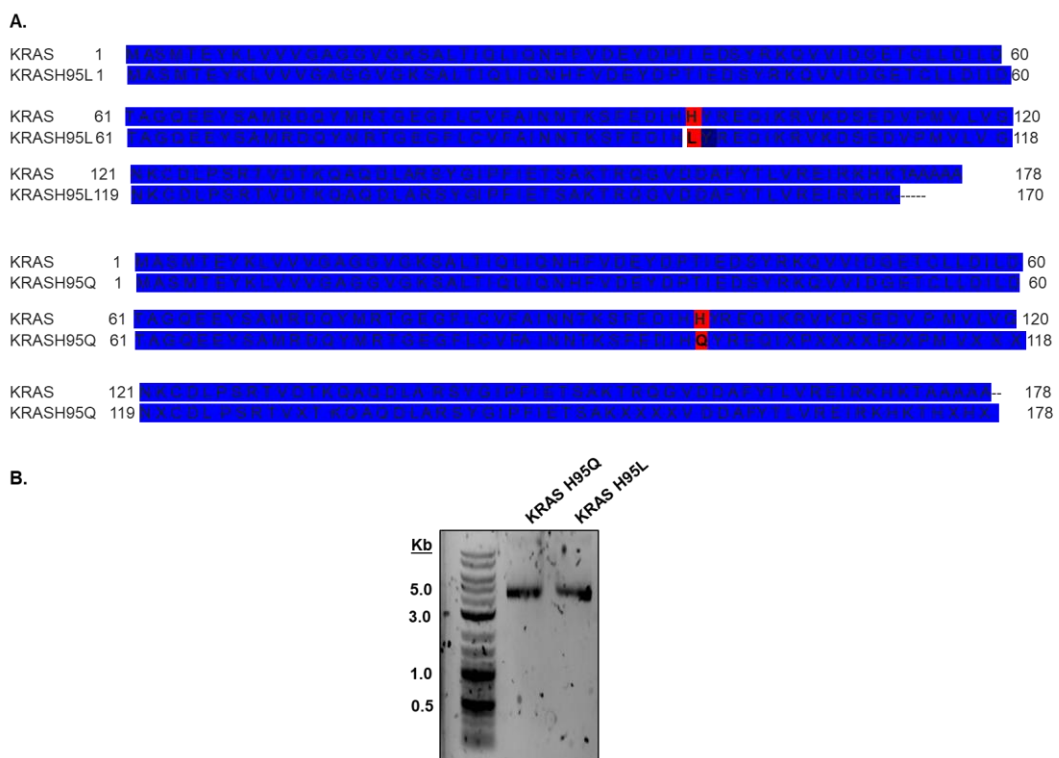


Figure 5.1 Site directed mutagenesis and sequence of KRas H95Q/L. A. Sequence alignment between KRas WT and KRas H95Q/L shows point mutation at 95 position to Gln and Leu. **B.** KRas was mutated to Q and L at H 95 via site directed mutagenesis protocol using KRas WT sequence as a template (pET11a 5677bp). DNA was loaded on agarose gel to verify presence of DNA and sent for sequencing.

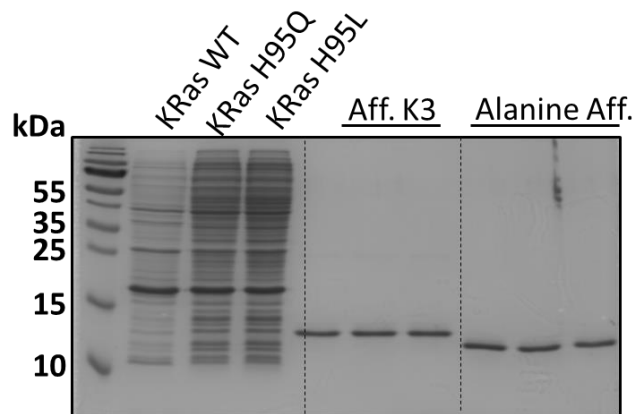


Figure 5.2 15% SDS PAGE gel showing protein expression of KRas WT, H95Q, H95L and Affimer K3/Alanine. Protein separation was performed on 15% Bis-Tris gel. Protein expression was carried in *E. coli* BL21 DE3 cell line. 20.5 KDa = KRas, KRas H95Q, KRas H95L *E. coli* cell lysates. 12 KDa =Affimer K3, 10.7 KDa =Alanine Affimer and KRas WT/H95Q= 20.5 kDa.

Once verified, mutated KRas cell lysates were produced in *E. coli* BL21 DE3 cells. Affimer K3 and Alanine Affimer (both VR1 and VR2) were also expressed and purified using Ni²⁺-NTA chromatography (See Figure 5.2). To analyse the effect of protein interactions between K3 Affimer and the mutated H95Q and H95L KRas, co-immunoprecipitation assay was carried out. K6 Affimer was used as positive control in this assay, since K6 binds to pocket between Switch I and II region and does not form hydrogen bond with H95 KRas (Haza, et al., 2020). Alanine Affimer was used as negative control for this assay since it does not bind to Ras (Figure 5.3 A). Prior to performing the assay Affimer K3, Alanine Affimer and K6 Affimer was purified and dialysed in PBS buffer (see section 2.2.3.1). 20 µg of purified Affimers (K3, K6 and Alanine Affimer) was pre-incubated with Ni²⁺-NTA magnetic agarose beads in separate tubes. These Affimers loaded beads were then added to KRas WT, H95Q and H95L proteins (without His-tag) present in *E. coli* cell lysate. For Affimer K3, a strong Ras band was observed for WT KRas, verifying the interaction between Affimer K3 and KRas (Figure 5.3B lane 9). For KRas H95Q (which represents HRas) there is 60% reduction in density compared to KRas WT (Figure 5.2B, C. lane 8). For H95L (which represent NRas) there is no Ras band, indicating K3 does not bind

to NRas isoform in this assay (Figure 5.3 B Lane 7). Affimer K6 shows nearly equal immunoprecipitation of Ras for KRas WT, H95Q and H95L protein samples (Figure 5.3 B lane 4, 5 and 6). This assay shows the preferential binding of Affimer K3 towards KRas isoform as compared to HRas and NRas.

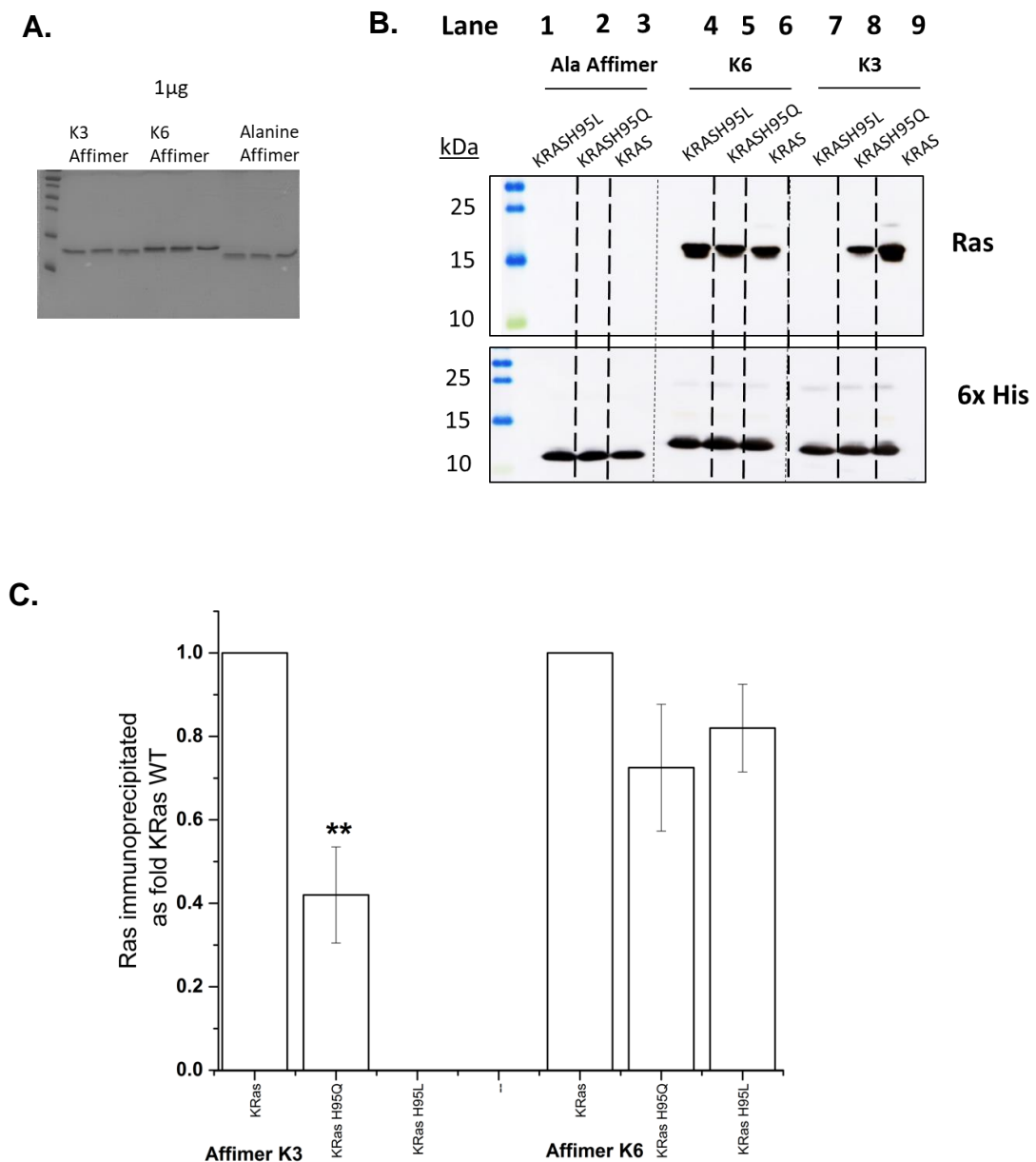


Figure 5.3 Immunoprecipitation of K3/K6 with KRas, KRas H95L and KRas H95Q. **A.** 1 μ g of Affimer K3, K6 and Alanine Affimer was run on 15% SDS-PAGE gel confirm concentration of Affimer. **B.** Pierce® Ni-NTA agarose magnetic beads were pre-incubated with 8x His tagged Affimer K3, K6 and Alanine Affimer. KRas WT/H95Q/H95L-Affimer complex was precipitated and pulled down proteins were analysed by western blot with anti-Ras and anti-His antibodies. Results are representative of three biological replicates (n=3). **C.** Densitometry analysis of Ras immunoprecipitated as fold KRas WT. Results are representative of three biological replicates (n=3). Error bars denote \pm SEM. Error bars are \pm SEM. p<0.05 (*), p<0.01 (**), p<0.001 (***) and p<0.0001 (****).

5.2.2 Structural analysis of Ras-Raf1RBD inhibition via Affimer K3

Ras is activated by GDP/GTP nucleotide exchange with the aid of guanine nucleotide exchange factors such as SOS1, Ras GRF, Ras GEF, PLCE1 etc. It triggers range of signalling cascades through interactions with multiple effectors. This includes effectors like Raf, PI3K, Tiam1, Ral GDS and Nore1 (Athuluri-Divakar et al., 2016). The well characterised Ras effectors such as Raf, PI3K γ and Ral GDS share a common Ras binding domain (RBD) that binds to Ras. Structural analysis of various RBD shows a common ubiquitin like fold that consists of five stranded β sheets flanked by two α helices. The structures of Ras and Raf complexes show Raf RBD interact with Ras via residues in β 2 and C terminal end of α 1 (Filchtinski et al., 2010). Efforts to develop small molecules that prevent Ras binding to effector proteins like Raf kinases have largely been unsuccessful. This is primarily because antiparallel β sheets that form the interface region between Ras and effector such as Raf, offer no pockets for small molecule to bind with high affinity (McCormick, 2018). In the previous chapters (Chapter 3 and 4). Affimer K3 when it binds to Switch II region of Ras, it causes a conformational shift in α -2 helix to reveal druggable binding pocket resulting in steric clash between M67 of Ras and R67 of RBD. This steric clash perturbs the salt bridge network that is formed between E37 of Ras and terminates at Raf RBD R100 (See Figure 5.4) (Fetics et al., 2015). If this steric clash is proven true, then this could explain the mechanism of inhibition of Ras/Raf inhibition when K3 binds to KRas. Point mutagenesis of these residues followed by pulldown assays was carried out in this chapter to verify the presence of the steric clash.

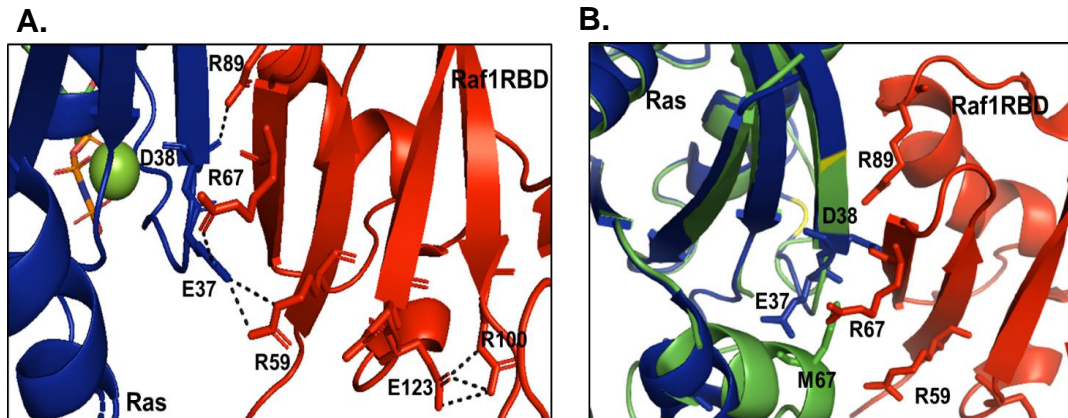


Figure 5.4 Structural overlay and comparison between HRas: Raf1RBD and KRas: Affimer K3. **A.** Crystal structure of HRas: Raf1RBD (PDB: 4G0N) shows E37 forming hydrogen bonds with R59 and R67 of Raf1RBD (as seen in dashed black lines). **B.** Crystal structure of HRas: Raf1RBD (blue) overlaid with KRas: Affimer K3 complex (green) shows shift in E37 and D38 (blue) side chain and perturbation of salt bridge network that begins with E37 and terminates at R100 of Raf1-RBD. Also shown is steric clash between M67 of α -2 helix after Affimer K3 binds to KRas and R67 of Raf1-RBD.

To verify steric clash between M67 side chain of α -3 and R67 of Raf RBD (Figure 5.4B), M67 KRas side chain was mutated to alanine (A) and R67 Raf RBD to alanine (A) or glutamic acid (E) using site-directed mutagenesis. This was done to see if mutating these residues might relieve the inhibition. After the sequence was verified the proteins were expressed and purified as described in the section 2.2.3 (See Figure 5.5).

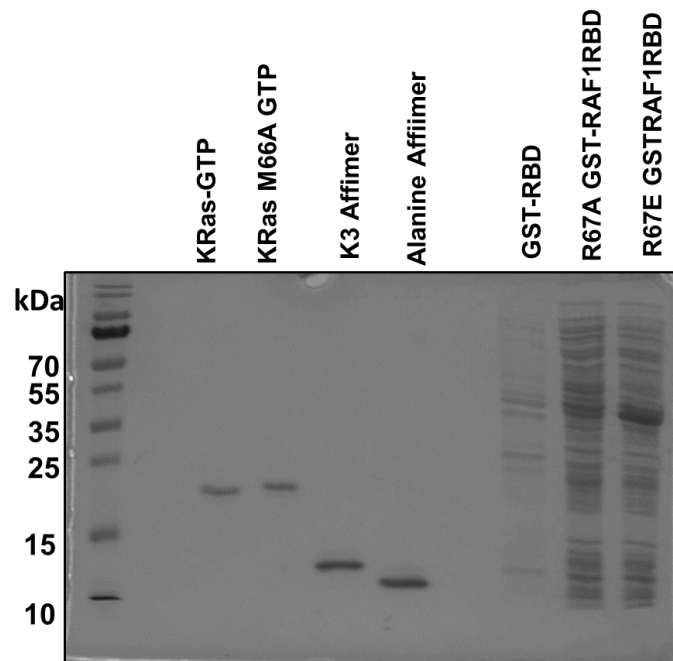


Figure 5.5 SDS PAGE to verify protein expression of KRas WT and GSTRBD. After site directed mutagenesis of KRas WT to KRas M66A and GST RBD to GSTRBDR67A and R67E, protein expression in *E. coli* BL21 DE3 was carried out. KRas WT and mutant proteins were purified via Ni²⁺-NTA chromatography. GST RBD WT and mutant proteins were expressed and run on 15% Bis-Tris gel via SDS-PAGE and Coomassie stained for visualisation. KRas -20.5 kDa, GST Raf1RBD = 42 KDa.

Initially, KRas WT and KRas M67A was loaded with GppNHp and verified using native mass spectrometry (refer sec 2.3.3). Following which Affimer K3 was pre-incubated with KRas WT and KRas M67A protein present in two separate tubes and added to glutathione coated magnetic beads. After incubation for an hour, GST RBD Raf1 WT was added to the protein complex of Affimer K3-KRas WT and KRas M67A separately. The same process was repeated using GST RBD Raf1R67A and R67E mutant Raf *E. coli* cell lysate (see section 2.2.6 for more details). The beads were washed three times, and protein complex was eluted and run on 15% w/v SDS PAGE gel and the blot was stained using anti Ras, GST and 6x His antibodies. This pulldown assay was carried out to analyse the effect of Affimer K3 on interaction between KRas WT and KRas M67A R67A/E of RBDRaf1. No Ras band was observed on the blot for WT Ras-Raf when Affimer K3 binds, indicating successful inhibition of Ras-Raf complex

(Figure 5.6 B lane 1). Also, when Raf R67 was mutated to glutamic acid (R67E), it relieved the inhibition in presence of Affimer K3 as observed by a Ras band in the output (Figure 5.6B lane 6). But when Alanine Affimer was used as control there is no band observed for Ras only as well as any RasM67A or RafR67A/E mutant lanes (Figure 5.6A lane 2-8), indicating failure to verify the presence of steric clash between M67 of Ras and R67 of Raf1RBD. This experiment was carried out only once and needs to be repeated.

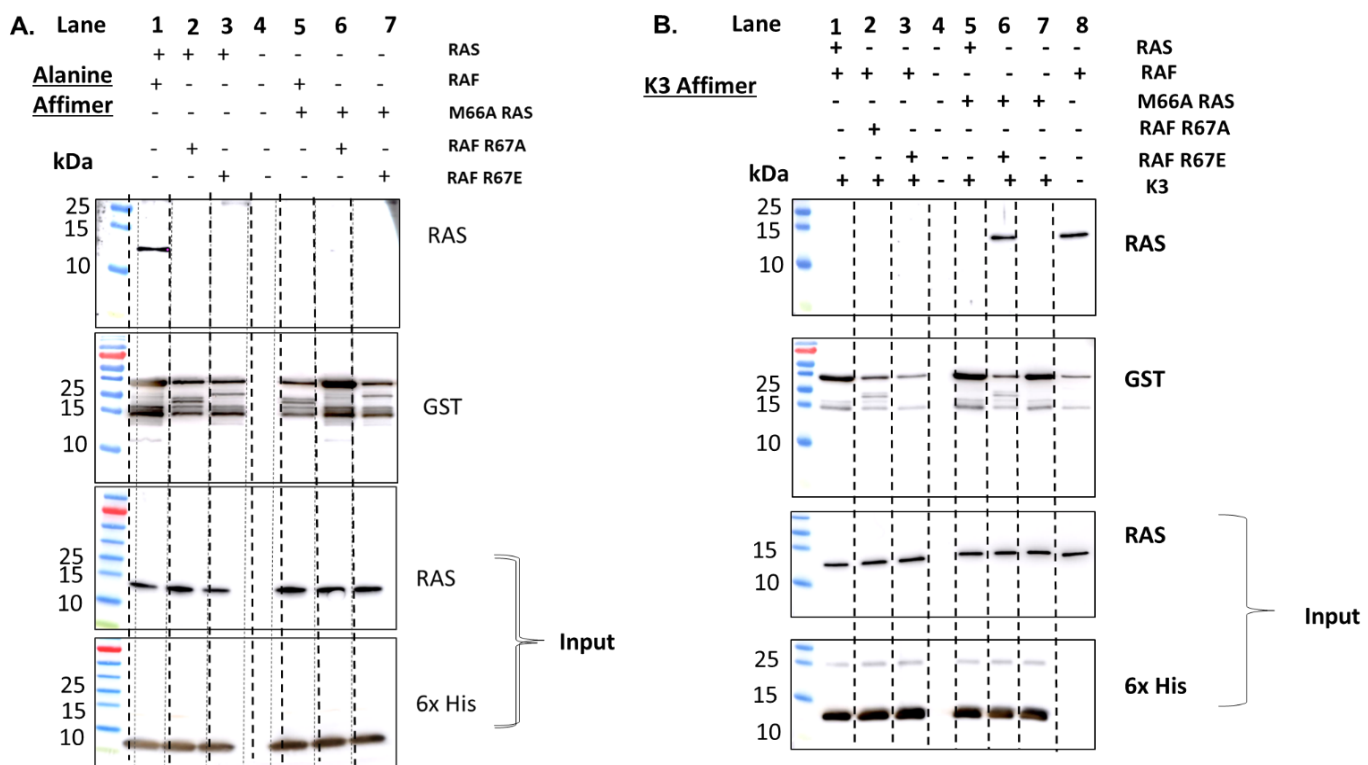


Figure 5.6 Co-immunoprecipitation assay showing effect of mutation on residues involved in Ras:Raf inhibition A. Prior to pulldown assay the samples was run on 15% SDS PAGE to verify the expression of the KRas and RAF1 RBD WT and point mutants. Following which K3 Affimer is incubated with KRas WT and M67A Ras and then allowed to interact with RafR67A and R67E with KRas and Raf1RBD as control and western blot of samples was carried out using Ras, GST antibodies for output and Ras and 6x His antibodies for input samples **B.** Same layout and western blotting was carried out using Alanine Affimer as control (n=1).

5.3 Discussion

In this chapter it has been demonstrated that Affimer K3 shows preferential specificity for KRas as compared to HRas and no binding affinity towards NRas. Affimer K3 has shown to bind in a pocket between SII α -2 and α 3 helix of Ras. W44 residue of Affimer K3 forms a hydrogen bond with H95 residue present in α -3 helix of KRas, which is only found in KRas, thereby confirming KRas selectivity. Recently KRas specific DARPins K13 and K19 have been isolated that can bind KRas at the allosteric lobe i.e. helix 3 loop7 and helix 4 region. However, the key difference is that DARPins that bind H95 do not probe SII/ α 3 pocket and instead binds to other side of α -3 helix, and therefore not revealing the novel conformation. Affimer K3 has shown preferential specificity towards KRas as compared to HRas (60% less fold) and no binding to NRas and is correlated by nucleotide exchange assays (chapter 3). The SII/ α 3 pocket identified by K3 Affimer may help achieve the first non-covalent small molecule inhibitors of KRas. These small molecules may have similar properties to the E3-ligase fused DARPins K19 and can be used in affinity directed protein missile system (AdPROM) (Roth et al., 2020). This system has shown to selectively degrade KRas and inhibit AKT, ERK and MEK phosphorylation in cell lines expressing mutant KRas (this include cell lines namely MIA PaCa2, H358 etc). This is an exciting avenue to be explored in the future studies.

The correct conformation of the switch II is important for Ras-Raf binding (Kiel et al., 2009). Upon Affimer K3 binding to KRas, it prevents the Switch II from adopting a correct conformation, preventing Ras: Raf RBD binding by shifting the α -2 helix of Ras. The positioning of the side chain of E37 and D38 of KRas changes when K3 Affimer binds and perturbs the H-bonding interactions with R59 and R89 of Raf1 respectively. The structural overlay with Ras: Raf1 RBD (PDB: 4G0N) with KRas: Affimer K3 shows a steric clash between M67Ras and R67 Raf1RBD which perturbs the salt bridge network. But in solution these side chains would move away and mutating to alanine would not make difference. Therefore, to verify the presence of steric clash, mutation of R67 to E was carried out helps relieve the inhibition. This was done based on the premise

that α -2helix dipole (with positive charge created at N terminus) helps repel the two arginine residues R59 and R67 of Raf1 away from Ras structure when K3 Affimer is used. Although, there is evidence of steric clash, as seen in the crystal structure of KRas: Affimer K3 M67 Ras and R67 of Raf1RBD would move away in solution, hence mutating these residues would not have any effect. Instead mutating E37Ras-R59Raf or D38Ras-R89Raf to alanine would be beneficial to understand how these residues play a role in Ras-Raf interaction.

In conclusion, data presented in this chapter demonstrates that Affimer K3 shows preferential binding to KRas as compared to HRas and no binding to NRas. Overall, these findings demonstrate the benefits of Affimer technology to identify and study the effects of different isoforms of Ras for research, diagnostics and therapeutic use.

Chapter 6

Discussion and future perspectives

Ras proteins are small GTPases that act as binary molecular switch and are involved in regulation of various cellular functions such as cell proliferation, differentiation, migration, and apoptosis (Karnoub and Weinberg, 2008). Ras proteins are frequently mutated in human cancers, with an average mutation incidence of 25% in all human tumours (Hobbs et al., 2016). The highest incidence of aberrant Ras signalling is due to single base missense mutations mostly occurring at codon 12, 13 and 61. These mutations impair GAP-induced GTP hydrolysis activity of Ras and therefore causing Ras to be in permanent active GTP bound state, which lead to uncontrolled cell growth (Prior et al., 2012) (Figure 6.1).

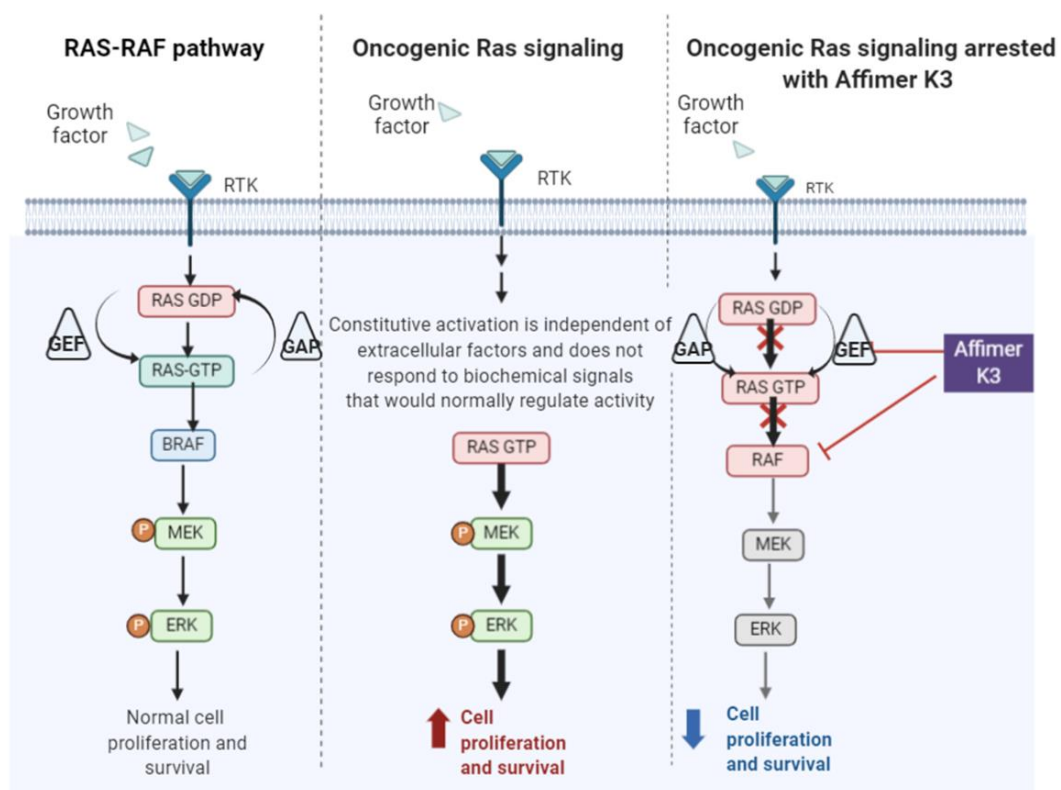


Figure 6.1 Comparison of normal, oncogenic Ras signalling and inhibition of oncogenic KRas with help of Affimer K3. Affimer K3 has shown to have dual mode of function-it inhibits SOS^{cat} (GEF) mediated nucleotide exchange as well as Ras-Raf interaction. Affimer K3, K6 and K37 has shown to bind to intracellular Ras and inhibit downstream signalling. Inset- Affimer K3 binding

(Figure 6.1 legend continued) between switch II and α 3 region of KRas. Adapted from “Vemuravenib in oncogenic BRaf signalling pathway in melanoma” by Biorender.com (2020).

Direct targeting of mutant Ras has been challenging due to two main reasons- firstly, due to lack of deep druggable pockets to which small molecule can bind. Secondly, it is due to high picomolar affinity of GTP towards the nucleotide-binding pocket making it difficult to develop effective competitive inhibitors (Ostrem and Shokat., 2016; Stephen et al., 2014; Dang et al., 2017). But recently there has been success in development of allele specific covalent inhibitors that selectively target KRAS^{G12C}, which is the most commonly found mutation present in non-small cell lung tumours (Mullard, 2019; McCormick., 2019; Canon et al., 2019; Janes et al., 2018). The inherent reactive nature of cysteine present at codon 12 of KRas^{G12C} has been leveraged to develop covalent small molecule inhibitors. These covalent compounds bind KRas in GDP bound state and blocked nucleotide exchange and KRas^{G12C} association with Raf (Moore et al., 2020). Covalent inhibitors of KRas^{G12C} have shown to bind exclusively to GDP bound state at the allosteric pocket behind Switch II (SII-P) (Ostrem and Shokat., 2016). However, resistant mutations could arise in KRas^{G12C} that could influence intrinsic GTPase activity or GDP/GTP exchange. Recently, small molecule compound namely 2C07 has been discovered that bind to both nucleotide states of Ras. 2C07 compound bind to a new Switch II groove (SII-G) adjacent to SII-P (Lu, J. et al., 2017; Gentile et al., 2017). Analysis of B factors from deposited GppNHp structure of HRas^{G12C} and NMR studies suggests that switch-II region is dynamic in nature and Ras transitions between multiple conformational states to accommodate effector binding and GTPase activities. Targeting both GTP and GDP bound states opens the possibility of inhibiting oncogenic Ras mutants which exists predominantly in GTP bound state (Gentile et al., 2017).

We have used phage display technology to identify seven unique Affimer proteins that bind to KRas irrespective of its nucleotide state. Three of the seven Affimers namely K3, K6 and K37 Affimers were identified as the most potent

inhibitors of SOS^{cat} mediated nucleotide exchange. Affimer K3 was the most potent inhibitor with IC₅₀ value of 200 nM ± 6 nM compared to K6 (594 ± 271 nM) and K37 (697 ± 158 nM) when using WT KRas. Further characterization of K3 binder revealed that K3 exhibits dual mode of inhibition i.e. it inhibits nucleotide exchange as well as Ras/Raf interaction (chapter 3) (Figure 6.1). The critical residues in K3 involved in binding and inhibition of KRas were identified using alanine scanning mutagenesis. Crystal structure of Affimer K3 binding to KRas showed that K3 Affimer selects a novel Ras conformation to reveal a druggable pocket between SII and α3 helix (chapter 4). Recently Gentile and colleagues have found that for non-covalent binding to SII-P, a substituted phenolic ring is required for insertion within the sub pocket formed by V9, R68, D69 and M72 (Gentile et al., 2017). Here we observed that Affimer K3 also has the aromatic ring of W44 extending into this sub-pocket. Aromatic ring of W44 has also shown to engage with His-95 residue, which may explain the specificity of K3 for KRas as demonstrated in our pulldown (chapter 5) and cellular assays (Haza, K.Z et al., 2020). The SII/α-3 pocket identified by K3 shares this key sub-pocket with the SII-P.

Taken together these findings show that Affimers can be used to inhibit KRas by identifying cryptic binding pockets that are not present in the unbound structure. Furthermore, this also highlights the use of Affimer technology to select novel conformers of various target proteins to reveal druggable regions.

6.1 Use of Affimers to inhibit KRas function

In recent years, there has been resurgence of research to directly target Ras, due to advances in drug discovery technologies such as fragment based lead discovery (FBLD) and disulphide-tethering technology (Sun et al., 2014). These technologies have helped to identify two pockets on surface of Ras that are amenable to drug discovery (O'Bryan., 2019). First is pocket between switch I and switch II of KRas (referred as SI/SII pocket) and second is SII-pocket, positioned above switch II loop. Researchers at Genentech (Maurer et al., 2012), Vanderbilt University (Sun et al., 2012) and the Rabbits group (Quevedo et al., 2018; Cruz-Migoni et al., 2019) identified small molecules that bind to SI/SII pocket. SI/SII pocket has been shown to be involved in interaction with

GEFs, GAPs and downstream effectors. Using Affimer technology, out of seven unique Affimer binders, Affimer K6 was shown to bind to both active and inactive forms of Ras with low nanomolar affinities and inhibit SOS^{cat} mediated nucleotide exchange reaction ($K_d=1.36\pm 0.87$ nM for GDP and $K_d=7.88$ nM for GppNHp) (Haza, Katarzyna Z et al., 2020; Kessler et al., 2019). All small molecules which have been shown to bind to SI/SII pocket (see appendix C) such as DCAI, compound 13 and Abd-7 have an aromatic ring inserting into SI/SII pocket (Sun et al., 2012; Maurer et al., 2012). This aromatic ring has shown to be easily reproduced by W43 side chain of Affimer K6, thereby highlighting the structural similarities of SI/SII molecules with K6 pharmacophore. Affimer K3 has also shown to inhibit SOS^{cat} mediated nucleotide exchange as it locks KRas in inactive conformation by stapling the switch regions through induced hydrogen bonding involving E37 of switch I and S65, A59 and G60 of switch II (chapter 4 Figure 4.8). Also, both K3 and K6 have shown to bind to endogenous Ras and have resulted in significant reduction in p-ERK levels (Haza, K.Z et al., 2020). However, the degree to which Affimers inhibit activation of Ras by other GEFs such as Ras-GRP, GRF has not being studied. Nevertheless, SOS^{cat} is most widely studied GEF for Ras activation and logical target for exchange assays. Thus, Affimer K3 and K6 can be used as useful *in-vitro* tool to study Ras signalling.

6.2 Identification of cryptic binding sites in Ras using Affimer K3

Besides using Affimers to study Ras signalling, Affimer K3 has been used to identify cryptic binding site between SII and alpha 3 helix. These cryptic sites can provide druggable targets and require a ligand to form a pocket that can be identified in ligand bound and not in unbound structure of protein (Vajda et al., 2018). Affimer K3 when it binds to KRas, caused a conformational shift in α -2 SII region to reveal a novel Ras conformation with druggable SII/ α -3 pocket (Chapter 4). This conformational shift generates a new network of intramolecular hydrogen bonds in KRas that has not being observed in unbounded WT KRas GDP or KRas GppNHp. However, The SII/ α 3 pocket has been previously being identified using cyclic peptide KRpep-2d in mutant

KRas^{G12D} (Sogabe et al., 2017). But K3 engages with KRas specific residue namely His-95, to which KRpep-2d does not bind. Additionally, Affimer K3 induces intramolecular hydrogen bonding between Q61 and Y96 without the involvement of residue 12, whereas KRpep-2d requires an Asp to induce similar bonding network. This specificity has been demonstrated in our pulldown (chapter 5) and cellular assays (Haza, K.Z et al., 2020). All these findings show that Affimer K3 binds to SII/ α 3 pocket in unique conformation different from peptides and small molecules. In addition to molecular dynamics, reliable cryptic site prediction can be improved by using highly specific binding proteins with small interaction surfaces (Beglov et al., 2018). Therefore, Affimers can be used as tools to identify cryptic binding pockets in 'difficult to drug/undruggable' protein targets.

6.3 Continuation of the project and future applications

Data obtained in this thesis can be expanded and improved upon in several ways. Firstly, Affimer K3 has shown to inhibit Ras-RBDRaf1 interaction via pulldown assay (Chapter 3 Fig 3.7). RBD has ubiquitin fold and is principle interface of interaction with GTP-Ras. But a cysteine rich domain (CRD) is required for full activation of Raf kinase (Okada et al., 1999). Therefore, further research by using live cell imaging experiments involving fluorescent proteins fused to the Ras binding domain and cysteine rich domain would provide an additional line of evidence of the effect of Affimers on regulation of Raf kinase activity. Techniques such as nano-bioluminescence resonance energy transfer (BRET) can be used to study the effect of Affimers on Ras-effectors such as PI3K and RalGDS. BRET is biophysical technique used to monitor proximity between proteins /molecules within live cells (Dale et al., 2019). The information will provide more insights on other signalling pathways besides MAPK pathway, involved in cell proliferation and differentiation.

Also, both variable regions of Affimer K3 have shown binding and inhibition of Ras via pulldown assays (Chapter 3 Fig 3.9 and 3.10). Additional experiments to know the affinity of each deleted loop mutants via SPR or ITC can provide

additional insights on the binding of K3VR2. This is important to understand why L73 and K80 residues of loop2 are involved in binding (Fig 3.13). If SPR shows weak binding in case of K3 Δ VR1 then this data can correlate with pulldown and CD studies. The effect of Affimers (K3, K6 and K37) on WT Ras and oncogenic Ras mutants can be further studied using electron microscopy (EM) spatial analysis using plasma membrane (PM) sheets to study the effect on PM localisation and nanoclustering. This is important since Ras proteins assemble into nanoclusters transiently and are sites for Ras effector recruitment and activation (Zhou and Hancock, 2015).

Structural characterisation has shown that Affimer K3 identifies a SII/ α 3 pocket in KRas using X-ray crystallography. Since X-ray crystallography is static snapshot, nuclear magnetic resonance (NMR) (Schulze-Sunninghausen et al., 2014) can provide supporting evidence to show the presence of SII/ α 3 pocket when K3 Affimer binds. Affimer K3 has shown to have preferential selectivity towards KRas over HRas and no binding to NRas isoform as evidenced by pulldown (chapter 5) and nucleotide exchange studies. Further experiments using BRET assay to see effect of mutating H95 residue to Q/L using Affimer K3 could add important information to this project.

Affimer K3 derived small molecule series obtained can be further characterised by obtaining KRas-compound co-crystal structures. This can be followed by studies of these compounds on cell proliferation, apoptosis and Ras-effector interactions. Obtaining KRas-K3 derived compounds crystal structures could inform structure-based optimisation of compounds to achieve better potency or new series like that observed using intracellular antibodies binding to KRas. Additionally, the effect of these compounds on cancer cell growth and proliferation could provide interesting insights on how the small molecules function.

Another strategy that can be employed for continuation of this project is not direct inhibition of KRas, but targeted degradation of KRas through ubiquitin proteasome system. Sapkota and colleagues have developed an affinity directed protein missile system (AdPROM) for targeted degradation of endogenous KRas using VHL-GFP-nanobody fusion (Roth et al., 2020). Affimer

K3 can be used by substituting the nanobody binder in AdPROM system and can be used to verify degradation of endogenous KRas or HRas.

6.3.1 Affimers as therapeutics

Apart from their use as pharmacological research tools, Affimers being utilised as therapeutics themselves is a future possibility. Biologics consisting of monoclonal antibodies have become the fastest growing class of cancer therapeutics. There are currently about 30 monoclonal antibodies approved by FDA for treatment of cancer (Lu, R.M. et al., 2020). However, while majority of these monoclonal antibodies in the market have been used against extracellular targets, the main limitation is that due to their large size (>150 kDa), it is unable to cross the cell membrane (Walker et al., 2017). Thus, leaving the intracellular targets out of their reach (Tsomaia, 2015). Since proteins are in general not cell permeable, intracellular applications needs to be accomplished by novel delivery technologies. Several strategies already exist to overcome this problem, and these include use of liposome based nanocarriers, engineered modular transport systems and fusion of antibodies with protein transduction domains (Slastnikova et al., 2018). For example, DARPins have been used to deliver into cytoplasm through engineered modular transport system involving *Pseudomonas* exotoxin A derived mechanism for translocation (Verdurmen et al., 2015). Despite these advances, intracellular delivery of proteins remains a challenging task for any new biologic therapy. Another hurdle to overcome concerns the immunogenicity of biologics. Administration of biotherapeutics carries a risk of production of anti-drug antibodies (ADAs), which in turn could impact the pharmacological properties of the therapeutic or trigger adverse side effects (Boehncke and Brembilla, 2018). Both Type I and Type II Affimer scaffolds did not induce a significant immunogenic response in an industry standard *in-vitro* immune cell assay namely peripheral blood mononuclear cells (PBMC) assay (Avacta Life Sciences, 2017). This, therefore, indicated that Affimer reagents do not possess fundamental immunogenicity problems and could progressed into therapeutic development.

Conclusions

Mutation in *RAS* genes have been found to present in 30% of all human cancers. Out of three *RAS* isoforms, *KRAS* is most frequently altered oncogene. Therapeutic strategies to target Ras mutant cancers have so far not being successful. A key aspect of this challenge is direct inhibition of Ras which has proven to be difficult leading to researchers terming Ras as 'undruggable' cancer target. In this thesis I have shown that Affimer technology has been used to identify binding pockets on KRas in very short timeframe, which scientific community has taken 30 years using traditional medicinal chemistry techniques.

The key findings of this study are:

1. Affimer K3 was shown to inhibit SOS^{cat} most potently with IC_{50} of 200 nM and inhibit Ras-RBDRaf1 interaction *in-vitro*.
2. Both variable regions of Affimer K3 have shown to be involved in binding and inhibition of KRas.
3. Crystal structure of Affimer K3-KRas protein complex was solved to 2.1 Å resolution. Affimer K3 selects a novel Ras conformer to reveal a druggable SII/ α 3 pocket.
4. Affimer K3 was shown to have preferential specificity to KRas isoform as it engages with His-95 residue which is present only in KRas and not in HRas and NRas.

Thus, Affimer K3 can be used to provide further insights into understanding KRas biology which will be of interest to cancer researchers.

References

- Adamson, H., Ajayi, M.O., Campbell, E., Brachi, E., Tiede, C., Tang, A.A., Adams, T.L., Ford, R., Davidson, A., Johnson, M., McPherson, M.J., Tomlinson, D.C. and Jeuken, L.J.C. 2019. Affimer-Enzyme-Inhibitor Switch Sensor for Rapid Wash-free Assays of Multimeric Proteins. *ACS Sens.* **4**(11), pp.3014-3022.
- Ahearn, I., Zhou, M. and Philips, M.R. 2018. Posttranslational Modifications of RAS Proteins. *Cold Spring Harb Perspect Med.* **8**(11).
- Ahearn, I.M., Haigis, K., Bar-Sagi, D. and Philips, M.R. 2011. Regulating the regulator: post-translational modification of RAS. *Nat Rev Mol Cell Biol.* **13**(1), pp.39-51.
- Aran, V. and Prior, I.A. 2013. Compartmentalized Ras signaling differentially contributes to phenotypic outputs. *Cell Signal.* **25**(9), pp.1748-1753.
- Athuluri-Divakar, S.K., Vasquez-Del Carpio, R., Dutta, K., Baker, S.J., Cosenza, S.C., Basu, I., Gupta, Y.K., Reddy, M.V., Ueno, L., Hart, J.R., Vogt, P.K., Mulholland, D., Guha, C., Aggarwal, A.K. and Reddy, E.P. 2016. A Small Molecule RAS-Mimetic Disrupts RAS Association with Effector Proteins to Block Signaling. *Cell.* **165**(3), pp.643-655.
- Baker, M. 2015. Reproducibility crisis: Blame it on the antibodies. *Nature.* **521**(7552), pp.274-276.
- Bar-Sagi, D. 2001. A Ras by any other name. *Mol Cell Biol.* **21**(5), pp.1441-1443.
- Beer. 1852. *Determination of absorption of red lights in coloured liquids.* [Online]. Available from: <https://onlinelibrary.wiley.com/doi/abs/10.1002/andp.18521620505>
- Beglov, D., Hall, D.R., Wakefield, A.E., Luo, L., Allen, K.N., Kozakov, D., Whitty, A. and Vajda, S. 2018. Exploring the structural origins of cryptic sites on proteins. *Proc Natl Acad Sci U S A.* **115**(15), pp.E3416-E3425.
- Bery, N., Legg, S., Debreczeni, J., Breed, J., Embrey, K., Stubbs, C., Kolasinska-Zwierz, P., Barrett, N., Marwood, R., Watson, J., Tart, J., Overman, R., Miller, A., Phillips, C., Minter, R. and Rabbitts, T.H. 2019.

KRAS-specific inhibition using a DARPIn binding to a site in the allosteric lobe. *Nat Commun.* **10**(1), p2607.

Binz, H.K., Amstutz, P., Kohl, A., Stumpp, M.T., Briand, C., Forrer, P., Grutter, M.G. and Pluckthun, A. 2004. High-affinity binders selected from designed ankyrin repeat protein libraries. *Nat Biotechnol.* **22**(5), pp.575-582.

Boehncke, W.H. and Brembilla, N.C. 2018. Immunogenicity of biologic therapies: causes and consequences. *Expert Rev Clin Immunol.* **14**(6), pp.513-523.

Boersma., Y.L. 2018. Advances in the Application of Designed Ankyrin Repeat Proteins (DARPin)s as Research Tools and Protein Therapeutics. *Methods Mol Biol.* **1798**, pp.307-327.

Boriack-Sjodin, P.A., Margarit, S.M., Bar-Sagi, D. and Kuriyan, J. 1998. The structural basis of the activation of Ras by Sos. *Nature.* **394**(6691), pp.337-343.

Bos, J.L., Rehmann, H. and Wittinghofer, A. 2007. GEFs and GAPs: critical elements in the control of small G proteins. *Cell.* **129**(5), pp.865-877.

Burslem, G.M., Kyle, H.F., Nelson, A., Edwards, T.A. and Wilson, A.J. 2017. Hypoxia inducible factor (HIF) as a model for studying inhibition of protein-protein interactions. *Chem Sci.* **8**(6), pp.4188-4202.

Canon, J., Rex, K., Saiki, A.Y., Mohr, C., Cooke, K., Bagal, D., Gaida, K., Holt, T., Knutson, C.G., Koppada, N., Lanman, B.A., Werner, J., Rapaport, A.S., San Miguel, T., Ortiz, R., Osgood, T., Sun, J.R., Zhu, X., McCarter, J.D., Volak, L.P., Houk, B.E., Fakhri, M.G., O'Neil, B.H., Price, T.J., Falchook, G.S., Desai, J., Kuo, J., Govindan, R., Hong, D.S., Ouyang, W., Henary, H., Arvedson, T., Cee, V.J. and Lipford, J.R. 2019. The clinical KRAS(G12C) inhibitor AMG 510 drives anti-tumour immunity. *Nature.* **575**(7781), pp.217-223.

Capon, D.J., Chen, E.Y., Levinson, A.D., Seeburg, P.H. and Goeddel, D.V. 1983. Complete nucleotide sequences of the T24 human bladder carcinoma oncogene and its normal homologue. *Nature.* **302**(5903), pp.33-37.

Carney., D.N. 1990. Molecular biology of cancer. *Ir J Med Sci.* **159**(6), p171.

Carter., P.J. 2011. Introduction to current and future protein therapeutics: a protein engineering perspective. *Exp Cell Res.* **317**(9), pp.1261-1269.

- Carugo, O. 2018. How large B-factors can be in protein crystal structures. *BMC Bioinformatics*. **19**(1), p61.
- Castellano, E. and Downward, J. 2011. RAS Interaction with PI3K: More Than Just Another Effector Pathway. *Genes Cancer*. **2**(3), pp.261-274.
- Chavan, T.S., Muratcioglu, S., Marszalek, R., Jang, H., Keskin, O., Gursoy, A., Nussinov, R. and Gaponenko, V. 2015. Plasma membrane regulates Ras signaling networks. *Cell Logist*. **5**(4), pe1136374.
- Chia, M.M., Holmes, M.D. and McLennan, G. 1991. The molecular biology of lung cancer. *Med J Aust*. **154**(8), pp.501-503.
- Clark, R., Wong, G., Arnheim, N., Nitecki, D. and McCormick, F. 1985. Antibodies specific for amino acid 12 of the ras oncogene product inhibit GTP binding. *Proc Natl Acad Sci U S A*. **82**(16), pp.5280-5284.
- Coffin, J.M., Hughes, S.H. and Varmus, H.E. 1997. The Interactions of Retroviruses and their Hosts. In: Coffin, J.M., et al. eds. *Retroviruses*. Cold Spring Harbor (NY).
- Colicelli., J. 2004. Human RAS superfamily proteins and related GTPases. *Sci STKE*. **2004**(250), pRE13.
- Cox, A.D. and Der., C.J. 2010. Ras history: The saga continues. *Small GTPases*. **1**(1), pp.2-27.
- Cox, A.D., Fesik, S.W., Kimmelman, A.C., Luo, J. and Der, C.J. 2014. Drugging the undruggable RAS: Mission possible? *Nat Rev Drug Discov*. **13**(11), pp.828-851.
- Cruz-Migoni, A., Canning, P., Quevedo, C.E., Bataille, C.J.R., Bery, N., Miller, A., Russell, A.J., Phillips, S.E.V., Carr, S.B. and Rabbitts, T.H. 2019. Structure-based development of new RAS-effector inhibitors from a combination of active and inactive RAS-binding compounds. *Proc Natl Acad Sci U S A*. **116**(7), pp.2545-2550.
- Cseh, B., Doma, E. and Baccarini, M. 2014. "RAF" neighborhood: protein-protein interaction in the Raf/Mek/Erk pathway. *FEBS Lett*. **588**(15), pp.2398-2406.
- Dale, N.C., Johnstone, E.K.M., White, C.W. and Pflieger, K.D.G. 2019. NanoBRET: The Bright Future of Proximity-Based Assays. *Front Bioeng Biotechnol*. **7**, p56.

- Dang, C.V., Reddy, E.P., Shokat, K.M. and Soucek, L. 2017. Drugging the 'undruggable' cancer targets. *Nat Rev Cancer*. **17**(8), pp.502-508.
- De Las Rivas, J. and Fontanillo., C. 2010. Protein-protein interactions essentials: key concepts to building and analyzing interactome networks. *PLoS Comput Biol*. **6**(6), pe1000807.
- Der, C.J., Krontiris, T.G. and Cooper, G.M. 1982. Transforming genes of human bladder and lung carcinoma cell lines are homologous to the ras genes of Harvey and Kirsten sarcoma viruses. *Proc Natl Acad Sci U S A*. **79**(11), pp.3637-3640.
- Dharmaiah, S., Bindu, L., Tran, T.H., Gillette, W.K., Frank, P.H., Ghirlando, R., Nissley, D.V., Esposito, D., McCormick, F., Stephen, A.G. and Simanshu, D.K. 2016. Structural basis of recognition of farnesylated and methylated KRAS4b by PDEdelta. *Proc Natl Acad Sci U S A*. **113**(44), pp.E6766-E6775.
- Dhillon, A.S., Hagan, S., Rath, O. and Kolch, W. 2007. MAP kinase signalling pathways in cancer. *Oncogene*. **26**(22), pp.3279-3290.
- Dimitrov., D.S. 2012. Therapeutic proteins. *Methods Mol Biol*. **899**, pp.1-26.
- Emsley, P. and Cowtan., K. 2004. Coot: model-building tools for molecular graphics. *Acta Crystallogr D Biol Crystallogr*. **60**(Pt 12 Pt 1), pp.2126-2132.
- End, D.W., Smets, G., Todd, A.V., Applegate, T.L., Fuery, C.J., Angibaud, P., Venet, M., Sanz, G., Poignet, H., Skrzat, S., Devine, A., Wouters, W. and Bowden, C. 2001. Characterization of the antitumor effects of the selective farnesyl protein transferase inhibitor R115777 in vivo and in vitro. *Cancer Res*. **61**(1), pp.131-137.
- Erlanson, D.A. and Hansen., S.K. 2004. Making drugs on proteins: site-directed ligand discovery for fragment-based lead assembly. *Curr Opin Chem Biol*. **8**(4), pp.399-406.
- Etienne-Manneville, S. and Hall., A. 2002. Rho GTPases in cell biology. *Nature*. **420**(6916), pp.629-635.
- Fetics, S.K., Guterres, H., Kearney, B.M., Buhrman, G., Ma, B., Nussinov, R. and Mattos, C. 2015. Allosteric effects of the oncogenic RasQ61L mutant on Raf-RBD. *Structure*. **23**(3), pp.505-516.
- Filchtinski, D., Sharabi, O., Ruppel, A., Vetter, I.R., Herrmann, C. and Shifman, J.M. 2010. What makes Ras an efficient molecular switch: a

- computational, biophysical, and structural study of Ras-GDP interactions with mutants of Raf. *J Mol Biol.* **399**(3), pp.422-435.
- Frejd, F.Y. and Kim., K.T. 2017. Affibody molecules as engineered protein drugs. *Exp Mol Med.* **49**(3), pe306.
- Gallardo, G., Wong, C.H., Ricardez, S.M., Mann, C.N., Lin, K.H., Leyns, C.E.G., Jiang, H. and Holtzman, D.M. 2019. Targeting tauopathy with engineered tau-degrading intrabodies. *Mol Neurodegener.* **14**(1), p38.
- Gauguin, L., Delaine, C., Alvino, C.L., McNeil, K.A., Wallace, J.C., Forbes, B.E. and De Meyts, P. 2008. Alanine scanning of a putative receptor binding surface of insulin-like growth factor-I. *J Biol Chem.* **283**(30), pp.20821-20829.
- Gebauer, M. and Skerra., A. 2019. Engineering of binding functions into proteins. *Curr Opin Biotechnol.* **60**, pp.230-241.
- Gentile, D.R., Rathinaswamy, M.K., Jenkins, M.L., Moss, S.M., Siempelkamp, B.D., Renslo, A.R., Burke, J.E. and Shokat, K.M. 2017. Ras Binder Induces a Modified Switch-II Pocket in GTP and GDP States. *Cell Chem Biol.* **24**(12), pp.1455-1466 e1414.
- Gorrec, F. 2009. The MORPHEUS protein crystallization screen. *J Appl Crystallogr.* **42**(Pt 6), pp.1035-1042.
- Grant, B.J., Lukman, S., Hocker, H.J., Sayyah, J., Brown, J.H., McCammon, J.A. and Gorfe, A.A. 2011. Novel allosteric sites on Ras for lead generation. *PLoS One.* **6**(10), pe25711.
- Greenfield., N.J. 2006. Using circular dichroism spectra to estimate protein secondary structure. *Nat Protoc.* **1**(6), pp.2876-2890.
- Grimm, S., Lundberg, E., Yu, F., Shibasaki, S., Vernet, E., Skogs, M., Nygren, P.A. and Graslund, T. 2010. Selection and characterisation of affibody molecules inhibiting the interaction between Ras and Raf in vitro. *N Biotechnol.* **27**(6), pp.766-773.
- Guillard, S., Kolasinska-Zwierz, P., Debreczeni, J., Breed, J., Zhang, J., Bery, N., Marwood, R., Tart, J., Overman, R., Stocki, P., Mistry, B., Phillips, C., Rabbitts, T., Jackson, R. and Minter, R. 2017. Structural and functional characterization of a DARPIn which inhibits Ras nucleotide exchange. *Nat Commun.* **8**, p16111.
- Gysin, S., Salt, M., Young, A. and McCormick, F. 2011. Therapeutic strategies for targeting ras proteins. *Genes Cancer.* **2**(3), pp.359-372.

- Haigis, K.M., Kendall, K.R., Wang, Y., Cheung, A., Haigis, M.C., Glickman, J.N., Niwa-Kawakita, M., Sweet-Cordero, A., Sebolt-Leopold, J., Shannon, K.M., Settleman, J., Giovannini, M. and Jacks, T. 2008. Differential effects of oncogenic K-Ras and N-Ras on proliferation, differentiation and tumor progression in the colon. *Nat Genet.* **40**(5), pp.600-608.
- Hall, B.E., Bar-Sagi, D. and Nassar, N. 2002. The structural basis for the transition from Ras-GTP to Ras-GDP. *Proc Natl Acad Sci U S A.* **99**(19), pp.12138-12142.
- Hanahan, D. and Weinberg., R.A. 2000. The hallmarks of cancer. *Cell.* **100**(1), pp.57-70.
- Hanahan, D. and Weinberg., R.A. 2011. Hallmarks of cancer: the next generation. *Cell.* **144**(5), pp.646-674.
- Hancock, J.F., Paterson, H. and Marshall, C.J. 1990. A polybasic domain or palmitoylation is required in addition to the CAAX motif to localize p21ras to the plasma membrane. *Cell.* **63**(1), pp.133-139.
- Harvey., J.J. 1964. An Unidentified Virus Which Causes the Rapid Production of Tumours in Mice. *Nature.* **204**, pp.1104-1105.
- Haylock, A.K., Nilvebrant, J., Mortensen, A., Velikyan, I., Nestor, M. and Falk, R. 2017. Generation and evaluation of antibody agents for molecular imaging of CD44v6-expressing cancers. *Oncotarget.* **8**(39), pp.65152-65170.
- Haza, K.Z., Martin, H.L., Rao, A., Turner, A., Saunders, S., Petersen, B., Tiede, C., Tipping, K., Tang, A.A., Ajayi, M., Taylor, T., Fishwick, K., Adams, T.L., Gaule, G.T., Trinh, C.H., Johnson, M., Breeze, A.L., T.A., E., McPherson, M.J. and Tomlinson, D.C. 2020. RAS-inhibiting biologics identify and probe druggable pockets including an SII- α 3 allosteric site. *BioRxiv.*
- Haza, K.Z., Martin, H.L., Rao, A., Turner, A.L., Saunders, S.E., Petersen, B., Tiede, C., Tipping, K., Tang, A.A., Ajayi, M., Taylor, T., Fishwick, K.M., Adams, T.L., Gaule, T.G., Trinh, C.H., Johnson, M., Breeze, A.L., Edwards, T.A., McPherson, M.J. and Tomlinson, D.C. 2020. RAS-inhibiting biologics identify and probe druggable pockets including an SII- α 3 allosteric site. p2020.2006.2004.133728.
- Haza., K. 2019. *Inhibition of Ras using Affimer reagents* PhD thesis, University of Leeds

- Heider, D., Hauke, S., Pyka, M. and Kessler, D. 2010. Insights into the classification of small GTPases. *Adv Appl Bioinform Chem.* **3**, pp.15-24.
- Hemmings, B.A. and Restuccia., D.F. 2012. PI3K-PKB/Akt pathway. *Cold Spring Harb Perspect Biol.* **4**(9), pa011189.
- Hillig, R.C., Sautier, B., Schroeder, J., Moosmayer, D., Hilpmann, A., Stegmann, C.M., Werbeck, N.D., Briem, H., Boemer, U., Weiske, J., Badock, V., Mastouri, J., Petersen, K., Siemeister, G., Kahmann, J.D., Wegener, D., Bohnke, N., Eis, K., Graham, K., Wortmann, L., von Nussbaum, F. and Bader, B. 2019. Discovery of potent SOS1 inhibitors that block RAS activation via disruption of the RAS-SOS1 interaction. *Proc Natl Acad Sci U S A.* **116**(7), pp.2551-2560.
- Hobbs, G.A., Der, C.J. and Rossman, K.L. 2016. RAS isoforms and mutations in cancer at a glance. *J Cell Sci.* **129**(7), pp.1287-1292.
- Hobbs, G.A. and Der., C.J. 2019. RAS Mutations Are Not Created Equal. *Cancer Discov.* **9**(6), pp.696-698.
- Hood, F.E., Klinger, B., Newlaczyk, A.U., Sieber, A., Dorel, M., Oliver, S.P., Coulson, J.M., Bluthgen, N. and Prior, I.A. 2019. Isoform-specific Ras signaling is growth factor dependent. *Mol Biol Cell.* **30**(9), pp.1108-1117.
- Hughes, D.J., Tiede, C., Penswick, N., Tang, A.A., Trinh, C.H., Mandal, U., Zajac, K.Z., Gaule, T., Howell, G., Edwards, T.A., Duan, J., Feyfant, E., McPherson, M.J., Tomlinson, D.C. and Whitehouse, A. 2017. Generation of specific inhibitors of SUMO-1- and SUMO-2/3-mediated protein-protein interactions using Affimer (Adhiron) technology. *Sci Signal.* **10**(505).
- Hunter, J.C., Manandhar, A., Carrasco, M.A., Gurbani, D., Gondi, S. and Westover, K.D. 2015. Biochemical and Structural Analysis of Common Cancer-Associated KRAS Mutations. *Mol Cancer Res.* **13**(9), pp.1325-1335.
- Irannejad, R., Tomshine, J.C., Tomshine, J.R., Chevalier, M., Mahoney, J.P., Steyaert, J., Rasmussen, S.G., Sunahara, R.K., El-Samad, H., Huang, B. and von Zastrow, M. 2013. Conformational biosensors reveal GPCR signalling from endosomes. *Nature.* **495**(7442), pp.534-538.
- Jancarik, J. and Kim, S.-H. 1991. Sparse matrix sampling: a screening method for crystallization of proteins. *Journal of Applied Crystallography.* **24**(4), pp.409-411.

- Janes, M.R., Zhang, J., Li, L.S., Hansen, R., Peters, U., Guo, X., Chen, Y., Babbar, A., Firdaus, S.J., Darjania, L., Feng, J., Chen, J.H., Li, S., Li, S., Long, Y.O., Thach, C., Liu, Y., Zariéh, A., Ely, T., Kucharski, J.M., Kessler, L.V., Wu, T., Yu, K., Wang, Y., Yao, Y., Deng, X., Zarrinkar, P.P., Brehmer, D., Dhanak, D., Lorenzi, M.V., Hu-Lowe, D., Patricelli, M.P., Ren, P. and Liu, Y. 2018. Targeting KRAS Mutant Cancers with a Covalent G12C-Specific Inhibitor. *Cell*. **172**(3), pp.578-589 e517.
- Janosi, L., Li, Z., Hancock, J.F. and Gorfe, A.A. 2012. Organization, dynamics, and segregation of Ras nanoclusters in membrane domains. *Proc Natl Acad Sci U S A*. **109**(21), pp.8097-8102.
- Johnson, C.W., Reid, D., Parker, J.A., Salter, S., Knihtila, R., Kuzmic, P. and Mattos, C. 2017. The small GTPases K-Ras, N-Ras, and H-Ras have distinct biochemical properties determined by allosteric effects. *J Biol Chem*. **292**(31), pp.12981-12993.
- Kanie, T. and Jackson., P.K. 2018. Guanine Nucleotide Exchange Assay Using Fluorescent MANT-GDP. *Bio Protoc*. **8**(7).
- Karnoub, A.E. and Weinberg, R.A. 2008. Ras oncogenes: split personalities. *Nat Rev Mol Cell Biol*. **9**(7), pp.517-531.
- Karnoub, A.E. and Weinberg., R.A. 2008. Ras oncogenes: split personalities. *Nat Rev Mol Cell Biol*. **9**(7), pp.517-531.
- Keeton, A.B., Salter, E.A. and Piazza, G.A. 2017. The RAS-Effector Interaction as a Drug Target. *Cancer Res*. **77**(2), pp.221-226.
- Kern, F., Niauxt, T. and Baccarini, M. 2011. Ras and Raf pathways in epidermis development and carcinogenesis. *Br J Cancer*. **104**(2), pp.229-234.
- Kessler, D., Gmachl, M., Mantoulidis, A., Martin, L.J., Zoephel, A., Mayer, M., Gollner, A., Covini, D., Fischer, S., Gerstberger, T., Gmaschitz, T., Goodwin, C., Greb, P., Haring, D., Hela, W., Hoffmann, J., Karolyi-Oezguer, J., Knesl, P., Kornigg, S., Koegl, M., Kousek, R., Lamarre, L., Moser, F., Munico-Martinez, S., Peinsipp, C., Phan, J., Rinnenthal, J., Sai, J., Salamon, C., Scherbantin, Y., Schipany, K., Schnitzer, R., Schrenk, A., Sharps, B., Siszler, G., Sun, Q., Waterson, A., Wolkerstorfer, B., Zeeb, M., Pearson, M., Fesik, S.W. and McConnell, D.B. 2019. Drugging an undruggable pocket on KRAS. *Proc Natl Acad Sci U S A*. **116**(32), pp.15823-15829.

- Khan, I., Rhett, J.M. and O'Bryan, J.P. 2020. Therapeutic targeting of RAS: New hope for drugging the "undruggable". *Biochim Biophys Acta Mol Cell Res.* **1867**(2), p118570.
- Khan, I., Spencer-Smith, R. and O'Bryan, J.P. 2019. Targeting the alpha4-alpha5 dimerization interface of K-RAS inhibits tumor formation in vivo. *Oncogene.* **38**(16), pp.2984-2993.
- Kiel, C., Filchtinski, D., Spoerner, M., Schreiber, G., Kalbitzer, H.R. and Herrmann, C. 2009. Improved binding of raf to Ras.GDP is correlated with biological activity. *J Biol Chem.* **284**(46), pp.31893-31902.
- Kirsten, W.H. and Mayer., L.A. 1967. Morphologic responses to a murine erythroblastosis virus. *J Natl Cancer Inst.* **39**(2), pp.311-335.
- Kissick, D.J., Wanapun, D. and Simpson, G.J. 2011. Second-order nonlinear optical imaging of chiral crystals. *Annu Rev Anal Chem (Palo Alto Calif).* **4**, pp.419-437.
- Koide, A., Bailey, C.W., Huang, X. and Koide, S. 1998. The fibronectin type III domain as a scaffold for novel binding proteins. *J Mol Biol.* **284**(4), pp.1141-1151.
- Krissinel, E. and Henrick, K. 2007. Inference of macromolecular assemblies from crystalline state. *J Mol Biol.* **372**(3), pp.774-797.
- Krontiris, T.G. and Cooper, G.M. 1981. Transforming activity of human tumor DNAs. *Proc Natl Acad Sci U S A.* **78**(2), pp.1181-1184.
- Kummer, L., Parizek, P., Rube, P., Millgramm, B., Prinz, A., Mittl, P.R., Kaufholz, M., Zimmermann, B., Herberg, F.W. and Pluckthun, A. 2012. Structural and functional analysis of phosphorylation-specific binders of the kinase ERK from designed ankyrin repeat protein libraries. *Proc Natl Acad Sci U S A.* **109**(34), pp.E2248-2257.
- Kunkel., T.A. 1985. Rapid and efficient site-specific mutagenesis without phenotypic selection. *Proc Natl Acad Sci U S A.* **82**(2), pp.488-492.
- Kyle, H.F., Wickson, K.F., Stott, J., Burslem, G.M., Breeze, A.L., Tiede, C., Tomlinson, D.C., Warriner, S.L., Nelson, A., Wilson, A.J. and Edwards, T.A. 2015. Exploration of the HIF-1alpha/p300 interface using peptide and Adhiron phage display technologies. *Mol Biosyst.* **11**(10), pp.2738-2749.
- Laemmli., U.K. 1970. Cleavage of structural proteins during the assembly of the head of bacteriophage T4. *Nature.* **227**(5259), pp.680-685.

Lambert., J.H. 1760. *Photometria*. [Online]. Available from:

https://books.google.co.uk/books/about/Photometria.html?id=tbM6AAAACAAJ&redir_esc=y

Lampson, B.L., Pershing, N.L., Prinz, J.A., Lacsina, J.R., Marzluff, W.F., Nicchitta, C.V., MacAlpine, D.M. and Counter, C.M. 2013. Rare codons regulate KRas oncogenesis. *Curr Biol.* **23**(1), pp.70-75.

Lanman, B.A., Allen, J.R., Allen, J.G., Amegadzie, A.K., Ashton, K.S., Booker, S.K., Chen, J.J., Chen, N., Frohn, M.J., Goodman, G., Kopecky, D.J., Liu, L., Lopez, P., Low, J.D., Ma, V., Minatti, A.E., Nguyen, T.T., Nishimura, N., Pickrell, A.J., Reed, A.B., Shin, Y., Siegmund, A.C., Tamayo, N.A., Tegley, C.M., Walton, M.C., Wang, H.L., Wurz, R.P., Xue, M., Yang, K.C., Achanta, P., Bartberger, M.D., Canon, J., Hollis, L.S., McCarter, J.D., Mohr, C., Rex, K., Saiki, A.Y., San Miguel, T., Volak, L.P., Wang, K.H., Whittington, D.A., Zech, S.G., Lipford, J.R. and Cee, V.J. 2020. Discovery of a Covalent Inhibitor of KRAS(G12C) (AMG 510) for the Treatment of Solid Tumors. *J Med Chem.* **63**(1), pp.52-65.

Leney, A.C. and Heck., A.J. 2017. Native Mass Spectrometry: What is in the Name? *J Am Soc Mass Spectrom.* **28**(1), pp.5-13.

Lobato, M.N. and Rabbitts., T.H. 2004. Intracellular antibodies as specific reagents for functional ablation: future therapeutic molecules. *Curr Mol Med.* **4**(5), pp.519-528.

Lu, J., Harrison, R.A., Li, L., Zeng, M., Gondi, S., Scott, D., Gray, N.S., Engen, J.R. and Westover, K.D. 2017. KRAS G12C Drug Development: Discrimination between Switch II Pocket Configurations Using Hydrogen/Deuterium-Exchange Mass Spectrometry. *Structure.* **25**(9), pp.1442-1448 e1443.

Lu, R.M., Hwang, Y.C., Liu, I.J., Lee, C.C., Tsai, H.Z., Li, H.J. and Wu, H.C. 2020. Development of therapeutic antibodies for the treatment of diseases. *J Biomed Sci.* **27**(1), p1.

Luft, J.R., Snell, E.H. and Detitta, G.T. 2011. Lessons from high-throughput protein crystallization screening: 10 years of practical experience. *Expert Opin Drug Discov.* **6**(5), pp.465-480.

- Mabonga, L. and Kappo, A.P. 2019. Protein-protein interaction modulators: advances, successes and remaining challenges. *Biophys Rev.* **11**(4), pp.559-581.
- Macaluso, M., Russo, G., Cinti, C., Bazan, V., Gebbia, N. and Russo, A. 2002. Ras family genes: an interesting link between cell cycle and cancer. *J Cell Physiol.* **192**(2), pp.125-130.
- Maertens, O. and Cichowski, K. 2014. An expanding role for RAS GTPase activating proteins (RAS GAPs) in cancer. *Adv Biol Regul.* **55**, pp.1-14.
- Mageean., C.J. 2014. *Cellular responses to oncogenic Ras signalling* PhD thesis, University of Liverpool.
- Malumbres, M. and Barbacid., M. 2003. RAS oncogenes: the first 30 years. *Nat Rev Cancer.* **3**(6), pp.459-465.
- Marsden, C.J., Eckersley, S., Hebditch, M., Kvist, A.J., Milner, R., Mitchell, D., Warwicker, J. and Marley, A.E. 2014. The Use of Antibodies in Small-Molecule Drug Discovery. *J Biomol Screen.* **19**(6), pp.829-838.
- Martin, H.L., Bedford, R., Heseltine, S.J., Tang, A.A., Haza, K.Z., Rao, A., McPherson, M.J. and Tomlinson, D.C. 2018. Non-immunoglobulin scaffold proteins: Precision tools for studying protein-protein interactions in cancer. *N Biotechnol.* **45**, pp.28-35.
- Maurer, T., Garrenton, L.S., Oh, A., Pitts, K., Anderson, D.J., Skelton, N.J., Fauber, B.P., Pan, B., Malek, S., Stokoe, D., Ludlam, M.J., Bowman, K.K., Wu, J., Giannetti, A.M., Starovasnik, M.A., Mellman, I., Jackson, P.K., Rudolph, J., Wang, W. and Fang, G. 2012. Small-molecule ligands bind to a distinct pocket in Ras and inhibit SOS-mediated nucleotide exchange activity. *Proc Natl Acad Sci U S A.* **109**(14), pp.5299-5304.
- McCormick, F. 2018. Targeting KRAS Directly. **2**(1), pp.81-90.
- McCormick., F. 2019. Progress in targeting RAS with small molecule drugs. *Biochem J.* **476**(2), pp.365-374.
- McCoy., A.J. 2007. Solving structures of protein complexes by molecular replacement with Phaser. *Acta Crystallogr D Biol Crystallogr.* **63**(Pt 1), pp.32-41.
- McGee, J.H., Shim, S.Y., Lee, S.J., Swanson, P.K., Jiang, S.Y., Durney, M.A. and Verdine, G.L. 2018. Exceptionally high-affinity Ras binders that remodel its effector domain. *J Biol Chem.* **293**(9), pp.3265-3280.

- Memon., A.R. 2004. The role of ADP-ribosylation factor and SAR1 in vesicular trafficking in plants. *Biochim Biophys Acta*. **1664**(1), pp.9-30.
- Milburn, M.V., Tong, L., deVos, A.M., Brunger, A., Yamaizumi, Z., Nishimura, S. and Kim, S.H. 1990. Molecular switch for signal transduction: structural differences between active and inactive forms of protooncogenic ras proteins. *Science*. **247**(4945), pp.939-945.
- Miles, J., Hobor, F., Trinh, C., Taylor, J., Tiede, C., Rowell, P., Jackson, B., Nadat, F., Ramsahye, P., Kyle, H., Wicky, B., Clarke, J., Tomlinson, D., Wilson, A. and Edwards, T. 2020. Selective Affimers Recognize the BCL-2 Family Proteins BCL-xL and MCL-1 through Non-Canonical Structural Motifs. *Chembiochem*.
- Miles, J.A., Hobor, F., Taylor, J., Tiede, C., Rowell, P.R., Trinh, C.H., Jackson, B., Nadat, F., Kyle, H.F., Wicky, B.I.M., Clarke, J., Tomlinson, D.C., Wilson, A.J. and Edwards, T.A. 2019. Selective Affimers Recognize BCL-2 Family Proteins Through Non-Canonical Structural Motifs. p651364.
- Mishra, A.K. and Lambright., D.G. 2016. Invited review: Small GTPases and their GAPs. *Biopolymers*. **105**(8), pp.431-448.
- Mo, S.P., Coulson, J.M. and Prior, I.A. 2018. RAS variant signalling. *Biochem Soc Trans*. **46**(5), pp.1325-1332.
- Moore, A.R., Rosenberg, S.C., McCormick, F. and Malek, S. 2020. RAS-targeted therapies: is the undruggable drugged? *Nat Rev Drug Discov*. **19**(8), pp.533-552.
- Mullard, A. 2019. Cracking KRAS. *Nat Rev Drug Discov*. **18**(12), pp.887-891.
- Mullard., A. 2019. KRAS's undruggability cracks? *Nat Rev Drug Discov*. **18**(7), p488.
- Murshudov, G.N., Skubak, P., Lebedev, A.A., Pannu, N.S., Steiner, R.A., Nicholls, R.A., Winn, M.D., Long, F. and Vagin, A.A. 2011. REFMAC5 for the refinement of macromolecular crystal structures. *Acta Crystallogr D Biol Crystallogr*. **67**(Pt 4), pp.355-367.
- Naylor, J. and Beech, D.J. 2013. Generation of antibodies that are externally acting isoform-specific inhibitors of ion channels. *Methods Mol Biol*. **998**, pp.245-256.

- Newlaczyl, A.U., Hood, F.E., Coulson, J.M. and Prior, I.A. 2014. Decoding RAS isoform and codon-specific signalling. *Biochem Soc Trans.* **42**(4), pp.742-746.
- Newman, J., Egan, D., Walter, T.S., Meged, R., Berry, I., Ben Jelloul, M., Sussman, J.L., Stuart, D.I. and Perrakis, A. 2005. Towards rationalization of crystallization screening for small- to medium-sized academic laboratories: the PACT/JCSG+ strategy. *Acta Crystallogr D Biol Crystallogr.* **61**(Pt 10), pp.1426-1431.
- Nguyen, A., Burack, W.R., Stock, J.L., Kortum, R., Chaika, O.V., Afkarian, M., Muller, W.J., Murphy, K.M., Morrison, D.K., Lewis, R.E., McNeish, J. and Shaw, A.S. 2002. Kinase suppressor of Ras (KSR) is a scaffold which facilitates mitogen-activated protein kinase activation in vivo. *Mol Cell Biol.* **22**(9), pp.3035-3045.
- O'Bryan., J.P. 2019. Pharmacological targeting of RAS: Recent success with direct inhibitors. *Pharmacol Res.* **139**, pp.503-511.
- Okada, T., Hu, C.D., Jin, T.G., Kariya, K., Yamawaki-Kataoka, Y. and Kataoka, T. 1999. The strength of interaction at the Raf cysteine-rich domain is a critical determinant of response of Raf to Ras family small GTPases. *Mol Cell Biol.* **19**(9), pp.6057-6064.
- Omerovic, J., Hammond, D.E., Clague, M.J. and Prior, I.A. 2008. Ras isoform abundance and signalling in human cancer cell lines. *Oncogene.* **27**(19), pp.2754-2762.
- Ostrem, J.M., Peters, U., Sos, M.L., Wells, J.A. and Shokat, K.M. 2013. K-Ras(G12C) inhibitors allosterically control GTP affinity and effector interactions. *Nature.* **503**(7477), pp.548-551.
- Ostrem, J.M. and Shokat., K.M. 2016. Direct small-molecule inhibitors of KRAS: from structural insights to mechanism-based design. *Nat Rev Drug Discov.* **15**(11), pp.771-785.
- Patgiri, A., Yadav, K.K., Arora, P.S. and Bar-Sagi, D. 2011. An orthosteric inhibitor of the Ras-Sos interaction. *Nat Chem Biol.* **7**(9), pp.585-587.
- Patricelli, M.P., Janes, M.R., Li, L.S., Hansen, R., Peters, U., Kessler, L.V., Chen, Y., Kucharski, J.M., Feng, J., Ely, T., Chen, J.H., Firdaus, S.J., Babbar, A., Ren, P. and Liu, Y. 2016. Selective Inhibition of Oncogenic KRAS Output

- with Small Molecules Targeting the Inactive State. *Cancer Discov.* **6**(3), pp.316-329.
- Pei, D., Chen, K. and Liao, H. 2018. Targeting Ras with Macromolecules. *Cold Spring Harb Perspect Med.* **8**(3).
- Peri, F., Airoidi, C., Colombo, S., Martegani, E., van Neuren, A.S., Stein, M., Marinzi, C. and Nicotra, F. 2005. Design, synthesis and biological evaluation of sugar-derived Ras inhibitors. *Chembiochem.* **6**(10), pp.1839-1848.
- Phillips, A.T. and Signs, M.W. 2005. Desalting, concentration, and buffer exchange by dialysis and ultrafiltration. *Curr Protoc Protein Sci.* **Chapter 4**, pUnit4 4.
- Pluckthun., A. 2015. Designed ankyrin repeat proteins (DARPs): binding proteins for research, diagnostics, and therapy. *Annu Rev Pharmacol Toxicol.* **55**, pp.489-511.
- Pol, E. 2010. The importance of correct protein concentration for kinetics and affinity determination in structure-function analysis. *J Vis Exp.* (37).
- Ponting, C.P. and Benjamin., D.R. 1996. A novel family of Ras-binding domains. *Trends Biochem Sci.* **21**(11), pp.422-425.
- Prior, I.A., Hood, F.E. and Hartley, J.L. 2020. The Frequency of Ras Mutations in Cancer. *Cancer Res.*
- Prior, I.A., Lewis, P.D. and Mattos, C. 2012. A comprehensive survey of Ras mutations in cancer. *Cancer Res.* **72**(10), pp.2457-2467.
- Quevedo, C.E., Cruz-Migoni, A., Bery, N., Miller, A., Tanaka, T., Petch, D., Bataille, C.J.R., Lee, L.Y.W., Fallon, P.S., Tulmin, H., Ehebauer, M.T., Fernandez-Fuentes, N., Russell, A.J., Carr, S.B., Phillips, S.E.V. and Rabbitts, T.H. 2018. Small molecule inhibitors of RAS-effector protein interactions derived using an intracellular antibody fragment. *Nat Commun.* **9**(1), p3169.
- Quimby, B.B. and Dasso., M. 2003. The small GTPase Ran: interpreting the signs. *Curr Opin Cell Biol.* **15**(3), pp.338-344.
- Rajalingam, K., Schreck, R., Rapp, U.R. and Albert, S. 2007. Ras oncogenes and their downstream targets. *Biochim Biophys Acta.* **1773**(8), pp.1177-1195.
- Reddy, E.P., Reynolds, R.K., Santos, E. and Barbacid, M. 1982. A point mutation is responsible for the acquisition of transforming properties by the T24 human bladder carcinoma oncogene. *Nature.* **300**(5888), pp.149-152.

- Repasky, G.A., Chenette, E.J. and Der, C.J. 2004. Renewing the conspiracy theory debate: does Raf function alone to mediate Ras oncogenesis? *Trends Cell Biol.* **14**(11), pp.639-647.
- Resat, H., Straatsma, T.P., Dixon, D.A. and Miller, J.H. 2001. The arginine finger of RasGAP helps Gln-61 align the nucleophilic water in GAP-stimulated hydrolysis of GTP. *Proc Natl Acad Sci U S A.* **98**(11), pp.6033-6038.
- Rhodes, K.J. and Trimmer, J.S. 2008. Antibody-based validation of CNS ion channel drug targets. *J Gen Physiol.* **131**(5), pp.407-413.
- Roberts, P.J. and Der, C.J. 2007. Targeting the Raf-MEK-ERK mitogen-activated protein kinase cascade for the treatment of cancer. *Oncogene.* **26**(22), pp.3291-3310.
- Robinson, J.I., Baxter, E.W., Owen, R.L., Thomsen, M., Tomlinson, D.C., Waterhouse, M.P., Win, S.J., Nettleship, J.E., Tiede, C., Foster, R.J., Owens, R.J., Fishwick, C.W.G., Harris, S.A., Goldman, A., McPherson, M.J. and Morgan, A.W. 2018. Affimer proteins inhibit immune complex binding to FcγRIIIa with high specificity through competitive and allosteric modes of action. *Proc Natl Acad Sci U S A.* **115**(1), pp.E72-E81.
- Rodrigues, G.A., Mason, M., Christie, L.A., Hansen, C., Hernandez, L.M., Burke, J., Luhrs, K.A. and Hohman, T.C. 2018. Functional Characterization of Abicipar-Pegol, an Anti-VEGF DARPIn Therapeutic That Potently Inhibits Angiogenesis and Vascular Permeability. *Invest Ophthalmol Vis Sci.* **59**(15), pp.5836-5846.
- Roth, S., Macartney, T.J., Konopacka, A., Chan, K.H., Zhou, H., Queisser, M.A. and Sapkota, G.P. 2020. Targeting Endogenous K-RAS for Degradation through the Affinity-Directed Protein Missile System. *Cell Chem Biol.*
- Rous., P. 1911. A Sarcoma of the Fowl Transmissible by an Agent Separable from the Tumor Cells. *J Exp Med.* **13**(4), pp.397-411.
- Rudack, T., Xia, F., Schlitter, J., Kotting, C. and Gerwert, K. 2012a. Ras and GTPase-activating protein (GAP) drive GTP into a precatalytic state as revealed by combining FTIR and biomolecular simulations. *Proc Natl Acad Sci U S A.* **109**(38), pp.15295-15300.
- Rudack, T., Xia, F., Schlitter, J., Kotting, C. and Gerwert, K. 2012b. The role of magnesium for geometry and charge in GTP hydrolysis, revealed by

- quantum mechanics/molecular mechanics simulations. *Biophys J.* **103**(2), pp.293-302.
- Ryan, M.B. and Corcoran., R.B. 2018. Therapeutic strategies to target RAS-mutant cancers. *Nat Rev Clin Oncol.* **15**(11), pp.709-720.
- Sathyan, K.M., Nalinakumari, K.R. and Kannan, S. 2007. H-Ras mutation modulates the expression of major cell cycle regulatory proteins and disease prognosis in oral carcinoma. *Mod Pathol.* **20**(11), pp.1141-1148.
- Schulze-Sunninghausen, D., Becker, J. and Luy, B. 2014. Rapid heteronuclear single quantum correlation NMR spectra at natural abundance. *J Am Chem Soc.* **136**(4), pp.1242-1245.
- Schulze, W.X., Deng, L. and Mann, M. 2005. Phosphotyrosine interactome of the ErbB-receptor kinase family. *Mol Syst Biol.* **1**, p2005 0008.
- Scolnick, E.M., Rands, E., Williams, D. and Parks, W.P. 1973. Studies on the nucleic acid sequences of Kirsten sarcoma virus: a model for formation of a mammalian RNA-containing sarcoma virus. *J Virol.* **12**(3), pp.458-463.
- Serebriiskii, I.G., Connelly, C., Frampton, G., Newberg, J., Cooke, M., Miller, V., Ali, S., Ross, J.S., Handorf, E., Arora, S., Lieu, C., Golemis, E.A. and Meyer, J.E. 2019. Comprehensive characterization of RAS mutations in colon and rectal cancers in old and young patients. *Nat Commun.* **10**(1), p3722.
- Sha, F., Salzman, G., Gupta, A. and Koide, S. 2017. Monobodies and other synthetic binding proteins for expanding protein science. *Protein Sci.* **26**(5), pp.910-924.
- Shih, C., Shilo, B.Z., Goldfarb, M.P., Dannenberg, A. and Weinberg, R.A. 1979. Passage of phenotypes of chemically transformed cells via transfection of DNA and chromatin. *Proc Natl Acad Sci U S A.* **76**(11), pp.5714-5718.
- Shima, F., Ijiri, Y., Muraoka, S., Liao, J., Ye, M., Araki, M., Matsumoto, K., Yamamoto, N., Sugimoto, T., Yoshikawa, Y., Kumasaka, T., Yamamoto, M., Tamura, A. and Kataoka, T. 2010. Structural basis for conformational dynamics of GTP-bound Ras protein. *J Biol Chem.* **285**(29), pp.22696-22705.
- Shima, F., Yoshikawa, Y., Ye, M., Araki, M., Matsumoto, S., Liao, J., Hu, L., Sugimoto, T., Ijiri, Y., Takeda, A., Nishiyama, Y., Sato, C., Muraoka, S., Tamura, A., Osoda, T., Tsuda, K., Miyakawa, T., Fukunishi, H., Shimada, J., Kumasaka, T., Yamamoto, M. and Kataoka, T. 2013. In silico discovery of

- small-molecule Ras inhibitors that display antitumor activity by blocking the Ras-effector interaction. *Proc Natl Acad Sci U S A.* **110**(20), pp.8182-8187.
- Shimizu, K., Goldfarb, M., Perucho, M. and Wigler, M. 1983. Isolation and preliminary characterization of the transforming gene of a human neuroblastoma cell line. *Proc Natl Acad Sci U S A.* **80**(2), pp.383-387.
- Silvius, J.R., Bhagatji, P., Leventis, R. and Terrone, D. 2006. K-ras4B and prenylated proteins lacking "second signals" associate dynamically with cellular membranes. *Mol Biol Cell.* **17**(1), pp.192-202.
- Simeon, R. and Chen., Z. 2018. In vitro-engineered non-antibody protein therapeutics. *Protein Cell.* **9**(1), pp.3-14.
- Slastnikova, T.A., Ulasov, A.V., Rosenkranz, A.A. and Sobolev, A.S. 2018. Targeted Intracellular Delivery of Antibodies: The State of the Art. *Front Pharmacol.* **9**, p1208.
- Smyth, D.R., Mrozkiewicz, M.K., McGrath, W.J., Listwan, P. and Kobe, B. 2003. Crystal structures of fusion proteins with large-affinity tags. *Protein Sci.* **12**(7), pp.1313-1322.
- Sogabe, S., Kamada, Y., Miwa, M., Niida, A., Sameshima, T., Kamaura, M., Yonemori, K., Sasaki, S., Sakamoto, J.I. and Sakamoto, K. 2017. Crystal Structure of a Human K-Ras G12D Mutant in Complex with GDP and the Cyclic Inhibitory Peptide KRpep-2d. *ACS Med Chem Lett.* **8**(7), pp.732-736.
- Sondka, Z., Bamford, S., Cole, C.G., Ward, S.A., Dunham, I. and Forbes, S.A. 2018. The COSMIC Cancer Gene Census: describing genetic dysfunction across all human cancers. *Nat Rev Cancer.* **18**(11), pp.696-705.
- Spencer-Smith, R., Koide, A., Zhou, Y., Eguchi, R.R., Sha, F., Gajwani, P., Santana, D., Gupta, A., Jacobs, M., Herrero-Garcia, E., Cobbett, J., Lavoie, H., Smith, M., Rajakulendran, T., Dowdell, E., Okur, M.N., Dementieva, I., Sicheri, F., Therrien, M., Hancock, J.F., Ikura, M., Koide, S. and O'Bryan, J.P. 2017. Inhibition of RAS function through targeting an allosteric regulatory site. *Nat Chem Biol.* **13**(1), pp.62-68.
- Spencer-Smith, R., Li, L., Prasad, S., Koide, A., Koide, S. and O'Bryan, J.P. 2019. Targeting the alpha4-alpha5 interface of RAS results in multiple levels of inhibition. *Small GTPases.* **10**(5), pp.378-387.

- Spoerner, M., Herrmann, C., Vetter, I.R., Kalbitzer, H.R. and Wittinghofer, A. 2001. Dynamic properties of the Ras switch I region and its importance for binding to effectors. *Proc Natl Acad Sci U S A.* **98**(9), pp.4944-4949.
- Stadler, L.K., Hoffmann, T., Tomlinson, D.C., Song, Q., Lee, T., Busby, M., Nyathi, Y., Gendra, E., Tiede, C., Flanagan, K., Cockell, S.J., Wipat, A., Harwood, C., Wagner, S.D., Knowles, M.A., Davis, J.J., Keegan, N. and Ferrigno, P.K. 2011. Structure-function studies of an engineered scaffold protein derived from Stefin A. II: Development and applications of the SQT variant. *Protein Eng Des Sel.* **24**(9), pp.751-763.
- Stahl, S., Graslund, T., Eriksson Karlstrom, A., Frejd, F.Y., Nygren, P.A. and Lofblom, J. 2017. Affibody Molecules in Biotechnological and Medical Applications. *Trends Biotechnol.* **35**(8), pp.691-712.
- Stenmark, H. and Olkkonen, V.M. 2001. The Rab GTPase family. *Genome Biol.* **2**(5), pREVIEWS3007.
- Stephen, A.G., Esposito, D., Bagni, R.K. and McCormick, F. 2014. Dragging ras back in the ring. *Cancer Cell.* **25**(3), pp.272-281.
- Sun, Q., Burke, J.P., Phan, J., Burns, M.C., Olejniczak, E.T., Waterson, A.G., Lee, T., Rossanese, O.W. and Fesik, S.W. 2012. Discovery of small molecules that bind to K-Ras and inhibit Sos-mediated activation. *Angew Chem Int Ed Engl.* **51**(25), pp.6140-6143.
- Sun, Q., Phan, J., Friberg, A.R., Camper, D.V., Olejniczak, E.T. and Fesik, S.W. 2014. A method for the second-site screening of K-Ras in the presence of a covalently attached first-site ligand. *J Biomol NMR.* **60**(1), pp.11-14.
- Tabin, C.J., Bradley, S.M., Bargmann, C.I., Weinberg, R.A., Papageorge, A.G., Scolnick, E.M., Dhar, R., Lowy, D.R. and Chang, E.H. 1982. Mechanism of activation of a human oncogene. *Nature.* **300**(5888), pp.143-149.
- Tanaka, T. and Rabbitts, T.H. 2003. Intrabodies based on intracellular capture frameworks that bind the RAS protein with high affinity and impair oncogenic transformation. *EMBO J.* **22**(5), pp.1025-1035.
- Tanaka, T., Williams, R.L. and Rabbitts, T.H. 2007. Tumour prevention by a single antibody domain targeting the interaction of signal transduction proteins with RAS. *EMBO J.* **26**(13), pp.3250-3259.
- Tate, J.G., Bamford, S., Jubb, H.C., Sondka, Z., Beare, D.M., Bindal, N., Boutselakis, H., Cole, C.G., Creatore, C., Dawson, E., Fish, P., Harsha, B.,

- Hathaway, C., Jupe, S.C., Kok, C.Y., Noble, K., Ponting, L., Ramshaw, C.C., Rye, C.E., Speedy, H.E., Stefancsik, R., Thompson, S.L., Wang, S., Ward, S., Campbell, P.J. and Forbes, S.A. 2019. COSMIC: the Catalogue Of Somatic Mutations In Cancer. *Nucleic Acids Res.* **47**(D1), pp.D941-D947.
- Taveras, A.G., Remiszewski, S.W., Doll, R.J., Cesarz, D., Huang, E.C., Kirschmeier, P., Pramanik, B.N., Snow, M.E., Wang, Y.S., del Rosario, J.D., Vibulbhan, B., Bauer, B.B., Brown, J.E., Carr, D., Catino, J., Evans, C.A., Girijavallabhan, V., Heimark, L., James, L., Liberles, S., Nash, C., Perkins, L., Senior, M.M., Tsarboboulos, A., Webber, S.E. and et al. 1997. Ras oncoprotein inhibitors: the discovery of potent, ras nucleotide exchange inhibitors and the structural determination of a drug-protein complex. *Bioorg Med Chem.* **5**(1), pp.125-133.
- Thornton., J.A. 2016. Splicing by Overlap Extension PCR to Obtain Hybrid DNA Products. *Methods Mol Biol.* **1373**, pp.43-49.
- Tiede, C., Bedford, R., Heseltine, S.J., Smith, G., Wijetunga, I., Ross, R., AlQallaf, D., Roberts, A.P., Balls, A., Curd, A., Hughes, R.E., Martin, H., Needham, S.R., Zanetti-Domingues, L.C., Sadigh, Y., Peacock, T.P., Tang, A.A., Gibson, N., Kyle, H., Platt, G.W., Ingram, N., Taylor, T., Coletta, L.P., Manfield, I., Knowles, M., Bell, S., Esteves, F., Maqbool, A., Prasad, R.K., Drinkhill, M., Bon, R.S., Patel, V., Goodchild, S.A., Martin-Fernandez, M., Owens, R.J., Nettleship, J.E., Webb, M.E., Harrison, M., Lippiat, J.D., Ponnambalam, S., Peckham, M., Smith, A., Ferrigno, P.K., Johnson, M., McPherson, M.J. and Tomlinson, D.C. 2017. Affimer proteins are versatile and renewable affinity reagents. *Elife.* **6**.
- Tiede, C., Tang, A.A., Deacon, S.E., Mandal, U., Nettleship, J.E., Owen, R.L., George, S.E., Harrison, D.J., Owens, R.J., Tomlinson, D.C. and McPherson, M.J. 2014. Adhiron: a stable and versatile peptide display scaffold for molecular recognition applications. *Protein Eng Des Sel.* **27**(5), pp.145-155.
- Vajda, S., Beglov, D., Wakefield, A.E., Egbert, M. and Whitty, A. 2018. Cryptic binding sites on proteins: definition, detection, and druggability. *Curr Opin Chem Biol.* **44**, pp.1-8.
- Vazquez-Lombardi, R., Phan, T.G., Zimmermann, C., Lowe, D., Jermutus, L. and Christ, D. 2015. Challenges and opportunities for non-antibody scaffold drugs. *Drug Discov Today.* **20**(10), pp.1271-1283.

- Verdurmen, W.P., Luginbuhl, M., Honegger, A. and Pluckthun, A. 2015. Efficient cell-specific uptake of binding proteins into the cytoplasm through engineered modular transport systems. *J Control Release*. **200**, pp.13-22.
- Vigil, D., Cherfils, J., Rossman, K.L. and Der, C.J. 2010. Ras superfamily GEFs and GAPs: validated and tractable targets for cancer therapy? *Nat Rev Cancer*. **10**(12), pp.842-857.
- Villanueva, M.T. 2019. Long path to MYC inhibition approaches clinical trials. *Nat Rev Drug Discov*.
- Waters, A.M., Ozkan-Dagliyan, I., Vaseva, A.V., Fer, N., Strathern, L.A., Hobbs, G.A., Tessier-Cloutier, B., Gillette, W.K., Bagni, R., Whiteley, G.R., Hartley, J.L., McCormick, F., Cox, A.D., Houghton, P.J., Huntsman, D.G., Philips, M.R. and Der, C.J. 2017. Evaluation of the selectivity and sensitivity of isoform- and mutation-specific RAS antibodies. *Sci Signal*. **10**(498).
- Watzinger, F., Mayr, B., Haring, E. and Lion, T. 1998. High sequence similarity within ras exons 1 and 2 in different mammalian species and phylogenetic divergence of the ras gene family. *Mamm Genome*. **9**(3), pp.214-219.
- Weiss, G.A., Watanabe, C.K., Zhong, A., Goddard, A. and Sidhu, S.S. 2000. Rapid mapping of protein functional epitopes by combinatorial alanine scanning. *Proc Natl Acad Sci U S A*. **97**(16), pp.8950-8954.
- Welsch, M.E., Kaplan, A., Chambers, J.M., Stokes, M.E., Bos, P.H., Zask, A., Zhang, Y., Sanchez-Martin, M., Badgley, M.A., Huang, C.S., Tran, T.H., Akkiraju, H., Brown, L.M., Nandakumar, R., Cremers, S., Yang, W.S., Tong, L., Olive, K.P., Ferrando, A. and Stockwell, B.R. 2017. Multivalent Small-Molecule Pan-RAS Inhibitors. *Cell*. **168**(5), pp.878-889 e829.
- Wennerberg, K., Rossman, K.L. and Der, C.J. 2005. The Ras superfamily at a glance. *J Cell Sci*. **118**(Pt 5), pp.843-846.
- Whitmore, L. and Wallace., B.A. 2004. DICHROWEB, an online server for protein secondary structure analyses from circular dichroism spectroscopic data. *Nucleic Acids Res*. **32**(Web Server issue), pp.W668-673.
- Wilkins, M.R., Gasteiger, E., Bairoch, A., Sanchez, J.C., Williams, K.L., Appel, R.D. and Hochstrasser, D.F. 1999. Protein identification and analysis tools in the ExPASy server. *Methods Mol Biol*. **112**, pp.531-552.

- Willumsen, B.M., Norris, K., Papageorge, A.G., Hubbert, N.L. and Lowy, D.R. 1984. Harvey murine sarcoma virus p21 ras protein: biological and biochemical significance of the cysteine nearest the carboxy terminus. *EMBO J.* **3**(11), pp.2581-2585.
- Winter, J.J., Anderson, M., Blades, K., Brassington, C., Breeze, A.L., Chresta, C., Embrey, K., Fairley, G., Faulder, P., Finlay, M.R., Kettle, J.G., Nowak, T., Overman, R., Patel, S.J., Perkins, P., Spadola, L., Tart, J., Tucker, J.A. and Wrigley, G. 2015. Small molecule binding sites on the Ras:SOS complex can be exploited for inhibition of Ras activation. *J Med Chem.* **58**(5), pp.2265-2274.
- Wortzel, I. and Seger, R. 2011. The ERK Cascade: Distinct Functions within Various Subcellular Organelles. *Genes Cancer.* **2**(3), pp.195-209.
- Wuo, M.G. and Arora, P.S. 2018. Engineered protein scaffolds as leads for synthetic inhibitors of protein-protein interactions. *Curr Opin Chem Biol.* **44**, pp.16-22.
- Xie, C., Tiede, C., Zhang, X., Wang, C., Li, Z., Xu, X., McPherson, M.J., Tomlinson, D.C. and Xu, W. 2017. Development of an Affimer-antibody combined immunological diagnosis kit for glypican-3. *Sci Rep.* **7**(1), p9608.
- Young, A., Lyons, J., Miller, A.L., Phan, V.T., Alarcon, I.R. and McCormick, F. 2009. Ras signaling and therapies. *Adv Cancer Res.* **102**, pp.1-17.
- Yu, X., Yang, Y.P., Dikici, E., Deo, S.K. and Daunert, S. 2017. Beyond Antibodies as Binding Partners: The Role of Antibody Mimetics in Bioanalysis. *Annu Rev Anal Chem (Palo Alto Calif).* **10**(1), pp.293-320.
- Zarich, N., Oliva, J.L., Martinez, N., Jorge, R., Ballester, A., Gutierrez-Eisman, S., Garcia-Vargas, S. and Rojas, J.M. 2006. Grb2 is a negative modulator of the intrinsic Ras-GEF activity of hSos1. *Mol Biol Cell.* **17**(8), pp.3591-3597.
- Zerial, M. and McBride., H. 2001. Rab proteins as membrane organizers. *Nat Rev Mol Cell Biol.* **2**(2), pp.107-117.
- Zhou, Y. and Hancock, J.F. 2015. Ras nanoclusters: Versatile lipid-based signaling platforms. *Biochim Biophys Acta.* **1853**(4), pp.841-849.

Appendix A

Vector Maps

Figure 1- Vector map of pBSTG phagemid vector (Tiede et., al 2014)

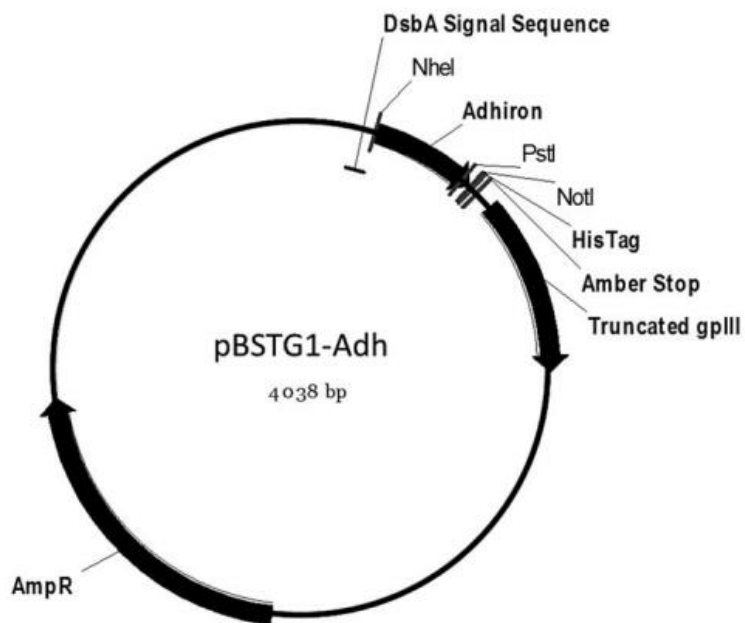


Figure 2- Vector map of pET11a Affimer containing expression vector (Tiede et. al., 2014)

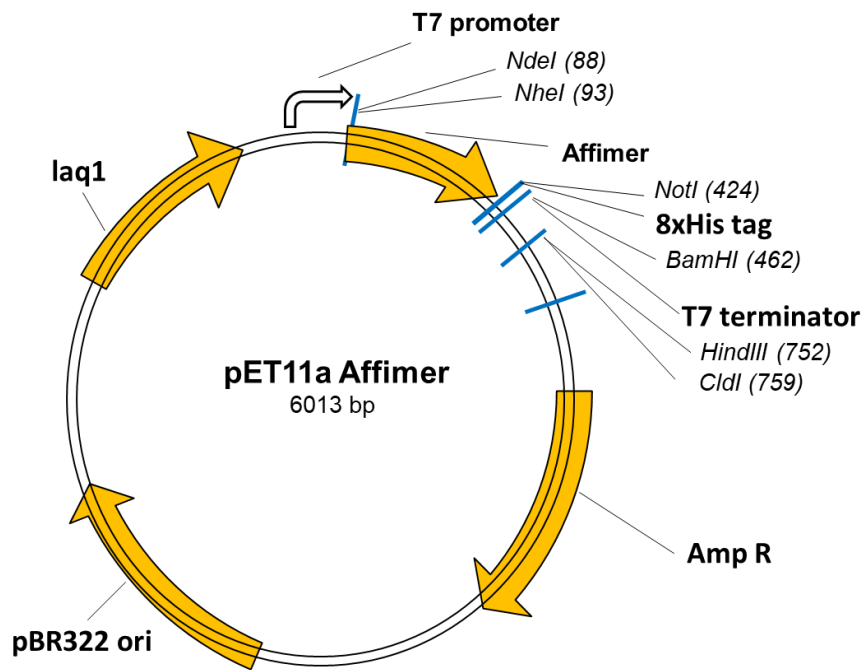


Figure 3- Vector map of GST-thr-Raf1RBD vector (Addgene® catalogue number 86033)

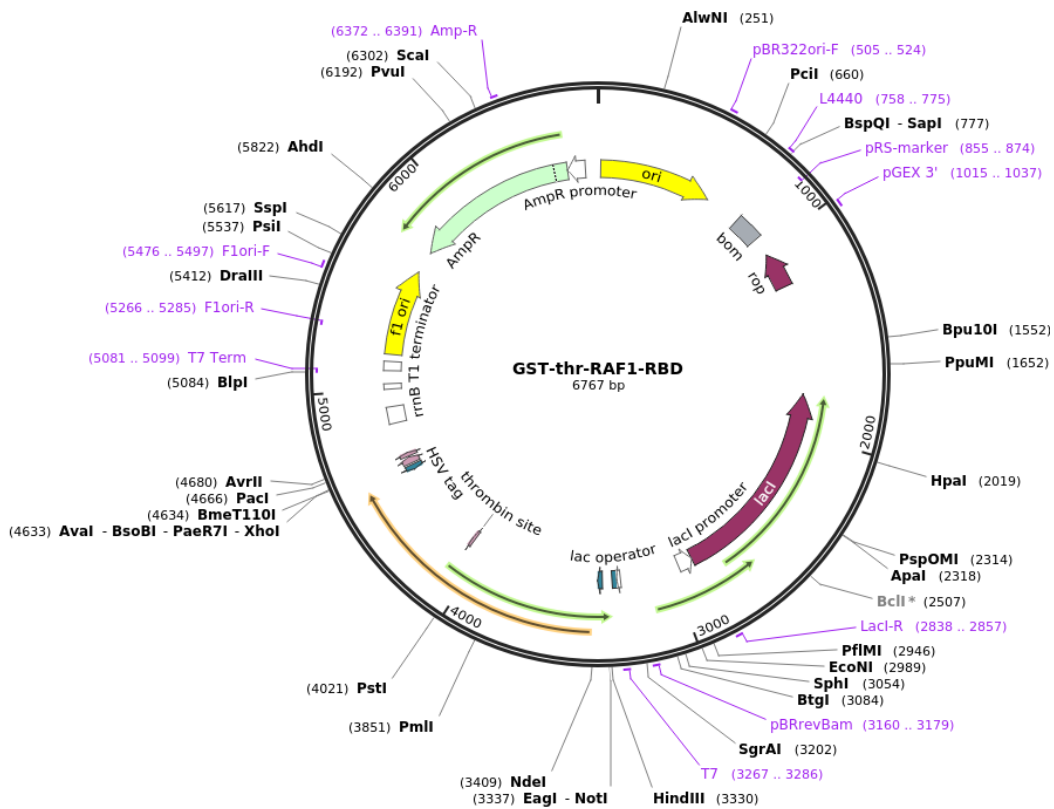


Figure 4- Vector map of pET11a KRas8x His containing expression vector

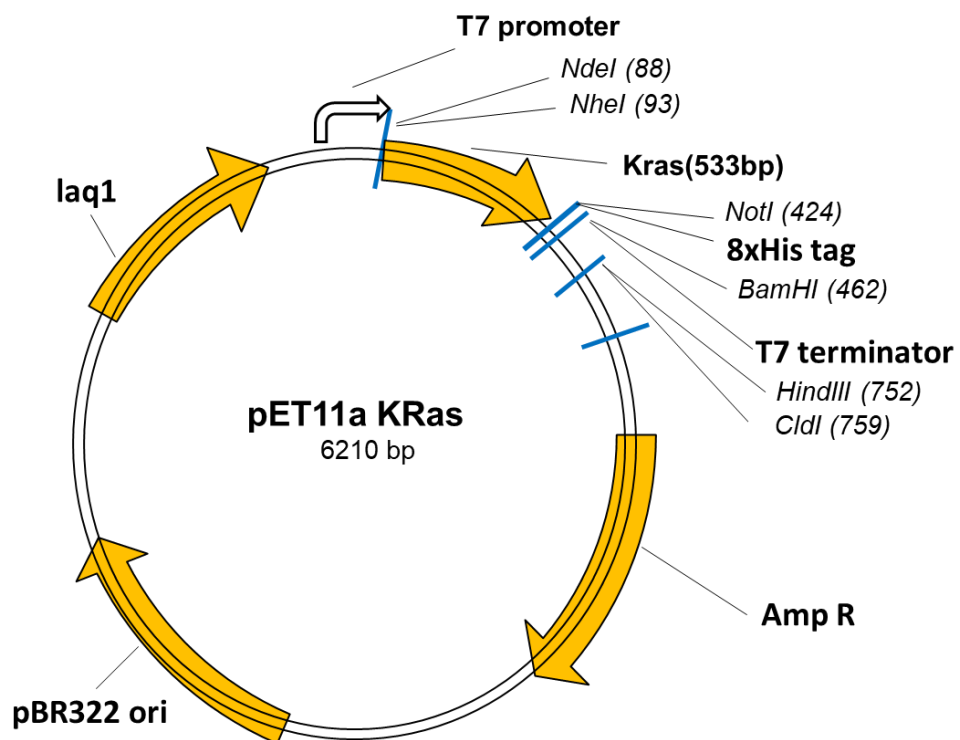
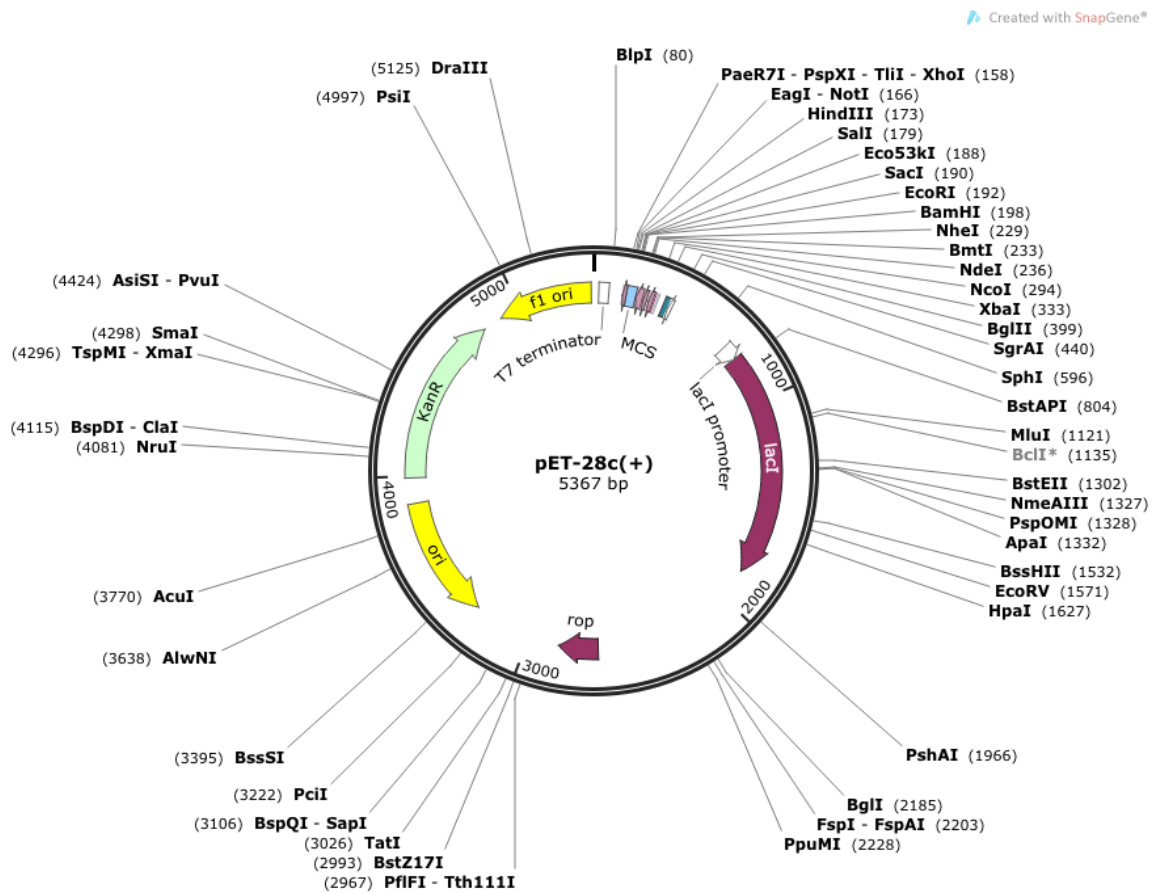


Figure 5- Vector map of pET28c containing expression vector in which SOS^{cat} 6xHis were encoded between



Appendix-B

Protein sequences of all proteins used in this thesis

Protein	Protein sequence
BAP taggedKRas-6xHis	M HHHHHH TEYKLVVVGAGGVGKSALTIQLIQNHFVDEYDPTIEDSYRKQVVIDGETCLLD ILDTAGQEEYSAMRDQYMRTGEGFLCVFAINNTKSFEDIHHYREQIKRVKDSQVPMVLV GNKCDLPSRTVDTKQAQDLARSYGIPFIETSAKTRQGVDDAFYTLVREIRKHKS GLNDIF EAQKIEWHE
K3 Affimer	MASNSLEIEELARFAVDEHNKKNALLEFVRVVKAKEQ HSIDIWYDFT MYYLTLLEAKDGGGKK LYEAKVWVK KLNSHTY KNFKELQEFKPVGDAAAAHHHHHHHHH
K6 Affimer	MASNSLEIEELARFAVDEHNKKNALLEFVRVVKAKEQ HFTPWFQRNT MYYLTLLEAKDGGGKK KLYEAKVWVK RMVTDKMRN FKELQEFKPVGDAAAA HHHHHHHH
K37 Affimer	MASNSLEIEELARFAVDEHNKKNALLEFVRVVKAKEQ QYNPWFQNT MYYLTLLEAKDGGGKK KLYEAKVWVK VIHGTRWGN NFKELQEFKPVGDAAAA HHHHHHHH
SOS1 catalytic domain	MGSS HHHHHH SSGLVPRGSHMEEQMRLPSADVYRFAEPDSEENIIFEENMQPKAGIPIKAGT VIKLIERLTYHMYADPNFVRTFLTYYRSFCKPQELLSLIERFEIPEPEPTADRIAIENGDQPLSA ELKRFRKEYIQPVQLRVLNVCRHWVEHHFYDFERDAYLLQRMEEFIGTVRGKAMKKWVESIT KIIQRKKIARDNGPGHNITFQSSPPTVEWHISRPGHIETFDLLTLHPIEIARQLTLLESPLYRAVQ PSELVGSVWTKEDKEINSPNLLKMIRHTTNLTLWFEKCVETENLEERVAVVSRIIEILQVFQEL NNFNGVLEVVSAMNSSPVYRLDHTFEQIPSRQKKILEEAHELSEDHYKKYLAKLRSINPPCVPF FGIYLTNLIKTEEGNPEVLKRHGKELINFSKRRKVAEITGEIQYQNPYCLRVESDIKRFFENL NPMGNSMEKEFTDYLFNKSLEIEPRNPKPLPRFPKKYSYPLKSPGVRPSNPRPGT*
Raf1RBD	ATGGAACATATCCAGGGCGCATGGAAACTATCAGCAATGGCTTCGGTTTCAAAGATGCG GTGTTTGTGATGGCTCCAGCTGCATTAGCCCGACCATCGTACAGCAGTTCGGTTACCAGCGT CGTGCGAGCGATGATGGCAAACGACCGATCCGAGCAAGACCAGCAACACGATTCGCGT TTTTCTGCCGAATAACAACGCACCGTCGTCAACGTTCTGTAACGGTATGAGCCTGCACGA TTGTCTGATGAAGGCTCTGAAAGTGCAGCGGTCTGCAACCGGAGTGTTCGCGCAGTTTTTCG TCTGTTACACGAGCACAAGGGTAAAAAGCCCGTCTGGACTGGAATACCGACGCGGCCA GCCTGATTGGCGAGGAAGTCAAGTCAATTTCTGGATCATGTGCCGCTGACGACCCAC AACTTCGCGCGTAAAACCTTT TTG AAG CTG GGT ATC CAT CGT GAC

Bold- Variable regions

Yellow- His tag

Red- Biotin acceptor peptide tag

Appendix C

Additional protein-based inhibitors binding to Ras

KRpep-2d peptide

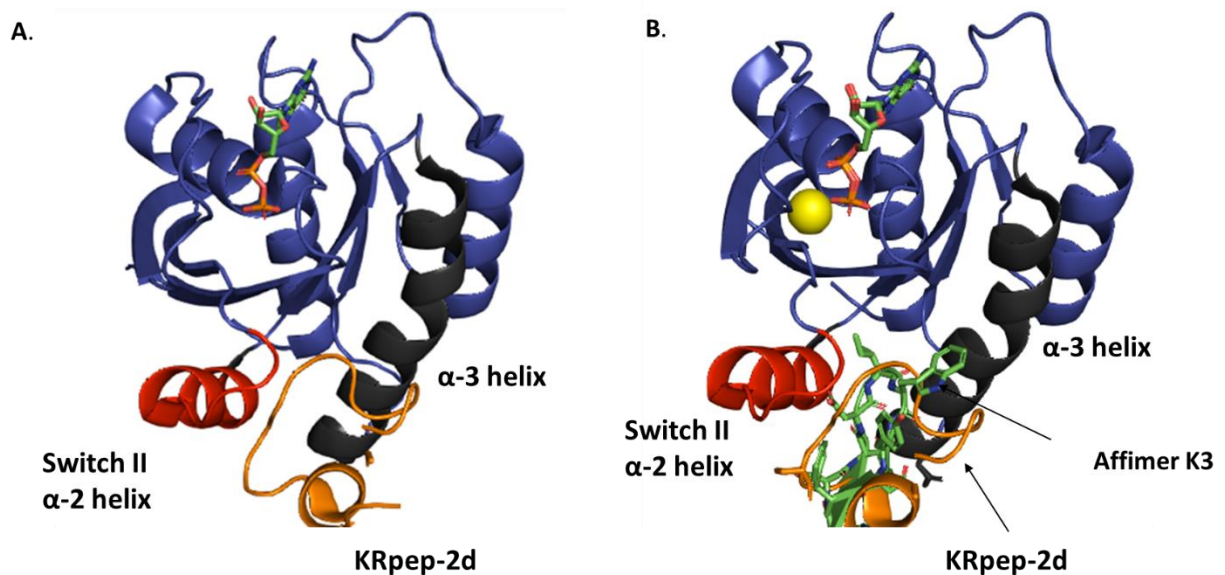


Fig 1. Comparison of KRpep2d peptide which binds between SII and α 3 helix region of KRas and Affimer K3. Affimer K3 shows different binding conformation as compared to KRpep-2d even though both bind to same druggable pocket.

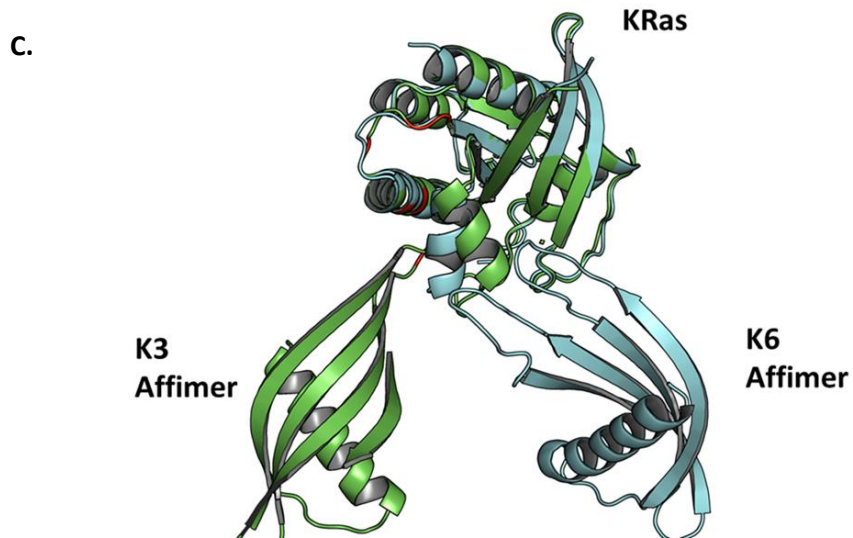


Fig 2. Comparison of Affimer K3 (green) and K6 Affimer (cyan). K3 Affimer binds between Switch II and $\alpha 3$ helix. K6 Affimer binds between Switch I and Switch II region of KRas.